HELSINKI INSTITUTE OF PHYSICS INTERNAL REPORT SERIES

HIP-2020-01

Probing the QCD Phase Diagram via Holographic Models

Jere Remes

Helsinki Institute of Physics &
Department of Physics, Faculty of Science
University of Helsinki
Finland

DOCTORAL DISSERTATION

To be presented for public discussion with the permission of the Faculty of Science of the University of Helsinki, in the auditorium D101 at Physicum, Gustaf Hällströmin katu 2, Helsinki, on the 14th of December 2020 at 14 o'clock.

Helsinki 2020

ISBN 978-951-51-1291-0 (print)
ISBN 978-951-51-1292-7 (pdf)
ISSN 1455-0563
http://ethesis.helsinki.fi
Unigrafia
Helsinki 2020

Die Menschen machen ihre eigene Geschichte, aber sie machen sie nicht aus freien Stücken, nicht unter selbstgewählten, sondern unter unmittelbar vorgefundenen, gegebenen und überlieferten Umständen.

Karl Marx
Der achtzehnte Brumaire des Louis Bonaparte (1852)

J. Remes: Probing the QCD Phase Diagram via Holographic Models,
University of Helsinki 2020, 97 pages,
Helsinki Institute of Physics, Internal Report Series, HIP-2020-01,
ISBN 978-951-51-1291-0,
ISSN 1455-0563.

Abstract

Quantum Chromodynamics (QCD) is the quantum field theory describing strong nuclear interactions. Due to the titular strong nature of these interactions, obtaining reliable predictions from the theory has proven challenging in many physically interesting regions of the phase diagram.

The most well-established current framework for handling strongly coupled, non-perturbative systems is that of lattice simulations. Even this framework has its weaknesses when applied to QCD, however, such as simulating systems where real-time dynamics are relevant or that have non-zero chemical potential. Such cases are found in *e.g.* the early-time dynamics of heavy-ion collisions and inside neutron stars, respectively. These nonperturbative systems provide us with an ideal testing ground for new methods such as holography.

Holography is an umbrella term for various dualities which connect a quantum field theory with a higher-dimensional theory of quantum gravity. One general property of these dualities is that they map operators in strongly coupled field theories into fields in weakly coupled classical gravity. It therefore seems natural to apply the methods provided by these dualities to the study of strong coupled real-world theories such as QCD. However, there is no known holographic dual for QCD yet, and we must resort to some modeling if we wish to compute predictions via holographic methods.

In this thesis, we apply holographic models of QCD – namely Improved Holographic QCD and its extension called V-QCD – in the study of both the thermalization of hot quark-gluon plasma produced in heavy-ion collisions and the structure and astrophysical properties of cold, dense matter in neutron stars. We also provide an introduction to the different facets concerning these applications from the motivation in QCD and the challenges the QCD phase diagram provides to current computational methods, to holography, heavy-ion collision phenomenology and neutron star observations.

Acknowledgments

First and foremost I thank Umut Gürsoy for agreeing to act as my opponent and Aleksi Vuorinen for performing the duties of the *kustos*. The pre-examiners of this thesis, Nick Evans and Tuomas Lappi, gave astute criticism and comments on this dissertation, and for that they have my gratitude.

The work done in this thesis would not have been possible without my supervisors: Kimmo Tuominen, Aleksi Vuorinen and Niko Jokela. I heartily thank you for conversations, guidance, support, challenging my thinking and for always answering my dire e-mails.

The research that forms the backbone of this thesis was not, and could not have been done alone. It was thanks to my collaborators, Timo Alho, Matti Järvinen and Govert Nijs that it reached the light of day, and having the privilege of working with them has taught me a lot about physics. I additionally thank Matti for his insightful and detailed comments on the manuscript of this thesis.

I also thank my colleagues at the Department of Physics and Helsinki Institute of Physics for discussions. Especially Keijo Kajantie has given me many timely comments and tips on research and academia. Fellow doctoral students of all stripes from various universities have also been of importance to my time at the university, and I wish to thank you all collectively for the comradery without naming names.

I would go amiss, if after spending nearly a decade at the campus, I would not thank all the staff and administration at Helsinki Institute of Physics, the Department of Physics, Faculty of Science, Doctoral School in Natural Sciences, Doctoral Programme in Particle Physics and Universe Sciences and especially at Physicum for their work. I have also had the privilege to be taught by many a wonderful teacher, to whom I owe much.

I also wish to extend a special recognition to all the wraiths – past and present – of the notorious A313. They have provided me with a worthwhile looking-glass, to which I can rave and ramble and which meanders in kind in response. *"Lasciate ogne speranza, voi ch'intrate"*?

Considering the circumstances that have greatly helped me in retaining some form of a life, especially through the pandemic, I thank Oranssi – and in particular my neighbors – for maintaining the fragile circle of light. And in a similar vein, I thank my co-orbiters for their flexibility and for distracting me from time to time.

I would not be here without the trouble with being born; my family has my gratitude for bringing me up and encouraging me to dive into the subjects I was interested in. Kiitos tuestanne, työstänne ja ennen kaikkea rohkeudestanne, joka on aina toiminut esimerkkinä muutoksen tavoittelussa.

The list is long, but I have saved the personally most significant recognition to last, as is the custom: I thank K for their love and over-extending patience with my occasional monomania. The amount of labor is roughly constant, no matter who is spending the time in the attic. Also, thank you Mila, even if you cannot read this.

Included Publications

This thesis is based on the following publications [**I**–**III**]

I N. Jokela, M. Järvinen, J. Remes: *Holographic QCD in the Veneziano limit and neutron stars*, JHEP **1903** (2019) 041. `arXiv:1809.07770 [hep-ph]`

II T. Alho, J. Remes, K. Tuominen, A. Vuorinen: *Quasinormal modes and thermalization in Improved Holographic QCD*, Phys. Rev. D101 (2020) 10, 106025. `arXiv:2002.09544 [hep-ph]`

III N. Jokela, M. Järvinen, G. Nijs, J. Remes: *Unified weak/strong coupling framework for nuclear matter and neutron stars* `arXiv:2006.01141 [hep-ph]`

The authors are listed alphabetically according to particle physics convention.

The author's contribution

In article **I**, the author co-wrote the numerical codes, produced the band plots and took part in writing the article. In article **II**, the author co-wrote the numerical codes, produced all the plots and co-wrote the article. In article **III**, the author wrote the numerical codes to produce the neutron star data, produced the data used in the final plots, produced most of the plots and co-wrote the article.

Contents

1 Introduction **1**

2 Quantum Chromodynamics **5**

2.1 Lagrangian and Parameters 7

2.2 Asymptotic Freedom 8

2.3 Confinement 10

2.4 On the Approximate Symmetries of the Lagrangian 11

2.4.1 Chiral symmetry 12

2.4.2 Conformal Invariance 13

2.5 Lattice QCD 14

2.6 QCD Phase Diagram 16

3 Holography **21**

3.1 A Primer on Anti-de Sitter Spacetimes 21

3.2 A Sketch of an Argument for AdS/CFT Duality 23

3.3 Holographic Thermodynamics 25

3.4 Building Models: Bottom-Up and Top-Down 27

4 Holographic QCD in the Veneziano limit **31**

4.1 Building Blocks of the Model 32

4.1.1 Improved Holographic QCD 32

4.1.2 Flavor Action 33

4.2 Matching the Model to QCD 37

4.2.1 Fitting Glue 38

4.2.2 Fitting Flavor 40

4.3 Thermodynamics of the Model 43

5 Heavy-Ion Collisions and Holography **47**

5.1 Time-evolution of Heavy-Ion Collisions 48

5.2 Holographic Thermalization 51

5.2.1 Thermalization in IHQCD 52

6 Neutron Stars and Holography **55**
6.1 Neutron Stars 55
6.1.1 Neutron Star Observations 56
6.1.2 Equation of State and the Structure of a Neutron Star 58
6.2 Neutron Stars in V-QCD 61
6.2.1 Hybrid Equations of State 61
6.2.2 Some Key Results 64

7 Summary **67**

References **69**

Chapter 1

Introduction

In his book *The Structure of Scientific Revolutions*, philosopher Thomas Kuhn argued that science does not progress solely in a linear manner – by accumulating more and more new knowledge – but also by undergoing revolutionary periods, during which the prevailing theory of the field in question is overthrown and replaced by a new one [1]. After this paradigm shift, one enters again the stage of conceptual continuity, of "normal science", where the new prevailing theory is explored and new experiments are made, until enough anomalies are discovered that lead the way to a new theory which again overthrows the now-old ruling theory.

Kuhn's theory of scientific revolutions can of course be easily critiqued. Paradigms can be seen as much more malleable and undergoing slight shifts even in the phase of normal science. One can also argue that the notion of incommensurability underlying the discrepancy between the prevailing theoretical paradigm and anomalous empirical results is too radical, or say that the model gives a simplified and after-the-fact account of the history of science and the development of theoretical models. We can nonetheless use some of Kuhn's terminology and ideas to make at least some heuristic statements about the position of the research being carried out; is it aiming for a revolution, or is it exploring the established theory of its field?

In view of this, the position of holography – and by association, of this thesis – in the historical process of science is somewhat curious. Holography provides a correspondence between quantum gravity and quantum field theory; between a string theory living in a higher-dimensional space and a highly symmetric field theory living on the boundary of this space. Therefore, one can take two disparate positions concerning how to preface a dissertation on holography; either you focus on holography as a gateway to quantum gravity and the Theory of Everything, and see the subsequent model as an application of the principle, or you focus on the problems of strongly coupled gauge theories and introduce holography as a computational tool – a hammer to hit nails with – within the established theories. One can either focus on the revolutionary gauge/gravity duality or solving the puzzles within current theories.

This thesis will take the latter approach, as we focus on bypassing the problems one is faced with when applying the usual methods of perturbation theory and lattice simulations to Quantum Chromodynamics (QCD).

1. Introduction

QCD is one of the theories making up the Standard Model of particle physics, which has, as a whole, proven time and time again to agree to an astonishing accuracy with experiments. However, the strong nature of the interactions that QCD describes makes it theoretically challenging to compute predictions from it in most circumstances. The reason one cannot currently just determine, say, the structure of neutron stars from QCD lies in the way we compute observables in quantum field theory at present. Most of the standard computational methods include the use of perturbation theory, in which one studies observables in different orders of an expansion with respect to the coupling constant of the theory. In many crucial cases though, the coupling constant is not small.

There are other tools available to assist one in these instances, namely effective field theories and lattice simulations. The problem with the former arises from their applicability, as the underlying approximations, such as chirality of the vacuum, fail, whereas the latter is at present the gold-standard method when dealing with strongly coupled field theories. The applicability of lattice methods is also limited to some extent, as the current computational methods are unable to cope with non-negligible chemical potentials due to the infamous sign problem [2], and with real-time processes due to their reliance on Euclidean discretization [3].

The problems plaguing non-perturbative approaches become most apparent when one considers the phase diagram of QCD. Even after almost half a century of research, the details of the diagram outside the region with vanishing chemical potential remain elusive to theoretical endeavors. From the empirical standpoint, the new century has provided us with new probes to QCD scales, as colliders such as RHIC and the LHC have been able to commence the study of quark-gluon plasma, the hot particle soup made of the constituent particles making up protons, neutrons and other hadrons. The heavy-ion collision experiments conducted in these facilities have actually allowed us to experimentally explore the properties of this phase, revealing that the plasma created in these experiments is strongly coupled and behaves like a nearly perfect relativistic fluid.

On another front, the recent LIGO/Virgo gravitational wave detection of a neutron star merger [4, 5], together with the observation of its electromagnetic counterpart [6], have opened up interesting possibilities. With the growing body of data on neutron stars and their dynamics, we are offered a laboratory to probe the phase diagram of QCD in the high-density limit that is manifest within neutron stars. These observations provide us with a possibility to constrain the equation of state of QCD by its connection to neutron star observables, such as the maximum observed mass, observed radii and tidal deformabilities.

Here the aforementioned holography steps in. Holographic dualities provide us with a tool to compute observables in strongly coupled field theories by describing them with fields in a higher-dimensional gravity theory. There are multiple known holographic dualities between different theories, the most famous being the AdS/CFT correspondence, which connects a type IIB string theory in $\mathrm{AdS}_5 \times S^5$ spacetime with an $\mathcal{N} = 4$ supersymmetric Yang-Mills theory living on the boundary of the AdS space [7].

Like is the case with AdS/CFT, in the known dualities the boundary theory is usually highly symmetric, with supersymmetries and conformal symmetry, which is not the case for real QCD. In fact, there is no known holographic dual for QCD, and so, if one wishes to compute predictions from QCD within the holographic framework, they need to resort in some form of model-building. There have been surprising successes in this modeling, most prominently in predicting the nature of the quark-gluon plasma as a near-perfect fluid [8]. Since then, holography has become a standard tool in the study of heavy-ion collisions [9].

The particular holographic framework in the center of this dissertation is called *Veneziano-QCD* (V-QCD). It is a family of models based on two building blocks: a holographic, bottom-up dilaton-gravity model for pure Yang-Mills theory – which in itself is known as Improved Holographic QCD (IHQCD) – and a flavor sector, where the dynamics of quarks are described by a Dirac-Born-Infeld action. These two sectors are fully backreacted with each other in the Veneziano limit. The action, motivated by string theory, is generalized to contain nontrivial potentials, which can be matched to QCD results both qualitatively, by requiring the model to *e.g.* be confining in the IR, and quantitatively where reliable lattice results are available.

Herein, in the application of this model, lies the *thesis* of this thesis: I claim that we can make reasonable qualitative predictions in the strongly coupled regime of QCD by using V-QCD. In this work, we apply holographic methods in the study of both the thermalization of the hot quark-gluon plasma formed in heavy-ion collisions and of the cold, dense matter that neutron stars comprise of.

In the first part of this thesis we look into the generalities behind the work exhibited in the accompanying publications: in Chapter 2 we review some relevant background in QCD, its Lagrangian and properties such as asymptotic freedom and confinement. We then introduce lattice QCD and discuss what is currently known about the QCD phase diagram. In Chapter 3, we introduce holography, starting from anti-de Sitter spaces, go through the argumentation behind the original AdS/CFT duality, study the implementation of thermodynamics in the holographic framework and review the different modeling philosophies. Coming to Chapter 4, we introduce V-QCD. We explain how the model is put together and what is the reasoning behind each part. We also examine the process of matching the model to QCD and the thermodynamics of the model. In Chapter 5, we review the time-evolution of heavy-ion collisions, and our studies concerning the thermalization process in the context of IHQCD. The matter of neutron stars is discussed next, in Chapter 6. We begin with a review of some of the observations and the state of knowledge concerning the equation of state, and continue on to summarize our research on the subject using V-QCD. We will end with concluding remarks in Chapter 7.

Chapter 2

Quantum Chromodynamics

The basis of our current understanding of subatomic physics is formulated in the language of quantum field theories (QFT). The Standard Model of particle physics, the best and the most rigorously tested theory concerning the matter content and the interactions governing our universe (excluding gravity), is built on such theories. The quantum field theories making up the Standard Model describe the different interactions between the matter fields via their respective gauge fields. These different interactions are named the *electromagnetic*, the *weak*, and the *strong* interaction. The electromagnetic and the weak interactions are unified under the Electroweak theory, and the strong interaction is described by *Quantum Chromodynamics* (QCD).

These different theories manifest different gauge symmetries, which – along with other symmetry requirements – uniquely determine the way in which the theory is constructed. The electroweak sector is described by a spontaneously broken gauge symmetry of $SU(2) \times U(1)$. The gauge bosons which mediate these interactions are the charged W^+ and W^-, and the neutral Z – all of which are massive particles – for the weak interaction, and the massless photon γ for the electromagnetic interaction. The strong interaction is described by QCD, which is a manifestation of $SU(3)$ gauge symmetry, the carriers of which are the *gluons*. The only matter particles in the Standard Model charged under $SU(3)$ are the six different types, or *flavors* of *quarks*, which are called *up*, *down*, *strange*, *charm*, *bottom*, and *top*, all of which are summarized with the other particles of the Standard Model in Fig. 2.1.

Unlike the electron, which carries a single unit of $U(1)$ charge, each of the different flavors of quarks can carry any of three different $SU(3)$ charges, also known as *color* charges (hence the name for the theory). One further and extremely important difference between the electromagnetic and strong interactions is in their respective gauge bosons; photons do not carry electric charge whereas gluons do carry color charge, meaning that gluons can interact with each other.

While the subject particles of the other facets of the Standard Model are, however briefly, observed as isolated particles, this is not the case for quarks and gluons, which are bound into color-neutral states known as hadrons[1]. Among these hadrons are the familiar proton

[1]It is worth also mentioning the color singlet states comprising entirely of gluons, called *glueballs*. Their existence has not yet been confirmed by experiments, but some of the observed light scalars exhibit properties similar to

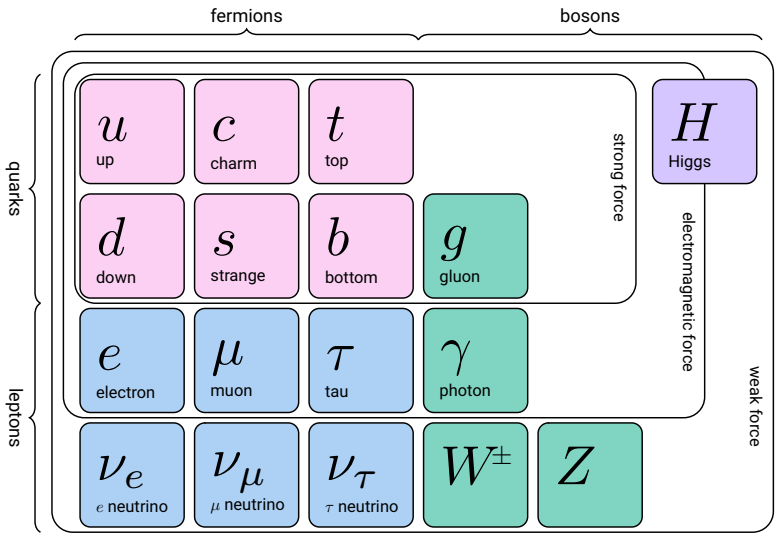

Figure 2.1: Particles making up the Standard Model, excluding the antiparticles. The fermions can be further divided into three generations by the column they are in, with each generation being heavier than the previous.

and neutron, which make up most of the visible mass in the Universe, and comprise of three constituent quarks. The composite particles consisting of an odd number of valence quarks are collectively known as *baryons*. The other option in making color-neutral states of quarks is by a quark and an antiquark with opposite color charges forming a bound state known as a *meson*.

In this chapter we will shortly review some central properties of QCD, in order to explain why we need to develop new tools to produce testable predictions from QCD in the strongly-coupled regime. This dissertation is meant to be but a pebble on that path.

QCD has been the subject of extensive theoretical and experimental inquiry for the majority of the past century, and there are inevitably too many phenomenologically interesting details and detours to be dealt with here. This chapter will mostly focus on the subjects especially relevant for the work done in this thesis. For a more complete and relatively up-to-date review of the current status of the study of QCD, see *e.g.* Ref. [12].

We will begin this chapter by recalling some of the basic properties and parameters of the QCD Lagrangian in Sec. 2.1. We will then focus on the corollaries that the QCD Lagrangian and Nature present us in the form of asymptotic freedom in Sec. 2.2 and confinement in Sec. 2.3 and review some aspects of a few approximate symmetries that aid us in the later discussion, more specifically chiral symmetry in 2.4.1 and conformal symmetry in 2.4.2. We will then introduce

what one expects from glueballs [10]. The lightest glueball state is expected to have a mass of around 1.7 GeV based on lattice simulations [11].

the very basics of lattice QCD in Sec. 2.5, as it will play a crucial role both in determining the structure of the QCD phase diagram and also in the building of our holographic model later on in the dissertation. After that, we review the current state of knowledge on the QCD phase diagram in Sec. 2.6.

2.1 Lagrangian and Parameters

To determine the dynamics and the kinematics of a QFT, it is usually helpful to write down the (classical) Lagrangian of the theory. The QCD Lagrangian can be written as

$$\mathcal{L}_{QCD} = \sum_q \bar{\psi}^q \left(i\not{D} - m^q\right)\psi^q - \frac{1}{4}G^a_{\mu\nu}G_a^{\mu\nu}, \tag{2.1}$$

where quarks ψ, labeled $q = u, d, \ldots, N_f$, transform in the fundamental representation of SU(3), and gluons, transforming in the adjoint representation of SU(3), have color indices a and b, which for N_c colors take values $a, b = 1, 2, \ldots, N_c^2 - 1 = 8$. Indices $\mu, \nu = 0, 1, \ldots, 3$ are Lorentz indices. The covariant derivative $\not{D} = \gamma^\mu D_\mu$ and the gluon field strength tensor G are defined through

$$D_\mu = \partial_\mu - igt_a\mathcal{A}^a_\mu, \tag{2.2}$$

$$G^a_{\mu\nu} = \partial_\mu\mathcal{A}^a_\nu - \partial_\nu\mathcal{A}^a_\mu + gf^a{}_{bc}\mathcal{A}^b_\mu\mathcal{A}^c_\nu, \tag{2.3}$$

where $t_a \equiv \frac{1}{2}\lambda_a$, with the Gell-Mann λ_a being the generators of SU(3), which have a traceless, Hermitian 3×3 matrix representation. The coefficients f_{abc} are the structure constants of the $\mathfrak{su}(3)$ algebra, defined by the commutation relation $[t_a, t_b] = if^a_{bc}t^c$. The γ^μ are Dirac gamma-matrices.

There is also freedom for a CP-violating term of the form

$$\mathcal{L}_\theta = \frac{\alpha_s}{4\pi}\theta G^a_{\mu\nu}\tilde{G}_a^{\mu\nu}, \tag{2.4}$$

to be present in the Lagrangian (2.1). The parameter θ is called the QCD vacuum angle, or simply θ-angle, and $\tilde{G}^a_{\mu\nu} \equiv \frac{1}{2}\epsilon_{\mu\nu\sigma\rho}G^{a\sigma\rho}$ is the dual of G. Experimental constraints limit the angle $|\theta| \lesssim 10^{-10}$ [13–15], the smallness of which poses a problem called the *strong CP problem*. This term is also relevant for the structure of the QCD vacuum, and θ is one of the few fundamental parameters of QCD alongside α_s[2]. All this, however, is outside the focus of this thesis, and interested readers can find more information *e.g.* in reviews such as Ref. [16, 17].

Alongside these terms, to produce the final Feynman rules from (2.1), one needs to include a gauge fixing term[3]

$$\mathcal{L}_{GF} = \frac{1}{2\xi}(\partial^\mu\mathcal{A}^a_\mu)^2, \tag{2.5}$$

where ξ appears from the Lagrange multiplier. One should note that adding the gauge fixing term obviously breaks gauge invariance, as a gauge is now chosen. If one chooses the above

[2]The others being the quark masses, which have their origin in the electroweak theory.
[3]Here, the R_ξ gauge is presented. It is a simple generalization of the Lorenz gauge.

gauge instead of the axial or temporal gauges, an additional term is needed to cancel unphysical polarization states of the gluons

$$\mathcal{L}_{FP} = \partial_\mu \bar{\eta}^a \partial^\mu \eta_a + g_s f^{abc} \mathcal{A}^\mu_a (\partial_\mu \bar{\eta}_b) \eta_c, \tag{2.6}$$

where η is a scalar Grassmann field called the *Faddeev-Popov ghost* [18]. The alternative gauges mentioned have unphysical singularities in the Feynman integrals, so the inclusion of these unphysical degrees of freedom is a worthwhile trade-off, and they are not relevant for the phenomenological conclusions we draw from the Lagrangian (2.1) [19].

There are multiple features that make QCD special compared to arguably simpler theories such as QED, and most of these properties are rooted in the non-Abelian gauge group $SU(3)$. One of the consequences of which is that gluons are self-interacting, *i.e.* they carry a color charge, as can be seen from the indices of the field strength tensor. These three- and four-gluon self-interactions contribute to the peculiar characteristics of QCD, among which are *asymptotic freedom* and *color confinement*.

2.2 Asymptotic Freedom

Almost immediately after QCD was formulated, Wilczek, Gross and Politzer [20, 21] discovered in 1973 that when QCD (or in fact, any suitable $SU(N_c)$ Yang-Mills theory) is examined at arbitrarily high energies – or equivalently, small distances – one is able to distinguish individual quarks and gluons, which do not form bound states. This observation is called asymptotic freedom.

One can see this behavior by examining the rate at which the coupling constant changes with the varying renormalization scale μ, as encoded in the behavior of the beta function β,

$$\beta(\alpha_s) = \mu^2 \frac{\partial \alpha_s(\mu^2)}{\partial \mu^2}, \tag{2.7}$$

with $\alpha_s \equiv g^2/4\pi$. This can be further expanded as

$$\beta(\alpha_s) = -b_0 \alpha_s^2(\mu^2) - b_1 \alpha_s^3(\mu^2) - b_2 \alpha_s^4(\mu^2) \ldots \tag{2.8}$$

where the expansion is taken up to a three-loop level. The lowest b_i can be written as [22]

$$\begin{aligned} b_0 &= \frac{33 - 2N_f}{12\pi}, \\ b_1 &= \frac{153 - 19N_f}{24\pi^2}, \\ b_2 &= \frac{77139 - 15099N_f + 325N_f^2}{3456\pi^3}. \end{aligned} \tag{2.9}$$

where N_f is the number of active flavors available at a given energy scale. One should note that coefficients b_0 and b_1 are renormalization-scheme-independent, unlike the ones at higher

orders, which are all dependent on the choice of renormalization scheme. The one adopted for this chapter is the modified minimal subtraction scheme ($\overline{MS}$) [23].

Given a renormalization scale μ, we can define $\Lambda \equiv \Lambda_{\overline{MS}}$, such that

$$\Lambda^2 = \frac{\mu^2}{\exp\left((b_0\alpha_s(\mu^2))^{-1}\right)}, \tag{2.10}$$

allowing us to write a formula for α_s by solving Eq. (2.7):

$$\alpha_s(\mu^2) = \frac{1}{b_0 \ln(\mu^2/\Lambda^2)}, \tag{2.11}$$

up to a one-loop contribution. From this equation, we see that for $N_f < 17$ flavors, as is the case for QCD, the strength of the interaction $\alpha_s(\mu^2) \to 0$ when $\mu \to \infty$, pointing us towards the realization that, at least when considering only the first loop, we could see free quarks at asymptotically high energies.

This theoretical observation – which naturally has been studied further than the mere one-loop level presented here – is also supported by the earliest experimental observations of quarks: in high-energy scattering experiments performed with electrons scattering from nucleons (Deep Inelastic Scattering [24]) one sees the scatterings occur from the constituent particles rather than the whole nucleon. The running of the coupling is demonstrated in Fig. 2.2, where we have shown the energy scale dependence of α_s up to the four-loop level, along with some observations from various experiments, as reported in Ref. [17].

In the formula for b_0 in Eq. (2.9), the factor of 33 comes from gluon self-interactions, and it is the factor that most clearly separates QCD and other Yang-Mills theories from QED and other Abelian theories. For $SU(N_c)$ Yang-Mills theories with N_c colors and N_f flavors, the term can be written as [20, 21]

$$b_0^{YM} = \frac{11}{12\pi}N_c - \frac{2}{12\pi}N_f, \tag{2.12}$$

whereas for QED the corresponding term is [25]

$$b_0^{QED} = -\frac{4N_f}{12\pi}. \tag{2.13}$$

Thus QED can effectively be handled perturbatively at all scales[4], whereas for QCD, perturbative methods – and the renormalization group equation (2.7) – are only valid at scales $Q \gg \Lambda_{QCD}$, where $\Lambda_{QCD} \sim 200$ MeV is the QCD scale, set by the confinement scale of ~ 1 fm.

One further aside to make here on Eq. (2.12) concerns the large-N_c expansion of the SU(N_c) theory [27], which will play a key role later in this thesis. By rescaling $g^2 \to \tilde{g}^2 = N_c g^2$, we can rewrite $b_0 = \frac{11}{3} - \frac{2}{3}N_f/N_c$, suppressing the fermion loop effects in the $N_c \to \infty$ limit. This points us towards a general feature of this limit; if one further keeps the rescaled coupling $\tilde{g}$ (usually denoted by $\lambda \equiv \tilde{g}^2$ and called the *'t Hooft coupling*) fixed, the limit is called the *'t Hooft*

[4]We are glossing over important subtleties here: QED has a perturbatively defined Landau pole at high energies, setting a definite higher limit in the applicability of the theory. There are more nuances to this discussion, and the interested reader can see *e.g.* Ref [26].

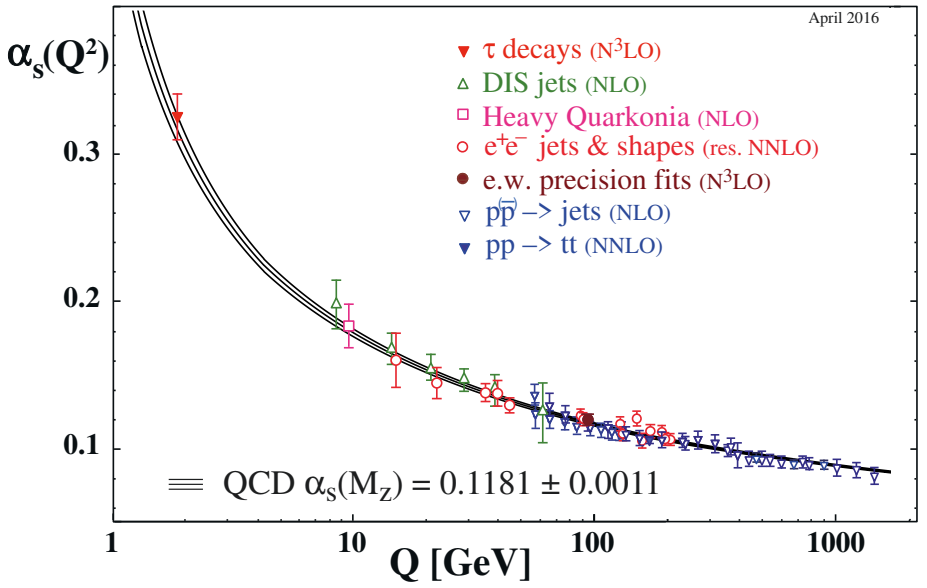

Figure 2.2: Summary of measurements of the strong coupling α_s as a function of the energy scale Q. The degree of QCD perturbation theory used in the extraction of the coupling from the data is indicated in brackets. Figure from Ref. [17].

limit. Taking this limit allows one to topologically classify Feynman diagrams, separating them into planar and non-planar diagrams, with non-planar ones being suppressed by $1/N_c$ for any given process, simplifying computations tremendously. The immediate question is of course, if the large-N_c limit provides any insight into QCD, which has $N_c = 3$. The answer is "yes" to a certain extent: one can gain insight to certain non-trivial nonperturbative aspects of QCD by studying the large-N_c limit (see *e.g.* Refs. [28, 29]), as the $1/N_c$ expansions seem to converge quite well to results close to ones at $N_c = 3$, if the scaling of the quantities is done correctly.

2.3 Confinement

While the nature of the theory at asymptotically high energies is both useful and revealing, the more familiar (from the everyday perspective) and simultaneously more challenging frontier is found in the low-energy regime of the theory. As we saw in Fig. 2.2, the perturbatively determined coupling constant becomes quite considerable at a high energy: in a back-of-the-envelope fashion, we see that if there are between two to five active flavors, Eq. (2.11) would give us $\alpha_s > 1$ at around $\mu \leq 0.1 \ldots 1$ GeV [30], signifying the definite breakdown of the perturbative expansion.

However naïve, this dabbling leads us to discuss the other aforementioned property of QCD, *confinement* – or the observation that we do not observe isolated color-charged particles in Nature. This (proposed) property conforms with our intuition: we only see color-neutral objects in the

world around us, not quarks and gluons. However, rigorously proving that QCD actually is a confining theory still provides a considerable, nonperturbative theoretical challenge, and is one of the reasons why the generalized problem of "Yang-Mills existence and mass gap" is a Millennium Problem. From a phenomenological point of view the problem is not that severe, as we are able to reproduce observationally valid bound state (*i.e.* hadron) spectra within the QCD framework by multiple different methods, some of which we have already mentioned in passing, while others we will later discuss. There is also a lot of theoretical work related to the topic of confinement [31–37], and the signs pointing towards QCD being confining are strong.

One way to gain intuition on confinement is by again contrasting Eq. (2.12) with Eq. (2.13). The fermionic contributions from the vacuum behave the same in both theories, but due to the non-Abelian nature, and the resulting self-interactions of the gauge fields, the gluonic contribution has an opposite effect to the fermionic one, which can be seen as the relative minus sign in Eq. (2.12). This effect is called *antiscreening* of the color charge, and it enhances the color charge at larger distances as $11N_c \gg N_f$, implying that separated particles attract each other the stronger the further away they are from one another.

The current state-of-the-art computations to address the question of confinement are provided by lattice simulations – which we will talk about a bit more in-depth later in this Chapter. One can see signs of confinement by studying the static quark-antiquark potential in pure $SU(3)$ gauge theory [19, 38, 39]

$$V(r) \approx -\frac{a}{r} + \sigma r + V_0, \tag{2.14}$$

where a, σ, V_0 are constants. What is important here is the linear term σr, which models a color-flux tube, and the parameter σ is often called the string tension. For very heavy quarks in a pure Yang-Mills theory, Eq. (2.14) implies that the binding energy of the pair grows without a limit, due to presence the linear term, as the separation $r \to \infty$. In real QCD, due to the presence of light quarks, the phenomenon of string breaking takes place: as the gluon field gains more energy, color singlet $\bar{q}q$ pairs are created between the original $\bar{q}q$ pair. Thus, no quarks can be isolated.

2.4 On the Approximate Symmetries of the Lagrangian

To fully understand some of the oncoming discussions, we need to briefly consider a few of the other symmetries associated with the QCD Lagrangian (2.1) besides those of gauge and Poincaré invariance. Some of the symmetries of the Lagrangian, such as CPT and $U(1)_B$ are conserved even in the full quantum theory, whereas others, like the axial symmetry [40], are broken by quantization. Some symmetries that have proven useful for effective computations are actually not exact symmetries of the complete Lagrangian, but approximate symmetries, such as isospin symmetry, conformal symmetry and chiral symmetry. The symmetries we are most interested in here are those of chirality and conformality.

2.4.1 Chiral symmetry

Chirality, in this context, refers to representations of the Lorentz group $SO(1,3)$. We can deform the group into $SL(2,\mathbb{C})_L \times SL(2,\mathbb{C})_R$, the representations of which can be labeled by half-integer numbers (m,n). Scalars naturally transform in the $(0,0)$ representation, whereas four-vectors such as x^μ transform in the $(\frac{1}{2},\frac{1}{2})$ representation. When transforming spinors, we have two possibilities: $(0,\frac{1}{2})$ and $(\frac{1}{2},0)$, or the right- and the left-handed representation respectively. We can write the full spinor ψ as a sum of spinors transforming in either representation, *i.e.* $\psi = \psi_L + \psi_R$, where $\psi_{R/L} = \frac{1}{2}(1 \pm \gamma^5)\psi$.

Using the anticommutation relations of Dirac gamma matrices, the part of the Lagrangian (2.1) concerning the quarks can be written using this decomposition as

$$\mathcal{L}_q = \bar{\psi}^q_L \not{D} \psi^q_L + \bar{\psi}^q_R \not{D} \psi^q_R - m_q \left(\bar{\psi}^q_L \psi^q_R + \bar{\psi}^q_R \psi^q_L \right), \tag{2.15}$$

where the summation over the flavors q is made implicit and we have suppressed the color indices.

Chiral symmetry refers to a property that the above Lagrangian does not explicitly have; a theory is considered chirally symmetric, if one can perform rotations in the flavor space independently for each chirality, *i.e.* if performing

$$\psi^i_L \mapsto L^{ij} \psi^j_L, \quad \psi^i_R \mapsto R^{ij} \psi^j_R, \tag{2.16}$$

where L and R are unitary matrices and i,j run from 1 to N_f, leaves the Lagrangian invariant. Chiral symmetry is thus an $SU(N_f)_L \times SU(N_f)_R$ symmetry.

The presence of the mass term in the Lagrangian (2.15) means that the Lagrangian is explicitly not chirally symmetric. However, in QCD the lightest of the quarks, the up and the down, have fairly small constituent masses – 2.2 MeV and 4.7 MeV respectively – compared to the masses of the nucleons, which are around $M \sim 1$ GeV [17]. Therefore one can treat the Lagrangian as effectively massless at hadronic scales, with the symmetry violation being around $m_q/M \sim 1\%$ for two massless flavors. For three massless flavors, the violation is of the order of 10 %, as the strange quark is comparatively heavy.

Even if chiral symmetry were an exact symmetry of the classical Lagrangian, it turns out that it is still broken spontaneously, *i.e.* by the vacuum of the theory. If chiral symmetry were respected, one expects $\langle \bar{\psi}_L \psi_R \rangle$ to equal zero [41]. However, even the simple chiral Lagrangian produces – when correctly quantized – a chiral condensate, and $\langle \bar{\psi}_{Li} \psi_{Rj} \rangle = -\Sigma \delta_{ij}$ [42, 43], with $\Sigma \neq 0$.[5] This breaks the global symmetry, as to preserve the Lorentz invariance of the vacuum one must require $L_{ij} = R_{ij}$.

The above consideration holds true at low temperatures, but the expectation value of the condensate lowers with temperature, and eventually vanishes and the chiral symmetry is restored [44–46]. The nature of the chiral transition is affected by the number of chiral quarks –

[5] The non-zero vacuum expectation value of $\langle \bar{\psi} \psi \rangle$ can be seen to signal that the vacuum harbors quark-antiquark pairs that come in and out of existence and contribute to the vacuum structure, as was alluded to earlier in this Chapter.

and in the massive Lagrangian the exact physical masses – which determine the chiral transition at finite temperature to be crossover (see the Columbia plot in Ref. [47]).

Why the chiral symmetry is relevant for the topic of this thesis is however its usefulness. The approximate chirality of the QCD Lagrangian serves as a starting point for some effective field theories [48–50], most notably Chiral Perturbation Theory (ChPT) [51, 52] and Chiral Effective Theory (CET)(see *e.g.* Ref. [53] for a review), which have proven remarkably useful in the study of nuclear forces, the structure of the nuclei and nuclear matter (see *e.g.* Refs. [53–59]), allowing for systematic and model-independent computations while respecting the symmetries of QCD.

2.4.2 Conformal Invariance

The other approximate symmetry relevant to our endeavors is the conformal symmetry, more due to its importance in holography and therefore the remainder of this thesis than the applications of the symmetry itself. To understand the connection of QCD to this topic, we need to begin with a brief refresher on conformal symmetry [60, 61].

Conformal transformations are angle-preserving spacetime transformations. They form a symmetry group, which in D-dimensional Minkowski space is $SO(2, D)$. The group has fifteen generators: ten corresponding to the full Poincaré group, one to dilatations and four to the special conformal group. It is easy to see why the Poincaré group is a part of the conformal group, as translations, rotations and Lorentz transformations naturally leave the Minkowski metric invariant. Simple scaling transformations $x^\mu \to x'^\mu = \lambda x^\mu$ also rightfully belong to the group, as they do not affect the angles between vectors. The final four generators correspond to the group of special conformal transformations, which can be parametrized with a vector b and written as

$$x^\mu \to x'^\mu = \frac{x^\mu - b^\mu x^2}{1 - 2b_\mu x^\mu + b^2 x^2}. \tag{2.17}$$

The field theories that are invariant under the conformal group are highly symmetric, scale-invariant theories, implying also the absence of any dimensionful parameters, such as mass, or scale dependence, such as a running gauge coupling. It is clear that the Lagrangian in Eq. (2.1) does not exhibit conformal behavior, as we have a scale introduced in the form of quark masses, and we have also discussed the running of the coupling in Section 2.2. However, if one considers the asymptotically high energies, where the gauge coupling tends to zero, in the absence of the mass terms we could expect QCD to manifest conformal symmetry [62]. And in fact, we do not even have to go to asymptotically high energies for perturbative $SU(N_c)$ Yang-Mills theory with N_f massless flavors for certain choices of N_f and N_c to have a fixed point[6] with nonzero coupling in the renormalization group flow, known as the Banks-Zaks fixed point [63, 64] (see also Refs. [65, 66]).

[6]Fixed points are points in the renormalization group flow where $\beta = 0$. More formally, if K is a coupling constant of the Hamiltonian that transforms as $R_\ell K$ under the renormalization group transformation R_ℓ, then K^* is a fixed point of the renormalization group flow iff $R_\ell K^* = K^*$.

The conformal symmetry of the classical Lagrangian is broken in quantization by quantum anomalies. We can easily see this by considering a scaling transformation of the coordinate $x \to \lambda x$, with the fermion field transforming as $\psi(x) \to \lambda^{3/2}\psi(\lambda x)$, and the gauge field as $\mathcal{A}^a_\mu(x) \to \lambda \mathcal{A}^a_\mu(\lambda x)$. Now the corresponding Noether current is $J^\mu = x_\nu T^{\mu\nu}$, where $T^{\mu\nu}$ is the energy-momentum tensor [19].

Noether's theorem requires the conservation of current J^μ, and thus $\partial_\mu J^\mu = T^\mu_{\ \mu} = 0$. If one however actually computes the trace of the energy-momentum tensor, it is [19]

$$T^\mu_{\ \mu} = \frac{\beta}{2g_s} G^{\mu\nu}_a G^a_{\mu\nu} + \sum_q m_q \bar{q} q, \tag{2.18}$$

which has a non-zero vacuum expectation value in the quantized theory. This discrepancy is called trace anomaly, or conformal anomaly, and it can be used to illustrate the origin of the mass of the nucleon, which is considerably larger than the mass of the constituent quarks due to the contribution from the gluon fields, which crowd the vacuum.

Although the full QCD Lagrangian is not conformal, the fact that aspects of conformality are still present in the theory, and that the theory is asymptotically conformal is encouraging, when we are considering the applicability of holography in the study of QCD.

2.5 Lattice QCD

As we have already seen, the usual perturbative methods only work in QCD for high energy processes, where the coupling constant is sufficiently small. However, quite a bit of interesting physics takes place well below these energies. One non-perturbative method that has proven very successful is *lattice gauge theory.* To understand some of the reasons why it has been so successful and why it ultimately fails at some tasks, we need to sketch a simple outline of lattice QCD. For a more complete introduction to the subject, see *e.g.* Ref. [67].

The naïve way one would go about discretizing spacetime would be to construct a lattice version of Minkowski space. This attempt is however ultimately doomed to fail, as the resulting action would be complex, and would hence interfere with the use of Monte Carlo methods. Success in discretization is achieved by working with Euclidean spacetime. This way, one can compute the correlator functions and spectra of the theory, as the resulting lattice theory is essentially a statistical system where the free energy is determined by the Euclidean action and where the lattice spacing a acts as a natural UV regulator. The downsides of the use of the imaginary time – resulting from the Wick rotation to the Euclidean coordinates – are however visible when dealing with real-time dynamics, such as is the case with out-of-equilibrium processes[7] [31, 69, 70].

Next, we encounter the question of placing the particles on the lattice. Again, the naïve attempt would be to put both fermions and gauge bosons on lattice points, but this effort glosses over what anyone familiar with differential geometry has recognized; the gauge field can be thought of as a connection, *i.e.* it can be interpreted to describe how the internal color degrees of

[7] Although much progress has happened at this front in the recent years. See *e.g.* Ref. [68].

freedom change when a particle is transported from a lattice point to another. From this picture it is clear that the gauge fields reside on the links between the lattice points.

The useful version of the continuum gauge fields $A_\mu(x)$ on lattice is the Wilson line $U_\mu(x)$ between the lattice points x and $x+\hat{\mu}$, defined as

$$U_\mu(x) = \mathcal{P}\exp\left[ig_s\int_x^{x+\hat{\mu}} \mathrm{d}x'_\mu A_\mu(x')\right], \tag{2.19}$$

with a slight abuse of the index notation – the repeated indices are not summed over. The operator $\mathcal{P}$ is the path-ordering operator.

Under a gauge transformation $\Lambda(x)$, $U_\mu(x) \to \Lambda(x)U_\mu(x)\Lambda^\dagger(x+\hat{\mu})$, and from the fact that the transformation only depends on the end points of the integration, it is easy to devise a gauge invariant combination of Wilson lines by taking a trace over a closed loop. We can define a *plaquette* $U_{\mu\nu}$ as

$$U_{\mu\nu}(x) = U_\mu(x)U_\nu(x+\hat{\mu})U_\mu^\dagger(x+\hat{\nu})U_\nu^\dagger(x). \tag{2.20}$$

Given that the trace over these plaquettes is gauge invariant, we can construct an action – called the Wilson action – from them [31]

$$S_W = \frac{6}{g_s^2}\sum_{x,\mu>\nu}\left(1-\frac{1}{6}\mathrm{Tr}\left[U_{\mu\nu}^\dagger(x)+U_{\mu\nu}(x)\right]\right). \tag{2.21}$$

In the continuum limit $a\to 0$, the Wilson action reduces to [71]

$$S_W \to \frac{1}{4}\int \mathrm{d}^4x \mathrm{Tr}\left[F_{\mu\nu}F^{\mu\nu}\right] + \mathcal{O}(a^2), \tag{2.22}$$

i.e. the usual pure gauge $SU(N)$ Yang-Mills action with a discretization error of $\mathcal{O}(a^2)$ in this particular case.

An easy attempt of a fermionic action is simply

$$S_F = \sum_q\sum_x \bar{\Psi}_q(x)\left(\not{D}+m_q\right)\Psi_q(x), \tag{2.23}$$

where Ψ are Grassmann vectors and $D_\mu = \frac{1}{2a}(V_\mu - V_\mu^\dagger)$ is a lattice difference operator, with $(V_\mu)_{x,y} = U_\mu(x)\delta_{x+\hat{\mu},y}$, and all the parameters are appropriately rescaled to be dimensionless. It bears stressing that this is a simple approach chosen for illustrative purposes, and this choice of fermionic action faces many problems, including 15 additional poles in the momentum space fermion propagator. This is an obstacle not just for our simple action, but a common problem when defining a lattice theory [72, 73], and there are multiple strategies to getting around it [31, 74, 75]. The current best way to include fermions to a lattice theory is to use something called staggered fermions [76], which we will not introduce here.

Combining these actions – which one should note, are gauge invariant, need no gauge fixing terms and do not rely on a perturbative expansion – one can crank out predictions by doing

Monte Carlo computations of the relevant path integrals, and then take the lattice spacing $a \to 0$ to gain the continuum theory.

Simplifying the notation a bit, the partition function Z can be written as a path integral on the Euclidean lattice

$$Z = \int \mathcal{D}A_\mu \mathcal{D}\bar{\Psi}\mathcal{D}\Psi \exp\left[-\int_0^\beta \mathrm{d}\tau \int \mathrm{d}^3x \mathcal{L}_E\right], \tag{2.24}$$

where β is the inverse temperature and $\mathcal{L}_E$ is the full Euclidean Lagrangian.

Because $\mathcal{L}_{QCD}$ is bilinear in the quark fields, we can perform the path integral over the Grassmann variables analytically, ending up with

$$Z = \int \mathcal{D}A_\mu \det(\not{D} + m_q - \mu\gamma_0) e^{-S_g}, \tag{2.25}$$

where S_g is the gluonic action, and we have already included the chemical potential μ in the Dirac operator.

Now, as performing the infinite-dimensional integral would be too numerically taxing, lattice computations rely on Monte Carlo methods and on the use of importance sampling. When $\mu = 0$, this works out fine, as the Dirac operator is γ_5-Hermitian, and the corresponding determinant is thus real. However, the inclusion of nonzero μ means that the operator is no longer Hermitian, and the corresponding determinant is no longer real-valued. Therefore the determinant can no longer be interpreted as a probability measure for the importance sampling. There is nothing wrong with the partition function itself, but the complex determinant still foils the use of Monte Carlo methods. This is known as the *sign problem*, and a lot of effort has been dedicated to either solving or bypassing it (see for example Refs. [77–88] and references therein), but no method has yet been shown to be reliable in the finite-μ regime of the QCD phase diagram.

It is worth stressing that, although we have honed in on some of issues with the lattice framework here, lattice simulations are the current gold-standard method when strongly coupled systems are concerned, one of the most remarkable feats being the reproduction of the (light) hadron spectrum (see *e.g.* [71, 89–91]). Outside of the $\mu/T \gg 1$ regime, lattice QCD has also proven itself extremely useful in determining the thermodynamics of QCD, as we shall see in in the following section.

2.6 QCD Phase Diagram

Having shortly reviewed some relevant aspects of QCD along with some of the most valuable computational tools, we can try to piece together what is known of the QCD phase diagram. The below discussion is summarized in the (μ_B, T) plane in Fig. 2.3. In the case of magnetars[8], the inclusion of an external magnetic field might be necessary, as strong magnetic fields induce Lorentz symmetry breaking expectation values. For a review on QCD phase diagram with magnetic fields, see *e.g.* Ref. [93].

[8]Magnetars are neutron stars with exceptionally strong magnetic fields, with field strengths up to 10^{15} Gauss [92].

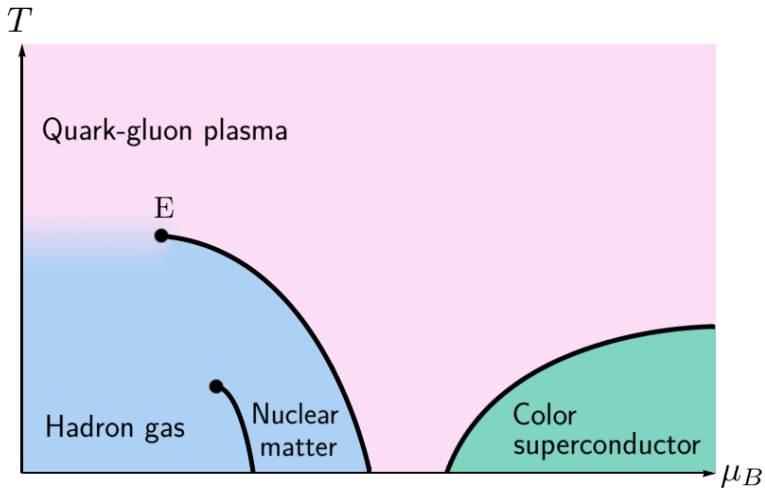

Figure 2.3: A sketch of the conjectured QCD phase diagram in the temperature – baryon chemical potential plane. The lines demarcate first order phase transitions and E denotes the possible critical endpoint to the deconfinement transition line. There are uncertainties related to the transitions marked here: the existence of the first-order deconfinement transition line is debatable, and the location of the transition to the color superconducting phase is unclear.

Even though the phase structure of QCD is now known to be extremely rich, our everyday experience with strongly interacting matter is only at relatively low temperatures and densities compared to the QCD scale Λ_{QCD}. In this low-energy phase, the relevant degrees of freedom needed to explain the thermodynamics of a given system are hadrons and their resonances. In the thermodynamic limit and at low chemical potential, this confined phase can be described as an ideal gas of hadrons embedded in the QCD vacuum. This is possible, because even though the interactions that confine the partons into hadrons are strong, the interhadronic interactions in a dilute enough hadron gas are considerably weaker, even negligible. This model, called Hadron Resonance Gas (HRG) [94, 95] agrees well with lattice Monte Carlo simulations for 2+1 flavors [96], and the agreement will likely still improve with the improvement of hadron resonance data [97].

Let us now follow the vertical axis up to higher temperatures. When analyzing asymptotically high temperatures, asymptotic freedom guarantees that the relevant degrees of freedom are quarks and gluons and we can use perturbative methods. At lower temperatures, gauge coupling becomes strong and we need to rely on lattice simulations, which at $\mu_B = 0$ connect the HRG and perturbative QCD results well [98, 99].

At low densities, this deconfined phase of quarks and gluons is called *quark-gluon plasma* (QGP). This phase is now routinely reproduced in heavy-ion experiments in colliders such as the Relativistic Heavy Ion Collider (RHIC) and the Large Hadron Collider (LHC). These heavy-ion

collisions create environments that are considered to have low net baryon density, as even though the initial state has an excess of quarks over antiquarks, the imbalance is negligible compared to the total number of particles created.

QGP is weakly interacting at asymptotically high temperatures, but at intermediate temperatures heavy-ion experiments have shown that the plasma is strongly coupled [100–105] and is a nearly perfect fluid [105–107] with an extremely low shear viscosity to entropy density ratio η/s [8, 108, 109] and so the dynamics of the (near-)equilibrium plasma can be accurately described by relativistic hydrodynamics [110, 111]. This also acts as an additional proof on the strongly coupled nature of the plasma, as perturbative computations give larger values for η/s [112, 113]. Also, pure gauge lattice simulations reproduce the shear viscosity closely [114], pointing towards the dynamics of QGP being determined to a high degree by gluonic contributions. We will discuss the evolution of heavy-ion collisions in more depth in Chapter 5.

It is worth nothing here that in the deconfined phase, chiral symmetry is also restored [105, 115–117]. The occurrence of the deconfinement transition and chiral restoration do not necessarily have to coincide, but if they do not, the deconfinement transition needs to occur first [118].

The transition between the hadronic and the quark-gluon phase at low baryon densities is known to be a crossover transition [105]. It is up to debate how to define a critical temperature T_c in the case of a crossover transition, and the exact value is dependent on the discretization of the fermionic action, but regardless of the definition used the transition occurs around 160 MeV [46, 119].

In Fig. 2.3, there is a critical point E at (μ_E, T_E) ending the deconfinement transition line, with the transition at $\mu_B > \mu_E$ being of first order. The existence of this point, and therefore also the first order phase transition line, are under intense research. Various effective models [120–128] predict the transition at higher μ_B to be of first order, pointing towards the existence of the critical point.

Current experiments do not show evidence for the existence of a critical point up to $\mu_B \sim 400$ MeV [129]. Also, recent $2+1$ flavor lattice QCD simulations exploring this area, both by using Taylor expansion of the thermodynamic potentials in μ_B/T [46] and the imaginary μ method [119] seem to disfavor the existence of a critical point at least up to $\mu_B \sim 300$ MeV. Some studies [130] suggest that the transition is probably weak at least below $\mu_B \sim 500$ MeV, and for example Dyson-Schwinger [131] and functional renormalization group [132] methods would expect the critical point to exist at around $\mu_E/T_E \approx$ 4-6.

The existence of the endpoint can be studied by future experiments at lower energies than those reached in RHIC and LHC, by studying larger baryon densities. These experiments include the Facility for Antiproton and Ion Research (FAIR) and Nuclotron-based Ion Collider fAcility (NICA). Also, RHIC has already commenced with the second phase of the Beam Energy Scan (BES) program [133], which could in its part help close on some of the questions about the critical point.

If we now consider the high-density part of the phase diagram, the first feature we encounter

at low temperatures is the liquid-gas transition in the hadronic phase between the hadron gas and nuclear matter phases, as the nuclei in the gas are packed closer and closer together until they overlap at around the nuclear saturation density $n_s = 0.16$ fm^{-3}. This transition occurs around $\mu_B \sim 425$ MeV at $T = 0$ MeV and has a second order critical point at about the same chemical potential and $T \sim 10$ MeV [134–136]. We can expect to compute the properties of this phase when the nucleons are weakly coupled with each other using *ab initio* methods such as CET [137–139].

Further right in Fig 2.3 we have a transition from the confined nuclear matter phase to the deconfined phase, which we have discussed above. The difference in this phase (besides the considerably lower temperature) is the quark density and the available degrees of freedom. Although the term "quark matter" is used quite indiscriminately to mean any phase where quarks are the relevant degrees of freedom, from QGP (*e.g.* the Quark Matter conferences) to superconducting phases, in this dissertation the meaning is limited to this low-temperature, quark-rich deconfined phase [140].

Then, lastly, at the high-μ_B end of the diagram, we have the color superconducting phases [124, 125, 141–146]. Here, we have hidden quite a lot of complications resulting from ongoing discussions on the exact structure of the region under the umbrella term of color superconductivity. The quark degrees of freedom can form Cooper pairs in multiple different ways, each resulting in a distinct phase. At extreme μ_B, the Color-Flavor Locked (CFL) phase, in which all three low-mass flavors participate symmetrically in forming Cooper pairs, is preferred [146]. It is also possible, depending on the exact model, that at lower chemical potential another color superconducting phase, such as the two-color superconducting (2SC) phase, in which u and d pair with two colors, is preferred [147, 148].

In the CFL phase, both the color and chiral symmetries are broken due to the locking, resulting in gluons acquiring mass among other exciting phenomena, making the phenomenology of the superconducting phases extremely rich [146, 149]

There are also some arguments to support that as a precursor to condensing in the superconducting phase, quark matter can exhibit various collective behaviors and pseudogaps reminiscent of superconductivity [150–159]. There is also a possibility of a crystalline superconducting phase [160] at sufficiently high densities.

The research presented in this thesis is not aimed towards probing the color superconducting area of the phase diagram, so we will not delve into more detail on it. For a recent review on the subject of color superconductivity, see Refs. [161, 162] and on the applications of holographic methods, see *e.g.* Ref. [163] and references therein.

We are left with an amount of unanswered questions. The next Chapter introduces us to a tool that is hopefully of use in alleviating these troubles.

Chapter 3

Holography

Holography is an umbrella term for a variety of dualities between lower-dimensional quantum field theories and higher-dimensional theories of quantum gravity. Originally, the holographic principle that states this correspondence was proposed in form by 't Hooft and Susskind in 1994 [164, 165], but the first[1] realization of the principle was found in the AdS/CFT duality in 1997 [7]. This conjectured duality states, in its strongest form that there is a correspondence between a type IIB string theory formulated in $\mathrm{AdS}_5 \times S^5$ spacetime, and a $\mathcal{N} = 4$ $SU(N)$ super-Yang-Mills theory living on the four-dimensional boundary of the string theory.

The original motivation behind holographic dualities was to study theories of quantum gravity, but the fact that duality connects a weakly coupled limit of the quantum gravity – *i.e.* classical gravity – to a strong coupled quantum field theory has opened up intriguing possibilities of application in the study of strongly coupled theories such as QCD. Because of this, holography has become one of the most actively studied topics in high-energy physics.

To familiarize the reader with the building of holographic dualities, we will begin this chapter by giving a brief review of the basics on anti-de Sitter spaces before introducing the original AdS/CFT duality. This chapter relies heavily on different limits of type IIB string theory that are not elaborated here in any detail, and the reader is referred to *e.g.* Refs [167–169] for a pedagogical introduction to string theory and holography. We will then expand upon the idea by looking into model-building within the holographic framework, with an eye on strongly coupled QCD.

3.1 A Primer on Anti-de Sitter Spacetimes

Anti-de Sitter (AdS) spacetimes (or at least spacetimes asymptotically so) are central to many parts of the following discussion, so it is necessary to expound upon some of the basic properties of AdS spaces.

[1] One could argue that Ref. [166] in 1986 was the first realization, as they found that a three-dimensional AdS spacetime has the same asymptotic symmetry group as a two-dimensional CFT, but this was done before the idea of holographic duality.

AdS_d spacetime is one of the three maximally symmetric[2] vacuum solutions to the Einstein-Hilbert action in d dimensions

$$S_{\mathrm{EH}} = \frac{1}{16\pi G_d}\int \mathrm{d}^d x\, \sqrt{|\det g|}(R - 2\Lambda)\,, \tag{3.1}$$

where G_d is Newton's gravitational constant in d dimensions, g is the metric, R is the Ricci scalar and Λ is the cosmological constant. With our choice of sign, the AdS solution corresponds to a negative cosmological constant, whereas de Sitter spaces result from a positive cosmological constant and Minkowski spaces from $\Lambda = 0$.

The Einstein field equations for action (3.1) are

$$R_{\mu\nu} - \frac{1}{2}g_{\mu\nu}R + \Lambda g_{\mu\nu} = 0\,, \tag{3.2}$$

the solutions of which, for $\Lambda < 0$ are of constant, negative curvature. Thus the AdS spaces can be considered the non-Euclidean counterpart of hyperbolic spaces. The solutions for Eq. (3.2) read

$$R_{\mu\nu} = \frac{2}{d-2}\Lambda g_{\mu\nu}\,, \quad R = \frac{2d}{d-2}\Lambda\,. \tag{3.3}$$

There are multiple useful ways to write the embedding of AdS_d in $\mathbb{R}^{2,d-1}$. One of the more illuminating ones is

$$-X_{-1}^2 - X_0^2 + X_1^2 + \cdots + X_{d-1}^2 = -\mathcal{L}^2\,, \tag{3.4}$$

with the metric signature $\mathrm{diag}(-1,-1,1,\ldots,1)$ and $\mathcal{L}$ is the AdS radius. In this formulation, the global $\mathrm{SO}(2,d-1)$ symmetry of the AdS space is manifest. From this one can already suspect why it is precisely AdS spaces that we are interested in when constructing dual theories. But we are getting ahead of ourselves.

We can now relate the cosmological constant to the AdS radius $\mathcal{L}$ by

$$\Lambda = -\frac{(d-1)(d-2)}{2\mathcal{L}^2}\,. \tag{3.5}$$

One of the most useful formulations of the metric is the Poincaré coordinate patch metric

$$\mathrm{d}s^2 = \frac{\mathcal{L}^2}{r^2}(\,\mathrm{d}r^2 + \eta_{\mu\nu}\,\mathrm{d}x^\mu\,\mathrm{d}x^\nu)\,, \tag{3.6}$$

where η is the $d-1$-dimensional Minkowski metric. From Eq. (3.6) it is straightforward to see that in the limit $r \to 0$ the metric is conformally equivalent to the Minkowski spacetime metric in $d-1$ dimensions. The coordinate patch in this case only covers a half-space, namely $r > 0$. The metric can be arrived at from the global coordinates in Eq. (3.4) by

$$X_{-1} = \frac{r}{2}\left(1 + \frac{\eta_{\mu\nu}x^\mu x^\nu + \mathcal{L}^2}{r^2}\right), \tag{3.7}$$

$$X_\mu = \frac{\mathcal{L}}{r}x_\mu, \tag{3.8}$$

$$X_{d-1} = \frac{r}{2}\left(1 + \frac{\eta_{\mu\nu}x^\mu x^\nu - \mathcal{L}^2}{r^2}\right), \tag{3.9}$$

where $\mu = 0, 1, \ldots, d-2$.

[2]That is, it has $\frac{d(d+1)}{2}$ Killing vectors and corresponding isometries.

3.2 A Sketch of an Argument for AdS/CFT Duality

The methods applied in this thesis rely on argumentation that is based on – or at least enlightened by – the original AdS/CFT duality [7]. To familiarize the uninitiated reader with the holographic jargon, it seems necessary to introduce the basic argument for holographic duality in wide brush strokes, mainly following Ref. [169].

Type IIB string theory is formulated with a 10-dimensional spacetime, and in addition to strings, it supports the existence of extended, dynamical, nonperturbative, p-dimensional objects called Dp-branes. The excitations of these branes are open strings, whereas closed strings can be considered excitations of the bulk spacetime. Each of the open strings attach to a brane by Dirichlet boundary conditions (thus the name "Dp-brane"). From the point of view of the branes, the endpoints of the open strings appear as point-like particles carrying $SU(N)$ charges, associated with a gauge group generated by a stack of N coincident branes[3].

To find the correspondence, let us consider the type IIB theory with a stack of N parallel, coincident $D3$-branes embedded in ten dimensions. There are now two equally correct ways to find the low-energy limit of this theory.

First, we can examine the open and closed string spectra separately. In the low-energy limit, we can write the complete action as $S = S_{\text{open}} + S_{\text{closed}} + S_{\text{int}}$, where the last term corresponds to interactions between the two sectors. It turns out that in the low-energy limit the interaction term S_{int} goes to zero [169] and the two sectors become decoupled. The dynamics of the particles on the branes is described by a Dirac-Born-Infeld (DBI) action [170, 171], which is a nonlinear generalization of the familiar Yang-Mills action, to which the DBI action also reduces to in the appropriate low-energy limit. Correspondingly, the low-energy theory of the open string sector on the four-dimensional $D3$-brane world-volume is the $\mathcal{N} = 4$ supersymmetric Yang-Mills theory, which is a highly symmetric conformal field theory (CFT). The low-energy theory of the closed string sector is a type IIB supergravity[4] in ten-dimensional Minkowski spacetime.

Second, we can simply regard the whole theory *in toto*, and examine its low-energy limit. We end up directly with the type IIB supergravity in ten dimensions, but with $D3$-branes embedded in the spacetime. Far from the stack of branes, the metric becomes ten-dimensional Minkowski, and there the theory is again a type IIB supergravity in Minkowski space. However, when observing the metric near the branes, it becomes that of $\text{AdS}_5 \times S^5$ [7] with a stack of branes at the boundary. At low energies, these two regions become decoupled. This can be seen by considering what kinds of excitations a distant observer can see in the low-energy limit: one immediately clear case are the massless excitations propagating in the ten-dimensional Minkowski, but which do not see the the branes due to their wavelength being much larger than the size of

[3]Each brane contributes U(1), but for a coincident stack, the symmetry is enhanced to U(N), and all string modes become massless. The symmetry can be however written as $SU(N)$, as there is a dynamically superfluous prefactor of U(1) corresponding to the location of the branes in the bulk.

[4]For our purposes, it is enough to know that in the low-energy limit, supergravity solutions satisfy the Einstein equations. Supergravity can be arrived to from two distinct but commensurate directions: either as gauged local supersymmetry, or as a supersymmetric theory of gravity. One can read more on the subject in Refs. [167, 172].

the brane [173]. The other possible excitations in the low-energy limit are actually arbitrarily energetic modes near the horizon. This is because for an observer placed at the asymptotic infinity, the measured energy E_∞ is related to the energy emitted at r by a redshift factor f, such that $E_\infty = f^{-1/4}E_r$. In the Maldacena limit, where the string length $\ell_s \to 0$ while keeping $\frac{r}{\ell_s^2}$ fixed, $E_\infty \sim (E_r\ell_s)\frac{r}{\ell_s^2}$ [169], and hence the high-energy modes near $r = 0$ are seen as low-energy modes by a distant observer, as the excitations close to the branes find it hard to climb from the gravitational well and into the asymptotic region. It follows that in the low-energy limit the two regions cannot interact. Thus, in this view, the low-energy limit of the full string theory can be described by a type IIB supergravity in ten-dimensional Minkowski spacetime plus a decoupled type IIB supergravity in $\mathrm{AdS}_5 \times S^5$.

With some caveats, for these two views on the low-energy limit to be equivalent, the resulting theories must be the same. As both of them include two decoupled theories, one of which is a type IIB supergravity in ten-dimensional Minkowski space in both of the descriptions, this leads us to conclude that $\mathcal{N} = 4$ $SU(N)$ super Yang-Mills in the four dimensions of the brane world-volume must correspond to a type IIB supergravity in $\mathrm{AdS}_5 \times S^5$ with the brane system at the boundary. This is an extremely powerful and surprising statement, as it equates a quantum field theory with a higher-dimensional classical theory of gravity.

The precise conjectured correspondence can be summed up in the equation that also defines the holographic dictionary, which tells us how different boundary operators are related to different fields in the bulk [174]

$$\left\langle \exp \int \phi_0 \mathcal{O} \right\rangle_{\mathrm{CFT}} = \mathcal{Z}_{\mathrm{AdS}}[\phi_0]\,, \tag{3.10}$$

where, in the CFT side, ϕ_0 acts as the source of the operator $\mathcal{O}$. On the AdS side, $\mathcal{Z}$ is the partition function and the field $\phi_0 \equiv \phi_0(x)$ is defined by $\phi_0(x) = \lim_{r\to 0} r^{\Delta-4}\Phi(x, r)$, where Φ is the bulk field, r is the bulk coordinate and Δ is the scaling dimension[5] of operator $\mathcal{O}$. For future reference, the correspondence between different fields and operators can be expressed schematically as

Bulk		Boundary
Φ	$\longleftrightarrow$	$\mathcal{O}$
A_μ	$\longleftrightarrow$	J_μ
$g_{\mu\nu}$	$\longleftrightarrow$	$T_{\mu\nu}$

The bulk scalar field Φ couples to the boundary scalar operator $\mathcal{O}$, the bulk vector A_μ is connected to the conserved boundary current J_μ and the metric $g_{\mu\nu}$ is coupled to the stress-energy tensor $T_{\mu\nu}$. The exact correspondence is tied to the definition of the on-shell supergravity action and the renormalization procedure, and it is discussed in detail in Ref. [175].

[5]For a coordinate transformation $x \to \lambda x$, $\phi_0(x) \to \lambda^{-\Delta}\phi_0(x)$.

We can immediately perform a nontrivial check on the duality by comparing the global symmetries of the theories. In the AdS side we have the aforementioned $\mathrm{SO}(2,4)$, combined with an $\mathrm{SO}(6)$ from the S^5. We also have 16 Poincaré supersymmetries and 16 superconformal supersymmetries, all in total giving the supergravity theory the symmetry group $\mathrm{PSU}(2,4|6)$ [176]. This matches the global symmetry group of the $\mathcal{N}=4$ super Yang-Mills, with the spacetime symmetries of $\mathrm{AdS}_5 \times S^5$ corresponding to the bosonic subgroup of the whole supergroup. There are additional tests, such as computing free field propagators protected by the symmetries from quantum corrections that also support the duality [173, 177].

We would go amiss if we would not immediately temper the statement (3.10) with the caveats only referred to above. Whilst taking the different decoupling limits, we have implicitly assumed that the string coupling g_s and N satisfy $\lambda \equiv 4\pi g_s N \gg 1$. This parameter λ can actually be identified with the 't Hooft coupling $\lambda = g_{\mathrm{YM}}^2 N$, to which the AdS radius $\mathcal{L}$ and the string length ℓ_s are related to by $(\mathcal{L}/\ell_s)^4 = \lambda$.

The classical supergravity limit $\lambda \to \infty$, $N \to \infty$, $g_s \to 0$ implies another alluring aspect of the duality: it connects a notoriously difficult strongly coupled quantum field theory to a classical, weakly coupled theory of gravity, which are remarkably simpler to solve.

The stronger form of Maldacena's conjecture states that the correspondence holds for any λ, as long as $g_s \to 0$, or equivalently $N \to \infty$ [7]. This limit corresponds to a classical string theory in the AdS side. What is intriguing about this limit is that fixing λ while taking $N \to \infty$ coincides with the 't Hooft limit in the Yang-Mills theory [27], making for considerable simplifications in computing diagrams in the field theory.

The strongest form of the conjecture posits that the equivalence holds for any N and λ, and is thus a duality between type IIB string theory in $\mathrm{AdS}_5 \times S^5$ and $\mathcal{N}=4$ $SU(N)$ super Yang-Mills in four-dimensional Minkowski spacetime. Above we have focused mostly on the weakest form of the duality, as it is sufficient for most of the practical contents of this thesis.

We have glossed over some extremely complicated issues here, but the main takeout one should have from this is that we are fairly certain that certain highly symmetric quantum field theories are dual to higher-dimensional gravity theories. The conjecture is by no means proven exactly correct yet, but the non-trivial tests that the duality passes make it as good as true for the purposes of model-building.

3.3 Holographic Thermodynamics

Before we delve into modeling, we should discuss thermodynamics. The conjectured equality (3.10) points us towards a fantastic statement: the partition functions of the two theories are the same, and thus there exists a one-to-one correspondence between the thermodynamic quantities between the bulk and the boundary once we generalize the duality to finite temperatures [178].

We can implement thermodynamics in the gravity theory by introducing a black hole, which are solutions to Einstein equations and have a temperature associated with them, into our

background. The correspondence stays intact as long as the studied Einstein manifolds in the bulk theory have the correct asymptotic behavior at the boundary [174, 178, 179]. This leaves the UV behavior unaffected, but allows us to modify the IR physics.

Given a generic AdS-Schwarzschild Ansatz

$$\mathrm{d}s^2 = \frac{\mathcal{L}^2}{r^2}(-f(r)\,\mathrm{d}t^2 + f(r)^{-1}\,\mathrm{d}r^2 + \mathrm{d}\mathbf{x}^2)\,, \tag{3.11}$$

where we have placed a Schwarzschild black hole with a horizon located at $r = r_h$ in the bulk, with f being a regular function with the near-horizon boundary condition $\lim_{r\to r_h} f(r) = 0$, we can write the metric with a Wick rotation to Euclidean time $\tau = it$ [180, 181]. In order to avoid a conical singularity in the radial coordinate, the Euclidian time must be 2π-periodic, and by identifying the period with inverse temperature [182], we get the Hawking temperature

$$T_H = \frac{|f'(r_h)|}{4\pi}\,. \tag{3.12}$$

We can use black hole thermodynamics even further. The Bekenstein-Hawking formula, which relates the entropy S and the area of the black hole A by $S_{\mathrm{BH}} = \frac{A}{4G_D}$ [183, 184], where G_D is the D-dimensional Newton's constant, determines the entropy of the bulk. However, as the black hole is actually extended in the $\mathbf{x}$-directions, the total entropy turns out infinite, and a more helpful, finite quantity is the entropy density $s = S_{BH}/V_3$, where V_3 is the volume of the brane in the extended directions.

For metric (3.11), taking $f(r) = 1 - r_h^4/r^4$, the entropy density is [169]

$$s = \frac{A}{4G_5V_3} = \frac{\pi^2}{2}N^2T_H^3\,, \tag{3.13}$$

which is concurrently somewhat surprising and altogether expected: our construction here depends on the limit $N, \lambda \to \infty$, but the expression (3.13) only differs from the result for the free $\mathcal{N} = 4$ $SU(N)$ super Yang-Mills by a factor of $3/4$ [185], and at the same time it agrees with the blackbody scaling law $S \sim VT^3$.

It is relieving to note that one can arrive at exactly the same expression for entropy by using the saddle point approximation [176]

$$Z \approx e^{-S_{\mathrm{E}}}\,, \tag{3.14}$$

$$F = -T\ln Z = TS_{\mathrm{E}}\,, \tag{3.15}$$

$$S = -\left(\frac{\partial F}{\partial T}\right)_V\,, \tag{3.16}$$

where Z is the partition function, S_{E} is the Euclidean supergravity action, and F is the Helmholtz free energy.

To include chemical potential among the thermodynamic quantities, we need to expand our considerations by considering charged solutions, such as AdS-Reissner-Nordström black holes. Why this is so is less obvious than the previous correspondences, and we need to consult our holographic dictionary.

We argued above that the global boundary current J^μ is sourced by the local[6] field A^μ. The standard way to include this sourcing of the current in the action is by the coupling term

$$\int \mathrm{d}^d x \; A_\mu J^\mu \,. \tag{3.17}$$

We should note now that for *e.g.* the conserved global $\mathrm{U}(1)_B$ symmetry in QCD, the associated conserved current is $J^\mu \sim \bar{\psi}\gamma^\mu\psi$. This leads us to realize that near the boundary [186–189]

$$A_0 \simeq \mu + nr^{-2} + \ldots, \tag{3.18}$$

where μ is the chemical potential and n is the associated number density. Therefore, the chemical potential can be included in the description of thermodynamics by turning on the temporal component of the bulk gauge field. There is no clear interpretation for the r-component of the gauge field, so it is better left turned off.

3.4 Building Models: Bottom-Up and Top-Down

The AdS/CFT duality is truly an awe-inspiring contraption. However, as it stands in the formulation above, it is of limited use in studying QCD. The $\mathcal{N} = 4$ super Yang-Mills theory is not confining, exhibits a continuous spectrum, has all the matter in the adjoint representation, has no running coupling and no chiral condensate, is considered at large N_c, and is maximally supersymmetric [190]. Multiple other dualities have been found [191, 192], but the field theory is usually supersymmetric and conformal.

Unfortunately, there is no algorithm to obtain a holographic dual for a given field theory[7]. If we are interested in obtaining a holographic dual to QCD, which is only asymptotically conformal and not at all supersymmetric, we have a choice between two approaches: *top-down* and *bottom-up*.

Before delving into modeling, we might want to address an obvious question: why do we even think QCD has a holographic dual? Which theories have? Unfortunately, there are no all-encompassing criteria yet. It is known that for a conformal gauge theory to have a semi-classical bulk counterpart, the bulk geometry must be encoded in the induced spacetime on the boundary [194]. QCD has many things going for it: we know that the theory is asymptotically conformal and has a well-established large-N_c expansion [27, 190, 195]. Considering the relative closeness of QCD and SYM it is tentatively believable that there might exist a reasonably QCD-like theory with a gravitational dual.

Top-down approaches start from a known duality and generalize it minimally to obtain a more realistic field theory dual. The constructions might include nontrivial brane configurations and

[6] As global symmetries in gravity theories are restricted, global symmetries in the boundary theory correspond to local isometries in the bulk.

[7] As I am writing this, an extremely interesting prerprint [193], which might prove to open new pathways to building bulk theories in the future, was uploaded to arXiv.

geometrical engineering, and they generally rely on a strong version of the conjectured duality. This way of constructing a duality is more or less rigorous, but often quite complicated and technically challenging. The constructions have gotten more and more realistic, as implementing more generic background manifolds [196, 197], and background deformations [198] have allowed for the boundary theory to be non-conformal and confining with chirally broken matter. Non-supersymmetric, non-conformal theories have also been achieved in Refs. [199–201]. Fundamental matter has also been implemented in the quenched approximation by embedding a probe D7-brane into the bulk [202], and also studied in the unquenched limit in *e.g.* Refs. [203–205] and generalized to finite temperatures in Refs. [206, 207] (for a review, see Ref. [208]).

As impressive as the current state of the top-down constructions is, with the most QCD-like models currently available being the Witten-Sakai-Sugimoto (WSS) model [202, 209–211] based on a $D4-D8-\overline{D8}$ brane configuration in type IIA string theory, and the $D3-D7$ models [204, 212, 213], they are still not QCD, and have limited applicability beyond the low-energy regime [214, 215].

Even if the top-down models are not exactly QCD, they still provide a way to make qualitative predictions about strongly coupled phenomena, especially at finite temperature[8]. Such feats as predicting properties such as jet quenching and the shear viscosity of strongly interacting plasma [8, 216–219] and the hydrodynamization of the fireball ensuing from heavy-ion collisions [220–223] have given a lot of credibility for holographic constructions as a promising line of inquiry into QCD matter.

Looking for the correct bulk dual, one might want to partake in some more phenomenologically-minded activities to obtain qualitative predictions by holographic methods, while also probing the applicability of said methods. This is the aim of bottom-up approaches. They involve generalizing the AdS/CFT conjecture maximally by claiming that any classical gravity theory that can be completed into a theory of quantum gravity is dual to a quantum field theory living on the boundary. Taking the bottom-up approach one does not always strictly know the bulk string theory, but starts from the wanted field theory and emulates it in the bulk by adding elements from string theory. This makes of course for an uncontrolled approximation and a more effective approach than the top-down constructions, but as the Russian proverb goes, "кто не рискует, тот не пьёт шампанское"[9].

Even with the more relaxed qualifications, building a viable gravity model is not straightforward. One still needs to consider how to build a consistent gravity model with the fields that correspond to the boundary operators one wants to study as the dictionary only fixes the boundary asymptotics of the fields. The IR behavior needs to be fixed by other information one has available. When one has fixed all the parameters, fields and functions one can from the *a priori* constraints, the rest are fitted by computing observables from the model and comparing them to observations, experiments, perturbation theory or lattice data.

[8] Introducing finite temperature breaks both the supersymmetry (due to bosons and fermions having different statistics) and the conformal invariance (due to the introduction of an energy scale).

[9] Tr. "Who takes no risk, drinks no champagne."

The clear downside of this procedure is that one has no other guarantee of the validity of the duality than success in reproducing known results. Even if the bulk theory could be traced to a theory of quantum gravity – justifying the duality between the bulk and the boundary – one cannot usually in practice even write down the boundary action.

Of the bottom-up models for QCD, the hard- and soft-wall AdS/QCD models, as constructed in Refs. [224–227], should be mentioned here. They are founded on a simple Einstein-dilaton action, with linear confinement and chiral symmetry breaking being imposed by boundary conditions at the IR boundary. They have been somewhat successful, especially in reproducing of meson spectrum and dynamics [228–231]. However the thermodynamics of the models have not been extensively studied.

The above taxonomy of dividing models into being either top-down or bottom-up is not as clear-cut as it might appear, as some approaches classified as being bottom-up base their structures somewhat rigidly in well-studied top-down constructs, but implement some effective potentials that can be used to fit the model to data. The V-QCD models that form the crux of this thesis belong among this class. This is done in an effort to be malleable enough to model QCD better than usual top-down approaches do, while being more rigorous in the construction than bottom-up models to ensure a solid basis. To achieve this, the model takes cues from top-down constructions, with the main difference being the ignorance about the correct brane action in curved spacetime. This ignorance is encoded in the effective potentials within the action, which are used to fit the model to qualitative and quantitative QCD behavior, as we will see in the following chapter.

Chapter 4

Holographic QCD in the Veneziano limit

Veneziano-QCD (V-QCD) is a family of models based on two building blocks: a holographic, bottom-up dilaton-gravity model for pure Yang-Mills theory called Improved-Holographic QCD (IHQCD), and a flavor brane sector, which are fully backreacted with each other in the Veneziano limit. The construction of the action is motivated by noncritical string theory, but it is generalized to contain nontrivial potentials, which can be matched to QCD results both qualitatively – *e.g.* by requiring the model to be confining in the IR – and quantitatively where reliable lattice results are available. In this way, one can hopefully retain some rigor in defining the holographic dictionary, but still have enough leeway compared to the top-down approaches to allow for a more realistic, QCD-like boundary theory.

In this Chapter, we will review this model, whose applications form the main body of this thesis. In articles **I** and **III**, we used the full V-QCD machinery in concert with nuclear physics models to produce equations of state at $T \sim 0$ to both gain insight to the physics of neutron stars and also to apply astrophysical constraints to the parameter space of V-QCD. In article **II**, we continued the line of work started in *e.g.* Refs. [232–235] by including the logarithmic corrections in the effective potential of IHQCD, and computing the quasinormal modes for tensor fluctuations in order to study aspects related to thermalization in heavy-ion collisions.

We will – for the sake of conciseness and the coherence of the thesis – discuss the totality of V-QCD as also including IHQCD, which V-QCD can be seen as an extension of. This point of view will slightly affect the way we define the potential Ansatz we use, as we will see when discussing the setup of article **II** in Section 5.2.1, where we do not consider flavor physics.

We begin in Section 4.1 by introducing and motivating the building blocks that make up V-QCD. In Section 4.2 we will then show how the effective potentials and parameters are matched to existing QCD results both in the UV and IR. We will end the chapter with Section 4.3, where we will review the thermodynamic properties and the phase structure of the model.

4.1 Building Blocks of the Model

V-QCD models are constructed from two basic building blocks: the glue and the flavor sector. The dynamics of gluons is described by IHQCD, a bottom-up holographic 5D Einstein-dilaton model for pure Yang-Mills theory [236–241]. The flavor sector is introduced through a tachyonic Sen-like Dirac-Born-Infeld (DBI) action, together with the associated Wess-Zumino (WZ) term, which describe dynamical quarks [202, 242–250]. These sectors are fully backreacted [251] in the Veneziano limit [252]

$$N_c \to \infty \quad \text{and} \quad N_f \to \infty\,, \quad \text{with} \quad x_f = \frac{N_f}{N_c} \quad \text{and} \quad g^2 N_c \quad \text{fixed}\,. \tag{4.1}$$

Most of the literature has been focused on the 't Hooft probe limit, but to accurately reproduce the dynamics of most strongly coupled systems where you have two to three flavors and three colors, it is truly important to study the backreaction of the flavor and color sectors.

The action of V-QCD can be schematically written as

$$S = S_g + S_f + S_a\,, \tag{4.2}$$

where S_g describes the gluon sector, S_f the flavor sector. We have delegated the CP-odd terms to S_a, which will not be relevant for our interests, as we are only concerned with manifest CP symmetry. The CP-odd effects in V-QCD have been studied in *e.g.* Ref. [253].

4.1.1 Improved Holographic QCD

Let us begin by sketching a motivation for the way IHQCD [236, 237, 240, 241] is built. First, we need to address the question: why noncritical string theory in five dimensions? With large-N theories, each independent adjoint field typically corresponds to one extra dimension in the bulk theory. QCD has four fields transforming in the adjoint representation, with only one of them being independent in flat, Lorentz-invariant background [254]. Thus we could reasonably expect the dual theory for QCD to be five-dimensional. This way, one can also dodge the problem of extraneous massive Kaluza-Klein modes that often plague higher-dimensional formulations [254].

Starting from the assumption we are working in a five-dimensional context, and aim to produce a boundary theory that is conformally symmetric in the extreme UV, we can already specify the metric Ansatz we will be using

$$\mathrm{d}s^2 = e^{2A(r)}(\,\mathrm{d}r^2 + \eta_{\mu\nu}\,\mathrm{d}x^\mu\,\mathrm{d}x^\nu), \tag{4.3}$$

where η is the conventional four-dimensional Minkowski metric and r is the holographic dimension. The conformal scale factor $e^{A(r)}$ goes asymptotically to $e^{A(r)} \sim \frac{\ell}{r}$ in the UV regime $r \to 0$, where ℓ corresponds to the radius of the AdS_5. Thus, the metric is asymptotically AdS_5, suggesting that the dual field theory, just like QCD, is asymptotically conformal in the UV. This, together with the monotonous behavior of $A(r)$ and arguments from gravitational red-shift [199, 236],

leads us to identify this factor with the boundary theory renormalization scale E in the UV regime by the relation $\ln(E) \propto A$.

Assuming we have a stack of coincident $D3$ branes in the bulk, which are responsible for the metric (4.3), we can start specifying the field content in the bulk. Pure Yang-Mills theory has no gauge-invariant space-time fermions, and thus the dual theory should not have NSR or RNS sectors. In the NSNS sector, the lowest-lying fields are[1] the metric $g_{\mu\nu}$, which is dual to the traceless stress tensor $T_{\mu\nu}$ in the Yang-Mills theory; the dilaton ϕ, which is dual to $\mathrm{Tr}\left[F^2\right]$; and the antisymmetric tensor $B_{\mu\nu}$, which is trivial in the vacuum [236].

The RR sector contains three independent fields that can be identified as the axion a, dual to $\mathrm{Tr}\left[F \wedge F\right]$; dC_4, which seeds the $D3$ branes; and dC_1, which couples minimally to baryon density on flavor branes [244]. The axion sources the θ-angle, and as we are only considering backgrounds with manifest CP symmetry here, we will neglect the a terms in the following discussion. In this section, we are only considering backgrounds without flavor, so we need not consider the RR-sector for now. These terms will become relevant once we have specified a flavor sector in the next section, and they will be incorporated into the V-QCD action there.

Before we go any further, let us define $\lambda \equiv N_c e^{\phi}$, which will be used here to define the action. We will further identify λ with the 't Hooft coupling near the boundary, as is conventional in an AdS/CFT duality with a dilaton.

Having laid out the lowest-lying bulk fields relevant for constructing the gluonic model, we can write the action in the Einstein frame as

$$S_g = M_P^3 N_c^2 \int \mathrm{d}^5x \, \sqrt{-g} \left[R - \frac{4}{3} \frac{(\partial\lambda)^2}{\lambda^2} + V_g(\lambda) \right] , \tag{4.4}$$

where the effective potential V_g is the ingredient that realizes our construction as a bottom-up model. Even though to some extent the potential can be seen as a term that has absorbed the higher-curvature contributions and non-dynamical fields that have been integrated out. [236, 254], we will here treat it as an arbitrary function that will be used to fit the model to the boundary theory in Section 4.2.1.

In Eq. (4.4), we have implied the Gibbons-Hawking boundary term [255], which can be written as [237]

$$S_{GH} = 2M_P^3 N_c^2 \int_{\partial M} \mathrm{d}^4x \, \sqrt{h} K \, , \tag{4.5}$$

where K is the extrinsic curvature and h the induced metric at the boundary ∂M.

4.1.2 Flavor Action

Adding flavor into a holographic model can and has been done in multiple different ways in top-down approaches depending on the exact details of the model in question, but from the dual string theory perspective, it necessitates adding a corresponding open string sector, and thus

[1]The higher-dimensional operators are analyzed in Ref. [236]. Here we will only work in the two-derivative level.

also D-branes – called flavor branes in this context – to the closed string background to carry flavor indices [202].

In our case, adding flavor and implementing dynamical chiral symmetry breaking is achieved by N_f pairs of coincident space-filling $D4$–$\overline{D4}$ branes [243, 244]. In this configuration, the lowest modes on open strings that are dual to dimension-3 operators on the boundary are the spin-0 bifundamental tachyon T_{ij} and the spin-1 gauge fields $A^\mu_{(L)i}$ and $A^\mu_{(R)i}$ (where we have marked the chiral label in parentheses), all of which are $N_f \times N_f$ matrices in the flavor space. The tachyon propagates between the $D4$ and $\overline{D4}$ branes and it is dual to the quark bilinear operator $\bar{q}_{(R)i}q_{(L)j}$, and the gauge fields arise from open strings with both endpoints on the same brane, which are the $D4$ and $\overline{D4}$ respectively, and are dual to the corresponding classically conserved currents $J^\mu_{(L/R)ij} = \bar{q}_{(L/R)i}\gamma^\mu q_{(L/R)j}$ [237, 243, 244, 247, 251].

The action that arises from this brane configuration can be written as

$$S_f = S_{DBI} + S_{WZ}\,, \tag{4.6}$$

where the dynamics are described by a Sen-like [256] DBI action

$$S_{DBI} = -\frac{1}{2}M_P^3 N_c\ \mathrm{Tr}\int \mathrm{d}^5x\ \left(V_f(\lambda, T^\dagger T)\sqrt{-\det \mathbf{A}^{(L)}} + V_f(\lambda, TT^\dagger)\sqrt{-\det \mathbf{A}^{(R)}}\right)\,, \tag{4.7}$$

where the trace Tr is taken over the flavor indices, and the determinant over the spacetime indices, V_f is the tachyon potential and

$$\mathbf{A}^{(L)}_{MN} = g_{MN} + w(\lambda,T)F^{(L)}_{MN} + \frac{\kappa(\lambda,T)}{2}\left[(D_MT)^\dagger(D_NT) + (D_NT)^\dagger(D_MT)\right]\,, \tag{4.8}$$

$$\mathbf{A}^{(R)}_{MN} = g_{MN} + w(\lambda,T)F^{(R)}_{MN} + \frac{\kappa(\lambda,T)}{2}\left[(D_MT)(D_NT)^\dagger + (D_NT)(D_MT)^\dagger\right]\,. \tag{4.9}$$

The field strengths $F^{(L/R)}$ and the covariant derivative D are defined as

$$F^{(L/R)} = dA_{(L/R)} - iA_{(L/R)}\wedge A_{(L/R)}\,, \tag{4.10}$$

$$D_M = \partial_M T + iTA^{(L)}_M - iA^{(R)}_M T\,. \tag{4.11}$$

The Wess-Zumino (WZ) term in (4.6) describes the coupling of the flavor branes to the background RR fields, and can be written as [244]

$$S_{WZ} = T_4\int_{M_5} C\wedge \mathrm{sTr}\,\exp\left[i2\pi\alpha'\mathcal{F}\right]\,, \tag{4.12}$$

where M_5 is the world-volume of the $D4$–$\overline{D4}$ branes, $T_4 \sim N_c$ is the $D4$-brane tension, sTr stands for supertrace, $C = \sum_n (-i)^{\frac{5-n}{2}}C_n$ is the sum of the RR potentials C_n, and $\mathcal{F}$ is the curvature of the superconnection $\mathcal{A}$, which can be expressed as [244, 257]

$$i\mathcal{A} = \begin{pmatrix} iA_{(L)} & T^\dagger \\ T & iA_{(R)}\end{pmatrix}, \tag{4.13}$$

so that $\mathcal{F} = \mathrm{d}\mathcal{A} - i\mathcal{A}\wedge\mathcal{A}$. The supertrace for a $2N_f \times 2N_f$ block matrix $M = \begin{pmatrix} A & B \\ C & D \end{pmatrix}$, where A, B, C, D are $N_f \times N_f$ matrices, is

$$\mathrm{sTr}\, M = \mathrm{Tr}A - \mathrm{Tr}B\,. \tag{4.14}$$

Setting $2\pi\alpha' = 1$, we can expand the action (4.12) as [244]

$$S_{WZ} = T_4 \int C_5 \wedge Z_0 + C_3 \wedge Z_2 + C_1 \wedge Z_4 + C_{-1} \wedge Z_6\,, \tag{4.15}$$

where the various Z_n are the forms coming from the expansion of the exponential of the superconnection. Of these, $Z_0 = 0$, to ensure gauge anomaly cancellation at the boundary [244]. The Z_2 term provides the mixing between the η' meson and the axion, connecting the term to the $U(1)_A$ axial anomaly[2] [244, 251]. The precise dual operator of C_1 is not known, but it is expected to source the topological baryon current at the boundary [251]. The final term is the one most interesting for the purposes of this thesis, as it automatically provides us with a Chern-Simons term; by writing $Z_6 = \mathrm{d}\Omega_5$, it can be written as

$$\int C_{-1} \wedge \mathrm{d}\Omega_5 = \int F_0 \wedge \Omega_5\,, \tag{4.16}$$

where $F_0 = \mathrm{d}C_{-1}$, is the zero-form field strength, which couples to bulk instantons. We will discuss the applications of this term in more detail below, when we introduce the role of instantons more properly.

Before we can use the expression (4.7), we need to address some issues. Firstly, this is not the full flavor action, which is as yet unknown [262, 263]. In the full picture, the trace would be more properly written as a symmetric trace, the exact definition of which in the case of non-Abelian fields is somewhat unclear. Here, as we are only considering the first nontrivial term in the DBI expansion for the non-Abelian fields, a normal trace suffices. Also, we have very few string theory guidelines to go by when trying to guess the correct potentials.

We can make some simplifying assumptions that ensure that the ambiguities of non-Abelianity do not enter the quadratic terms, and work the DBI action to a more usable form. First, we can choose to suppress the flavor structure for now, and fix the complex tachyon $T = \tau\mathbb{I}_{N_f}$, where $\tau \in \mathbb{R}$, which is dual to the quark bilinear $\bar{q}q$. This choice, besides making the terms flavor-independent, also suppresses the chirality of the terms, as now $T^\dagger = T$. The quark masses are, naturally, now fixed to be equal. Furthermore, we will not be considering massive quarks in this thesis. For an analysis on massive flavors, see Ref. [264].

We will also choose the tachyon dependence of the potential V_f to be $V_f(\tau) = e^{-a\tau^2}$, which matches what is seen to work in the probe limit [245, 246].The full tachyon potential can be now expressed as

$$V_f(\lambda, \tau) = V_{f0}(\lambda)e^{-\tau^2}, \tag{4.17}$$

[2]The connection between the η' meson and axial anomaly is discussed in *e.g.* Refs. [258–261].

where the dilaton dependence is delegated to the function V_{f0}, and the constant a is absorbed into the tachyon normalization. This form is also motivated by the requirement that the tachyon should diverge in the IR to ensure vanishing gauge anomaly [244], and thus this choice of potential suppresses the DBI action in the IR.

Also assuming that the couplings w and κ depend only on the dilaton λ, as they do in the conventional DBI action, the action can now be written as

$$S_{DBI} = -M_P^3 N_f N_c \int \mathrm{d}^5x \; V_{f0}(\lambda) e^{-\tau^2} \sqrt{-\det(g_{MN} + \kappa(\lambda)\partial_M\tau\partial_N\tau + w(\lambda)F_{MN})} \,. \tag{4.18}$$

We will discuss the determination of the potentials V_{f0}, κ and w in Section 4.2.

Baryonic matter

Including baryons in the V-QCD framework is still a rather new area of study. In article **III** we expanded on the model we previously used in article **I** by including baryons in the model following Ref. [265] to describe the strongly coupled nuclear matter phase.

Critical string theory-based top-down descriptions of baryons in the four-dimensional boundary theory are known to arise from Dp branes wrapped in the compactified dimensions in the bulk theory [209, 266], appearing in the low-energy limit as small point-like topological defects in the bulk. These solitonic objects have been studied extensively in the $\mathcal{N} = 4$ SYM, and the description has also been expanded to other top-down approaches, such as the Witten-Sakai-Sugimoto model [267–273].

To describe baryons in a holographic context, we need to examine solitonic configurations, and it turns out that the interactions of solitons with the background are described by the CS term included in the WZ action. It is worth underlining here that the CS term and the resulting baryon physics are not an artificial add-on to the V-QCD framework, but the physics of the branes automatically provides us with the relevant term.

The CS term can be written as

$$S_{CS} = \frac{iN_c}{4\pi^2} \int \Omega_5 \,. \tag{4.19}$$

The explicit form of Ω_5 was derived, and can be found in Eq. (3.13) in Ref. [244].

However, solving for interacting solitons with nontrivial spatial profiles is extremely difficult and computationally taxing, as it involves solving groups of PDEs. So, here too, is the time for approximations. In article **III**, we adopted the second approximation scheme introduced for V-QCD in Ref. [265], in which a high-density soliton configuration is described by a homogeneous configuration of non-Abelian gauge fields. An analogous approach has been studied in the WSS model [270, 274–276]. In the high density approximation, it is preferable for the solitons to lie at finite distance $r = r_c$ from the UV. Around r_c the configuration is highly inhomogeneous, but far from this "soliton center", the gauge fields can be well approximated by a homogeneous field structure.

The homogeneous $SU(N_f = 2)$ Ansatz for the spatial components of the gauge fields reads

$$A_L^i = -A_R^i = h(r)\sigma^i \,, \tag{4.20}$$

where $h(r)$ can be considered the baryon field and σ^i are the Pauli matrices. When plugged into the CS and DBI terms as probes on top of a thermal gas background, the Ansatz produces [**III**, 265]

$$S_{\rm DBI} = -2c_b M^3 N_c \int d^5x\, V_{f0}(\lambda) e^{-\tau^2} e^{5A} \sqrt{\Xi} \Big[1 + 6\kappa(\lambda)\tau^2 e^{-2A} h^2 \tag{4.21}$$

$$+ 6w(\lambda)^2 e^{-4A} h^4 + \frac{3}{2} w(\lambda)^2 e^{-4A} f \Xi^{-1} \left(h'\right)^2 \Big] \,, \tag{4.22}$$

$$S_{\rm CS} = -\frac{2c_b N_c}{\pi^2} \int d^5x\, \Phi(r) \frac{d}{dr} \left[e^{-b\,\tau(r)^2} h(r)^3 (1 - 2b\,\tau(r)^2) \right] \,, \tag{4.23}$$

$$\Xi = 1 + e^{-2A} f \kappa(\lambda) (\tau')^2 - e^{-4A} w(\lambda)^2 (\Phi')^2 \,, \tag{4.24}$$

where c_b fixes the pressure normalization and b controls the location of the instanton in the bulk and how it is coupled to the tachyon field. The function $f(r)$ is called the blackening factor, and it will be discussed in Section 4.3.

Now, if $h(r)$ is a smooth function, the CS term reduces to a boundary integral, which evaluates to zero, because the tachyon diverges in the IR and the baryon field $h(r)$ must vanish in the UV. This points towards $h(r)$ being discontinuous, which is actually a well-motivated choice. As mentioned above, the solitons reside at some finite distance r_c in the bulk. The homogeneous approximation is expected to work well both at the boundary $r \ll r_c$ and in the IR $r \gg r_c$, but at $r \sim r_c$, the configuration is nontrivial. This nontriviality can be modeled by introducing a discontinuity in $h(r)$ at $r = r_c$, while keeping the charge density continuous.

Neglecting the inhomogeneities in the instanton configuration introduces some uncertainty on the exact normalization of the action, which needs to be resolved in order to reliably compute thermodynamic observables from the model [265]. We parametrized this ignorance in article **III** by introducing the normalization factor c_b, which can be – along with the parameter b – determined by matching the holographic equation of state with established nuclear matter models, which are known to be reliable at low densities. We will discuss this matching procedure in Chapter 6.

4.2 Matching the Model to QCD

In this section, we will review fitting the potentials V_g, V_f, κ and w in Eqs. (4.4) and (4.18) to both qualitative [**I**, 236, 237, 251, 264, 277] and quantitative [**I**, 240, 278] constraints from QCD. This is also done in detail in Appendix A in article **I**, so we will keep this review short and focus more on some of the details that are not elaborated on in the articles included in this thesis.

In the work done in this thesis, the common starting Ansatz for all potentials V_g, V_f, $1/w$ and

$1/\kappa$ can be taken to be of the form

$$V(\lambda) = \sum_{k=0}^{n_{UV}} V_k \lambda^k + e^{-\lambda_0/\lambda}(\lambda/\lambda_0)^\alpha (\ln(1+\lambda/\lambda_0))^\beta \sum_{k=0}^{n_{IR}} v_k (\lambda/\lambda_0)^{-k} \tag{4.25}$$

where α and β control the IR asymptotics, as in the UV ($\lambda \to 0$) the potential tends to a constant value, and at small λ, the first term dominates. The second term introduces nonperturbative contributions and the powers α and β can be determined to match the wanted features of QCD. This form is chosen, as it has been seen to be able to reproduce important qualitative constraints such as confinement and linear glueball and meson trajectories and gapped spectra in the IR, and asymptotic freedom in the UV [236, 237, 251, 277].

Ansatz (4.25) is also close to what one would expect based on string theory arguments: simple power laws with logarithmic corrections in the IR. Intriguingly, the powers α usually correspond exactly to the string theory expectations [236, 237]. One should however keep in mind that the potentials are not unique to the detail, and there is a lot of fixing-by-hand involved – V-QCD is, after all, a bottom-up model.

In this section, we will first present how the glue sector is fit to QCD data, and then analyze the flavor sector. We will also shortly argue for the form of the Ansätze we employ at the start of the each section.

4.2.1 Fitting Glue

For fitting the glue sector, we can start from two broad requirements, which also argue for the form of Eq. (4.25):

1. In the UV ($\lambda \to 0$), the potential should be represented by the power expansion

$$V_g(\lambda) \sim V_0(1 + V_1\lambda + V_2\lambda^2)\,, \tag{4.26}$$

   in order to guarantee the agreement with the Yang-Mills RG flow, thus also implementing asymptotic freedom. Also, to guarantee the existence of an AdS_5 solution near the UV boundary, we require $V_0 \neq 0$.

2. In the IR ($\lambda \to \infty$), the potential should asymptote to

$$V_g(\lambda) \sim \lambda^{2Q}(\ln\lambda)^P\,, \tag{4.27}$$

   where either P is arbitrary and $2/3 < Q < 2\sqrt{2}/3$, or $Q = 2/3$ and $P \geq 0$ [251]. This form guarantees confinement, as determined by the Wilson loop test, and the avoidance of "bad" singularities [236, 237, 251, 279]. There is a unique solution with $Q = 2/3$ and $P = 1/2$, which reproduces an asymptotically linear glueball spectrum with $m_n^2 \sim n$ [237]. We will use this solution.

The form of Ansatz in Eq. (4.25) fulfills both of these limits. From here on, we will choose to specifically work with the Ansatz

$$V_g(\lambda) = 12\left[1 + V_1\lambda + \frac{V_2\lambda^2}{1+\lambda/\lambda_0} + V_{IR}\, e^{-\lambda_0/\lambda}(\lambda/\lambda_0)^{4/3}\sqrt{\ln(1+\lambda/\lambda_0)}\right], \tag{4.28}$$

which has been shown to work especially well with backreacted flavors [278]. In article **II**, we used a slightly altered form, as there we did not incorporate any flavor structure to our analysis, but the general arguments made here are true for all gluonic IHQCD and V-QCD potentials.

The potential (4.28) has four unfixed parameters; V_1, V_2, V_{IR} and λ_0. Additionally, in order to perform thermodynamic computations, we need to fix the Planck mass M_P and the dynamically generated energy scale Λ_{UV}, which can be defined by the UV expansion of the dilaton λ [236]:

$$\lambda = -\frac{1}{b_0\ln(r\Lambda_{UV})} - \frac{8b_1\ln(-\ln(r\Lambda_{UV}))}{9b_0^2\ln(r\Lambda_{UV})^2} + \mathcal{O}\left(\frac{1}{\ln(r\Lambda_{UV})^3}\right), \tag{4.29}$$

where b_i are beta function expansion coefficients, which are defined shortly.

Let us begin the fitting from the UV coefficients. Because we have identified λ with the 't Hooft coupling and the conformal factor $E \equiv e^A$ with the renormalization scale, we contrast the UV expansion of the holographic beta function $\beta(\lambda)$ with the Yang-Mills beta function $\beta_{\rm YM}$ up to renormalization-scheme-independent two-loop level

$$\beta(\lambda) \equiv \frac{\mathrm{d}\lambda}{\mathrm{d}\ln E} = \frac{\mathrm{d}\lambda}{\mathrm{d}A} = -b_0\lambda^2 + b_1\lambda^3 + \mathcal{O}(\lambda^4), \tag{4.30}$$

$$\beta_{\rm YM} = \beta_0\lambda^2 + \beta_1\lambda^3 + \mathcal{O}(\lambda^4). \tag{4.31}$$

We can write b_i in terms of V_i and demand the two β-functions to be equal in the UV. This, together with the Einstein equations, fixes the coefficients V_1 and V_2 to be [236]

$$V_1 = \frac{11}{27\pi^2}, \quad V_2 = \frac{4619}{46656\pi^4}. \tag{4.32}$$

In the IR, we have no reliable perturbative results to use, and thus we fix the remaining parameters to fit the lattice data [280] at $\mu = 0$ [240]. To produce the fit presented in Fig. 4.1, the parameter values are fixed to [278]

$$\lambda_0 = 8\pi^2/3, \quad V_{IR} = 2.05. \tag{4.33}$$

The global parameters Λ_{UV} and M_P are determined later, together with the flavor sector. The values used for plotting are $\Lambda_{UV} = 1.28T_c$, where T_c is the critical temperature for the lattice data, and $M_P^3 = 1.3/45\pi^2$. Note that to reproduce the Stefan-Boltzmann law for the pressure in the high-T limit, one would need $M_P^3 = 1/45\pi^2$. This overshooting of the limit by around[3] 30% is needed for a good fit, and it is actually to be anticipated; we do not expect to reproduce the behavior of the system deep in the perturbative regime, as we are modeling the strongly coupled limit of QCD, where holographic methods are applicable. We have also seen already in article **I** that for these values the pressure given by the model coincides with the pQCD pressure at finite chemical potential, in the region where pQCD is expected to break down.

[3]The actual value depends on the chosen flavor parameters, as we shall note in the next section.

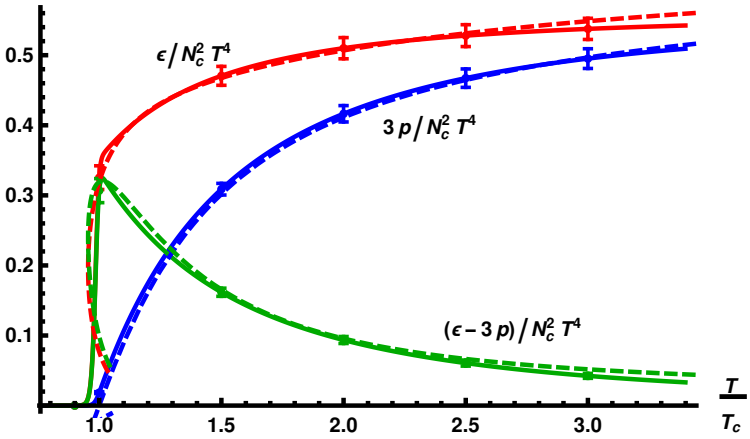

Figure 4.1: Comparison of the pressure p, energy density ε and interaction measure $\varepsilon - 3p$ of the glue sector of V-QCD to large N_c Yang-Mills lattice data from Ref. [280]. The solid lines and error bars represent the extrapolation of lattice data to $N_c \to \infty$, and the dashed lines are the results for the holographic model [278].

4.2.2 Fitting Flavor

The fitting of the flavor sector was done in detail in articles **I** and **III**, and the exact details and parameter values can be found there in Appendices A. Here, we will go through the basic idea and show the resulting fits.

Let us concentrate on $V_{f0}(\lambda)$ first. In the UV, the potential should have a regular power expansion

$$V_{f0}(\lambda) = W_0 + W_1\lambda + W_2\lambda^2 + \dots \tag{4.34}$$

With the flavor turned on, the dilaton effective potential can now be written $V_{\text{eff}}(\lambda) = V_g(\lambda) - x_f V_{f0}(\lambda)$, and we can use the holographic β-function to determine W_1 and W_2 from the full QCD β-function. Up to two-loop level, the coefficients are

$$b_0 = \frac{2}{3}\frac{11 - 2x_f}{(4\pi)^2}, \quad \frac{b_1}{b_0^2} = \frac{34 - 13x_f}{(11 - 2x_f)^2}, \tag{4.35}$$

If we take[4] $x_f = 1$, we can write W_1 and W_2 as

$$W_1 = \frac{8 + 3W_0}{9\pi^2} \quad W_2 = \frac{66488 + 999W_0}{15552\pi^4}. \tag{4.36}$$

[4]As mentioned previously, the parameter x_f makes sure that flavor is as important as color in the large-N_c limit. In this thesis, we are mostly using $x_f = 1$ in the computations presented here, and therefore I do not discuss the parameter at length. However, a rich phase structure reveals itself when varying x_f, as analyzed in length in Refs. [251, 264]

Also, the AdS radius ℓ is fixed by

$$\ell = \frac{1}{\sqrt{1 - x_f W_0/12}}\,, \tag{4.37}$$

In the IR, the DBI action is suppressed by the tachyon diverging. The divergence is required, among other considerations, to reproduce bulk flavor anomalies similar to QCD and reasonable meson spectra [244, 245]. This can been seen as a result of the $D4$ and $\overline{D4}$ branes annihilating in the IR, analogously to the WSS model.

The exact potential $V_{f0}(\lambda)$ is determined by the fit to lattice thermodynamics. Here, we have adopted the simple Ansatz

$$V_{f0}(\lambda) = W_0 + W_1\lambda + \frac{W_2\lambda^2}{1+\lambda/\lambda_0} + W_{\rm IR}e^{-\lambda_0/\lambda}(\lambda/\lambda_0)^2\,, \tag{4.38}$$

which produces regular solutions with non-zero θ-angle [253], *i.e.* when the axion is turned on, as well as a phase diagram as a function of x_f, which is qualitatively in agreement with that from QCD in the Veneziano limit [251]. The inclusion of the exponent in the Ansatz is to ensure that the UV part does not dominate in the IR.

The remaining parameters W_0 and W_{IR} are determined by the fit to the lattice data, which we will discuss below.

The couplings $\kappa(\lambda)$ and $w(\lambda)$ can be treated in a similar manner by demanding that their UV expansions are regular, and that the Ansätze reproduce the correct asymptotics in the IR . Namely, if we start from the common Ansatz $V(\lambda) \sim \lambda^\alpha(\ln\lambda)^\beta$, demanding that the meson trajectories are asymptotically linear and that axial and vector meson towers have different slopes, together with the demand for a hadronic phase at non-zero μ [265], fixes the powers α and β in the IR asymptotics of both $\kappa(\lambda)$ and $w(\lambda)$ [251, 264, 277]. Here we will use the Ansätze

$$\frac{1}{\kappa(\lambda)} = \kappa_0\left[1 + \kappa_1\lambda + \bar\kappa_0\left(1+\frac{\bar\kappa_1\lambda_0}{\lambda}\right)e^{-\lambda_0/\lambda}\frac{(\lambda/\lambda_0)^{4/3}}{\sqrt{\ln(1+\lambda/\lambda_0)}}\right], \tag{4.39}$$

$$\frac{1}{w(\lambda)} = w_0\left[1 + \frac{w_1\lambda/\lambda_0}{1+\lambda/\lambda_0} + \bar w_0 e^{-\lambda_0/\lambda}\frac{(\lambda/\lambda_0)^{4/3}}{\ln(1+\lambda/\lambda_0)}\right]. \tag{4.40}$$

Analogously to using the β-function to constrain $V_{\rm eff}$, we go about constraining the parameters of $\kappa(\lambda)$ by demanding that the UV behaviour of the model needs to reproduce the quark mass anomalous dimension

$$\gamma = -\frac{{\rm d}\ln m_q}{{\rm d}\ln E} = -\gamma_0\lambda + \dots\,, \tag{4.41}$$

up to the scheme-independent one-loop level, where $\gamma_0/b_0 = 9/(22-4x_f)$. The holographic equivalent is defined by [282]

$$\gamma \equiv 1 + \frac{{\rm d}\ln\tau}{{\rm d}A}\,, \tag{4.42}$$

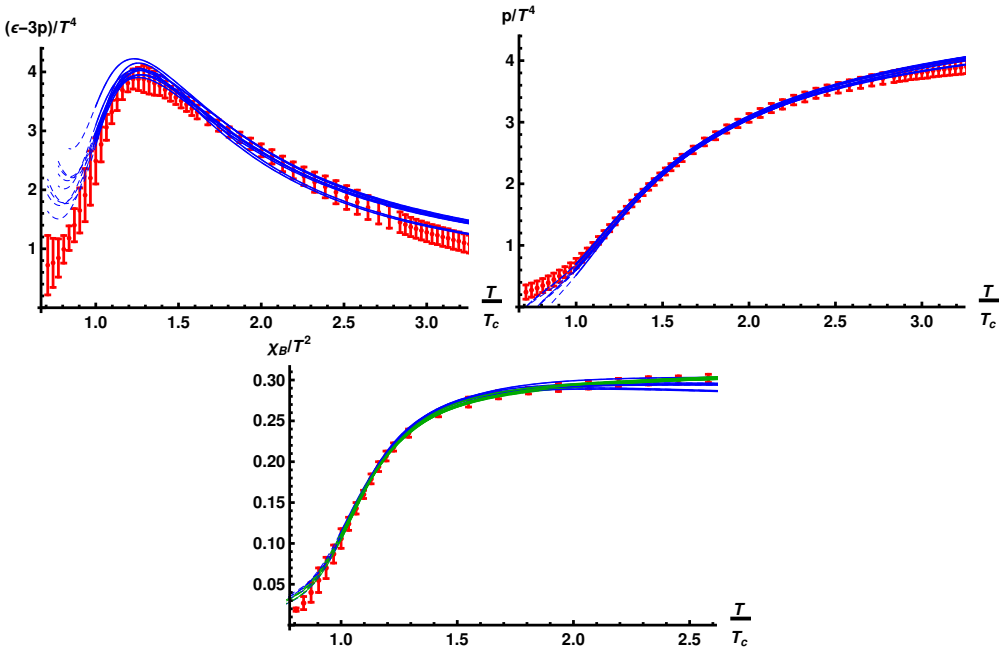

Figure 4.2: Comparison of different thermodynamic quantities between V-QCD and lattice QCD data [98, 281] with $2+1$ flavors. The red dots and error bars are lattice data and the various curves represent different fit results with slightly different parameter values. Top left: interaction measure versus temperature in units of critical temperature. Top right: pressure versus temperature. Bottom: baryon number susceptibility $\chi_B = \mathrm{d}^2 p/\,\mathrm{d}\mu^2$ at $\mu = 0$ versus temperature. The different color curves represent different fit strategies.

where the addition of 1 is due to the perturbative dimension of the quark mass operator. Plugging in the equations of motion and demanding the two γ to be equal fixes [**III**, 264]

$$\kappa_0 = \frac{12 - W_0}{8}, \quad \kappa_1 = \frac{11}{24\pi^2}\,. \tag{4.43}$$

The rest of the parameters need to be determined by a fit to lattice data at $\mu = 0$. In the case of the gluon sector, we were able to use large N_c Yang-Mills data, but for full QCD, no such data exists. The available lattice data is for $N_c = 3$ and $N_f = 2+1$ [98, 281]. We used this data – which roughly corresponds to $x_f = 1$, although the approximation is uncontrolled and corrections for finite N are challenging to obtain – to constrain the holographic model. There are multiple different choices of parameters that result in excellent fits, and we analyzed 18 different sets of parameters in article **I**. These fits are presented in Fig. 4.2, and the exact parameter values can be found in Appendix A in article **I**.

4.3 Thermodynamics of the Model

We have touched upon some of the thermodynamic quantities while fitting the potentials, but let us now discuss the phase structure of the model in a more systematic manner. Determining the thermodynamics with the nontrivial potentials we established in Section 4.2 is numerically somewhat involved, as the resulting equations of motion are also quite nontrivial. Here we will gloss over most of the numerical details for the sake of brevity. The thermodynamics with massless quarks has been studied in the case of IHQCD in Refs. [238, 239], for $\mu = 0$ in V-QCD in Refs. [278, 283], for nonzero μ in V-QCD in Refs. [**I**, 282] and including baryons in Refs. [**III**, 265]. Here we will only consider the case of massless quarks. The effects of nonzero quark masses on the thermodynamics have been considered in Ref. [264].

Generally speaking, in V-QCD, there are two classes of vacuum solutions for the geometry: the thermal gas (TG) solution and the black hole (BH) solution. The metric in Eq. (4.3) corresponds to the thermal gas solution, which is a horizonless metric with trivial thermodynamics, with the pressure scaling as $\mathcal{O}(N_c^0)$ [278, 283]. The solution can be thus identified with the vacuum or thermal gas solution in the boundary theory – or more succinctly, with the confined phase [239, 282, 283]. The BH solution can be identified with the deconfined phase, due to the Polyakov loop having non-zero expectation value [251, 282, 283].

As is conventional in holography, we incorporate non-trivial thermodynamics in the model by introducing a black hole horizon to our bulk geometry. This reflects upon our metric Ansatz, which becomes

$$\mathrm{d}s^2 = e^{2A(r)}\left(-f(r)\,\mathrm{d}t^2 + \mathrm{d}\mathbf{x}^2 + \frac{\mathrm{d}r^2}{f(r)}\right). \tag{4.44}$$

The bulk direction r is now truncated by the horizon at $r = r_h$, and the coordinate runs $r \in (0, r_h)$. The function $f(r)$ is called the blackening factor, and we impose upon it the boundary conditions $f(r = 0) = 1$ (so we retain the asymptotically AdS metric in the UV) and $f(r = r_h) = 0$.

Now the boundary thermodynamics are essentially determined by the bulk black hole thermodynamics. Thus, we can introduce temperature T and entropy density s by

$$T = -\frac{\dot{f}(r_h)}{4\pi}, \quad s = 4\pi M_P^3 N_c^2 e^{3A(r_h)}\,, \tag{4.45}$$

from which we can deduce the pressure p and the energy density ϵ by the conventional thermodynamic relations

$$\mathrm{d}p = s\,\mathrm{d}T + n\,\mathrm{d}\mu\,, \tag{4.46}$$

$$\epsilon = Ts + n\mu - p\,, \tag{4.47}$$

where n is the number density, and μ is the chemical potential. As was elaborated in Section 3.3, the chemical potential is introduced by turning on the temporal component of the gauge field $A^0(r) \equiv \Phi(r)$ in the DBI action.

The thermodynamics can now be determined by first finding pressure as a function of temperature at $\mu = 0$ by integrating $s(T) = p'(T)$, which sets a boundary condition for determining $p(\mu)$ at a given temperature by integrating Eq. (4.46). The process of determining the thermodynamic quantities is quite involved, and the exact details on how this is done can be found in Ref. [282], with the nuclear matter quantities being determined in Ref. [265].

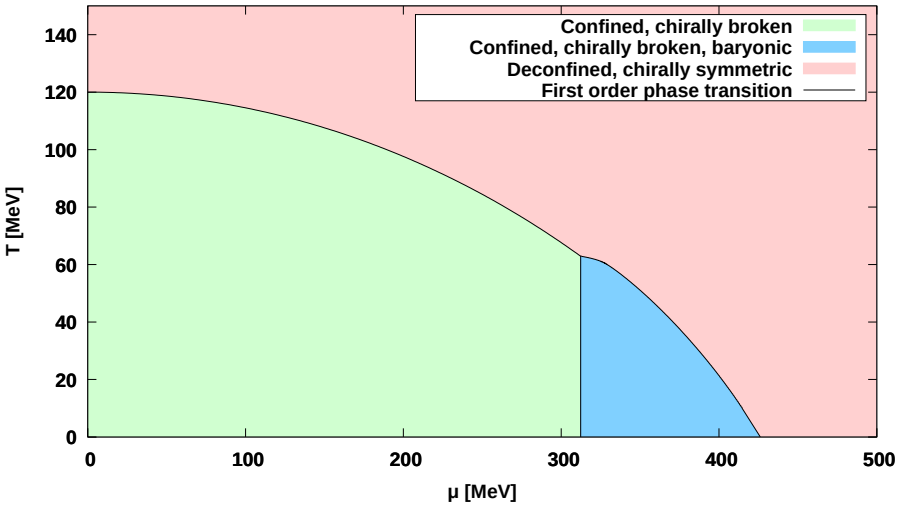

Figure 4.3: The V-QCD phase diagram at $m_q = 0$ with the homogeneous approximation for baryons, presented in Section 4.1.2. The lines correspond to first order phase transitions. In the green region, the thermodynamically favored solution is the thermal gas background with non-zero tachyon. The thermal gas solution with baryons, corresponding to strongly coupled nuclear matter, is dominant in the blue region. In the red region, the black hole solution with no tachyon condensate is favored, the phase being thus chirally symmetric as well as deconfined. Figure from Ref. [265].

As we are transitioning between a horizonless geometry to a one with a horizon, the transition between these two states is a first-order Hawking-Page transition [238]. The transition is actually generically strong at $T = 0$, as discussed in articles **I** and **III**, but it is expected to weaken with rising temperature [219] and stringy loop corrections [278].

There is a further distinction to be made when discussing the possible phases; we can have solutions with or without the tachyon, and thus states which are chirally symmetric or have spontaneously broken chiral symmetry. This, along with the prevalent metric, results in four distinct baryonless phases. Three of these four possibilities can be thermodynamically dominant [282]

- Confined phase with broken chiral symmetry, corresponding to a thermal gas solution with non-zero tachyon condensate.

- Deconfined, chirally symmetric phase, corresponding to a tachyonless black hole solution.

- Deconfined phase with broken chiral symmetry, corresponding to a black hole solution with non-zero tachyon condensate.

The last of these is quite an exotic state that is also found in top-down models, such as models based on the $D3-D7$ brane system [284] as well as the WSS model [285, 286]. The appearance of this state in the phase diagram is strongly dependent on the choice of potentials. Fits to lattice results seem to disfavor the potentials enabling the dominance of this state [**I**], and in the phase diagram presented here with the current fits, the deconfined phase with broken chiral symmetry is absent.

Additionally, we must address the nuclear matter phase. Baryons are introduced as a probe on top of the thermal gas background, corresponding to a hadron gas state with condensed baryons. There occurs a first order phase transition between the vacuum and the nuclear matter phase, which is exactly vertical in the phase diagram, as the temperature dependence is suppressed by N_c^2. If one takes the parameter b in the CS action to be $b = 10$, the transition occurs at $\mu = 313$ MeV [265]. The thermodynamics of this phase was studied in Ref. [265] as well as in Article **III**.

As is clear from Fig. 4.3, when contrasted with the conjectured QCD phase diagram in Fig. 2.3, the model reproduces most of the expected features of the real QCD phase diagram. We have a confined and a deconfined phase, with the dense nuclear matter phase appearing where it should. Here, I would like to remind the reader that all quantitative fitting to lattice QCD data is done at $\mu_B = 0$, and thus the relatively faithful reproduction of the phase diagram – as well as the equation of state, as is shown in the articles – at finite μ_B is a significant *tour de force* concerning the predictivity of the model.

The feature clearly missing from Fig. 4.3 is the crossover. The nature of the deconfinement transition in the bulk theory makes it extremely difficult to modify it into a crossover. One possibility, which also ensures a more complete fit to lattice data at low temperatures, would be to match the holographic model with the hadron resonance gas solution [278]. The possibility of the Hawking-Page transition in an Einstein-scalar model being able to accommodate a higher order transition in the boundary theory in some scenarios has been studied in Ref. [287].

Here we did not consider the effect of a magnetic field to the thermodynamics of the model, which has been studied in Refs. [288–290]. The inclusion of the magnetic field, by inverse magnetic catalysis [93], weakens the chiral condensate, decreasing the temperature of the chiral transition at small density. This effect has also been observed in lattice studies [291].

Chapter 5

Heavy-Ion Collisions and Holography

We can create quark-gluon plasma (QGP) in a laboratory by means of heavy-ion collisions (HIC). In the LHC and RHIC, heavy ions such as lead and gold nuclei are accelerated to near the speed of light, and hence these nuclei appear as discs in the lab frame due to Lorentz contraction. The discs then collide, interacting with each other and creating a plethora of new particles – a medium with a temperature of around 300 MeV. Forming this medium, quarks, antiquarks and gluons quickly start behaving as a strongly coupled fluid, the properties of which can be described by relativistic hydrodynamics. Expanding, driven by pressure, the QGP cools until the temperature and energy density are low enough for the partons to form new hadrons, which stream freely until they are picked up by the detectors.

The above is a short, coherent-seeming story about the time-evolution of heavy-ion collisions, also depicted in Fig. 5.1, but there are still some question marks hidden in the text. Firstly, the story is told chronologically – as we will continue to do shortly – but it is constructed inversely. The experiments do not see the plasma as it forms, but the resulting shower of particles with some global observables such as particle multiplicities and energies, from which the collision can be reconstructed using some theoretical framework. The global observables from *e.g.* Au+Au collisions can be used to constrain the model, which in turn can be used to predict other events, such as Pb+Pb collisions. Examples of this kind of analysis can be found in *e.g.* Refs [292–295]. Here, for the sake of simplicity, we will recount the events chronologically based on the results from such global observable analyses.

Secondly, there are some holes in the description of the very early stages of the strongly coupled far-from-equilibrium plasma. Some of the remaining open questions are related to the timescales associated with the processes: the hydrodynamic description of the plasma seems to be valid extraordinarily quickly after the collision, but exactly how quickly? How soon does the plasma thermalize? In this thesis, we are interested in the latter question.

Because of the strongly coupled nature of the plasma, combined with the out-of-equilibrium nature of these real-time processes, both perturbative methods and lattice simulations are of limited use in answering the above questions. However, as discussed shortly in Section 3.4, holographic methods have proved themselves extremely useful in the study of HIC as they are well

suited to study strongly coupled systems and even far-from-equilibrium processes. Unsurprisingly, there have been a lot of studies of HIC within the AdS/CFT framework ever since the seminal article by Policastro, Son and Starinets [8], and a lot of insight has been gained by studying the super Yang-Mills theory [9]. Still, it is clear that for the results to be applicable to real QCD, one needs to implement finite gauge coupling and conformal invariance breaking. And truly, there have been multiple finite coupling, nonconformal studies in different contexts, featuring shockwave collision in the bulk [296–298], but often restricted to the study of the quasinormal mode (QNM) spectra of undulating black hole solutions [299–301]. We will discuss these approaches more later.

Encouraged by the success of holographic descriptions in predicting the behavior of the plasma, in article **II** we applied the IHQCD model to the study of the QNM spectra. The spectrum allows us to determine how the black hole system equilibrates when subjected to small perturbations. The equilibration of the bulk system is of course closely related to the equilibration on the boundary, allowing us to determine the poles of the retarded Green's function through the duality.

We will use the first part of this chapter to shortly discuss the big picture and some details of the time-evolution in heavy-ion collisions. For recent reviews on the subject from different perspectives, see *e.g.* Refs. [9, 302–305]. We use the latter part of this chapter to discuss the use of QNMs in the study of thermalization and elaborate on the work done in article **II**.

5.1 Time-evolution of Heavy-Ion Collisions

Let us begin complicating the story we told to start this chapter. One must first remind oneself of the fact that the nuclear discs are not homogeneous; the nucleons making up the nuclei are made up of quarks, antiquarks and gluons (collectively called partons), with each nucleon having exactly three more quarks than antiquarks. The density profile of these partons fluctuates within each nucleon, making the nucleus a complex system. Thus, the discs could be thought of more realistically as having ragged edges.

In the following, we are only talking about central collisions, *i.e.* ones where the nuclei, A, collide head-on. Usually the collisions are of course off-center, but by restricting ourselves to central collisions, we remove some complications that are not central for the work at hand. When considering off-center collisions, the picture changes by the initial shape of the overlap region being lenticular, and that only a fraction of the nucleons take part in the interactions, but all general points made here also apply for off-central collisions.

In the initial stage of the collision, the nuclei interact via hard scatterings, yielding high-energy, large transverse momentum (*i.e.* momentum perpendicular to the beam line) parton pairs and electroweak bosons, which decay into jets of hadrons. These large-p_T particles act as hard probes of the medium created in the HIC. The processes behind the hard probes are well-understood; the conventional pp cross-sections with their large-p_T scatterings are accurately described by pQCD methods, and from observations from both pA collisions and AA collisions we know that the processes in AA collisions are essentially the same, but modified by the number of colliding

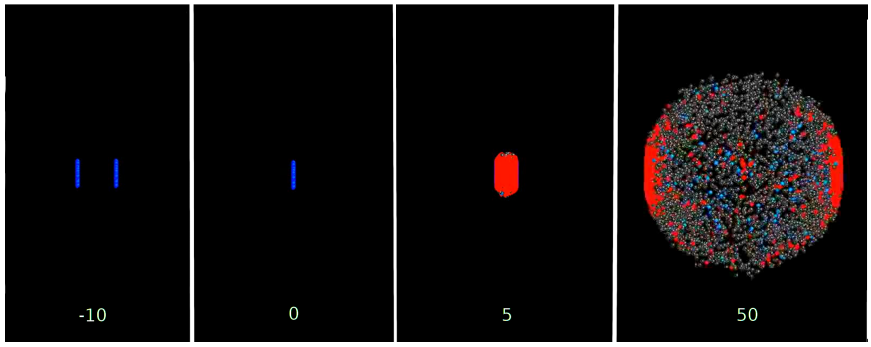

Figure 5.1: Stills from a central Pb-Pb collision at $\sqrt{s_{NN}} = 2.76$ TeV. Hadrons are represented by blue and gray spheres and QGP by red spheres. The number under each column indicates the time since the collision in fm/c. Figure adapted from animation in Ref. [313].

nucleons. This is attested to by the measured production rates of electroweak bosons, which are not affected by the colorful environment [306–308]. Especially photons are interesting, as they provide us with the information from which the temperature of the system can be determined.

Naturally, particles charged under $SU(3)_c$ are also created in the initial processes. The lighter quarks, u, d and s, are created in ratios well represented by a system in chemical equilibrium [309–311], but the heavier b and c quarks are too heavy to reach chemical equilibrium, and only a few of them are ever produced per event. The heavier quarks form heavy Υ and J/ψ mesons that are affected by the charged environment.

Continuing forward on the timeline, the discs overlap at time which we take as $\tau = 0$, and interact, passing through each other. Longitudinal color fields fill the space between the distancing discs, slowing them down, and eventually the field decays into a multitude of $q\bar{q}$ pairs and gluons. The initial energy density of the system is also enormous, clearly exceeding the value needed for the deconfinement transition (see *e.g.* Refs. [292, 312] for analyses on the initial energy density). Initially this body of particles is obviously not isotropic or in thermal equilibrium. However, soon after the collision, the plasma seems to behave as a strongly coupled, relativistic fluid. The hydrodynamic description of the plasma seems to be applicable very early in the evolution, with kinetic theory estimations being ≤ 1 fm/c [314], while some holographic simulations favor hydrodynamization as early as 0.35 fm/c [315].

One should note that hydrodynamization does not necessarily need thermalization [316]. A hydrodynamic description can work before the plasma is completely isotropic, so the fast hydrodynamization need not imply that the thermalization is also fast. There are some implications that the system is completely isotropic only later in the evolution [315], but there is still no consensus on the exact thermalization timescale, the study of which necessitates studies of far-from-equilibrium, real-time dynamics at strong coupling [317].

Going back to the large-p_T probes, we can provide some of the reasons why we know the plasma is strongly coupled and behaves like a fluid. The initially produced color charged jets

show considerable energy loss as they propagate through the medium created in the collision [318, 319]. In the case of the $b\bar{b}$ and $c\bar{c}$ pairs, forming Υ and J/ψ mesons respectively, their presence in the observations is suppressed, as the quark-antiquark pairs see the attractive force binding them being weakened in the color charged environment due to Debye screening. If the plasma was a weakly coupled gas, the jet quenching would be less severe, but as it stands, the suppression of quarkonium serves as an indicator of the strongly coupled nature of the plasma.

The differences in the suppression of different flavors is an interesting feature: due to their heavier mass, b quarks end up with a smaller multiplicity in the initial high-p_T processes than c quarks. If we look at Υ suppression, it is quite severe. Smaller excitations are more tightly bound than the ones with larger radii, and thus have a higher change of making it through the plasma [320, 321]. The case with the more abundant charmonium, J/ψ, is slightly different. Due to c being more abundant, the quarks separated from their antiparticle pairs have a higher chance of meeting a similar quark in the plasma sufficiently close to hadronization, and this is reflected in their final abundance [322–325].

Additional support for the strongly-coupled, fluid nature of the plasma is provided by the anisotropies in the final momentum distribution; if the plasma was a weakly interacting gas, the initial lumpiness of the nuclei would be smoothed out as the plasma expands and random movement erases the traces of the initial spatial anisotropies. However, as it stands, we see the effects of both the initial spatial anisotropies and centrality in the resulting momentum distribution [295, 326–328]. This is due to the anisotropies in the local fluid pressure driving the expansion, and which results in velocity anisotropies in the fluid that can be observed in the momentum distributions of the final state particles.

The QGP has some interesting hydrodynamic properties, the predominant one being the lowest specific shear viscosity η/s of any known fluid, enunciating the near-perfect fluidity of the medium. While the plasma has extremely large values of both η and s, the relativistically interesting, dimensionless ratio η/s is close to the conjectured lower bound $1/4\pi$ [329], with η/s in the range of $0.08 - 0.16$ being consistent with the RHIC data [330–333]. Recent Bayesian parameter analysis suggests $\eta/s = 0.07^{+0.05}_{-0.04}$ near the transition temperature [334] (see Fig. 5.2). This low-viscosity system, driven by the pressure, expands radially and cools. The system stays in the plasma phase until the energy density drops below that of a hadron, at which point the plasma begins to break apart into individual hadrons. Soon after this hadronization, the resonances having decayed into stable particles, the composition of this hadron gas freezes in what is called the *chemical freeze-out*. After a while, the system becomes dilute enough for the scatterings to cease (*kinetic freeze-out*), and the resulting composition of particles is in free streaming until it ends up in a detector.

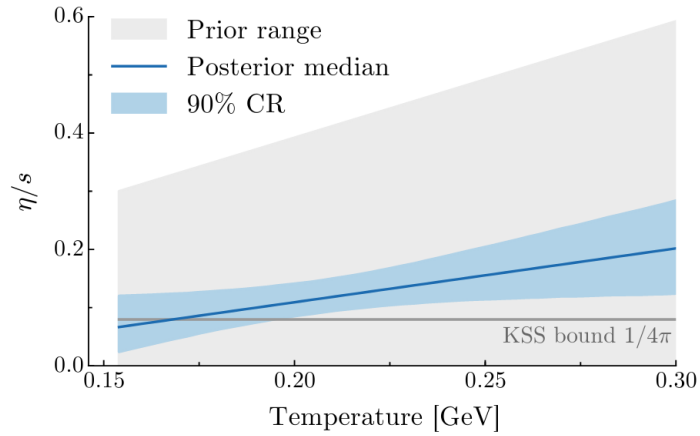

Figure 5.2: Temperature dependence of the shear viscosity $(\eta/s)(T)$ from Bayesian analysis. The blue line indicates the posterior distribution median with the blue band being the 90% credible region. The gray region indicates the prior range for the linear $(\eta/s)(T)$ parametrization. The holographic bound $\eta/s = 1/4\pi$ is also indicated as the KSS bound. Figure from Ref. [334].

5.2 Holographic Thermalization

When it comes to the study of heavy-ion collisions, holography has by now become a standard tool in the field [9]. This is not least due to the above-mentioned article [8] and its extensions proving that one can gain not only qualitative insight but also quantitative predictions from holographic models. Most of the early studies were naturally done in $\mathcal{N} = 4$ super Yang-Mills at infinite coupling, but there is a growing, not-insignificant body of work looking at HIC at finite-coupling in nonconformal theories. Rightfully so, as there is evidence (see Fig. 5.2) that for higher temperature plasma, there is an evident need for finite coupling corrections to the transport coefficients.

However, here we are not applying the model presented in Chapter 4 to hydrodynamization, but to thermalization, the quantitative description of which is a notoriously complicated problem. Luckily, this problem has been extensively studied in recent years in different holographic frameworks, and thus there are some established frameworks that are able to provide us with tools to study equilibration processes in gauge/gravity context.

One way to approach the problem is by numerical general relativity simulations of shock wave collision. This is possible, because if the Lorentz-contracted nuclei are approximated by infinitely expanded planar shock waves in the boundary theory, the collision can be described by colliding gravitational shock waves in bulk. This approach is described in detail in Refs. [220, 222, 335, 336] and the references therein. The shock-wave description has been successful, being able to see the onset of hydrodynamization and even the elliptic flow in off-central collisions [222, 337–339]. See also Refs. [296–298].

One other, less numerically taxing method to study heavy-ion collisions in the boundary is by studying a shell collapsing into a black hole in the bulk [340, 341]. The rationale behind this description can be seen by working backwards from equilibrated QGP, which corresponds to a black hole in equilibrium in the bulk theory. Therefore, the formation and evolution of a far-from-equilibrium plasma in the boundary theory should correspond to the formation and evolution of a black hole[1], and thus the thermalization corresponds to the relaxation of the horizon [343]. This ringing down of the black hole is encoded in the quasinormal mode (QNM) spectrum [329]. The QNMs corresponding to electromagnetic and gravitational perturbations in the bulk theory can be identified with poles of the corresponding Green's functions in boundary field theory (see also Refs. [344–347] for different treatments on the subjects, and Refs. [299–301] for studies of QNMs at finite coupling).

Furthermore, Ref. [348] argues that the thermalization time of a Wightman function in the boundary theory dual to a bulk system undergoing gravitational collapse should be inversely proportional to the imaginary part of the lowest QNM of the same correlator in thermal equilibrium, which would allow us to relate the QNM spectrum straight to the thermalization timescale of the boundary system.

5.2.1 Thermalization in IHQCD

In article **II**, we studied the QNM spectrum of a gauge-invariant scalar field dual to the retarded Green's function of the corresponding boundary operator in the context of IHQCD. This can be seen to be in continuum with *e.g.* Refs. [232–235] and Refs. [349–355], with the difference lying in the use of the IHQCD potential introduced in [283], including the logarithmic corrections.

In the article, we use the metric Ansatz

$$\mathrm{d}s^2 = b(r)(-f(r)\,\mathrm{d}t^2 + f(r)^{-1}\,\mathrm{d}r^2 + \mathrm{d}\mathbf{x}^2)\,, \tag{5.1}$$

where we have denoted $b(r) \equiv e^{A(r)}$. Note that and we are using notation consistent with the earlier chapters, but which differs from the one used in article **II**.

We used the IHQCD action (4.4), together with the potential

$$V(\lambda) = 12\left(1 + \frac{88\lambda}{27} + \frac{4619\lambda^2}{729(1+2\lambda)} + 3e^{-1/2\lambda}(2\lambda)^{4/3}\sqrt{1+\ln(1+2\lambda)}\right), \tag{5.2}$$

which is modified slightly with respect to the one in Eq. (4.28), which is used in tandem with the full V-QCD model [283].

For $\mathbf{q} = 0$, the equation of motion for the gauge-invariant scalar fluctuation $\phi(\omega, r)$ in the absence of mixing with the metric fluctuations can be written as [232, 356, 357]

$$\ddot{\phi} + \frac{d}{dr}\ln(fb^3)\dot{\phi} + \frac{\omega^2}{f^2}\phi = 0\,, \tag{5.3}$$

[1]Here, we are strictly talking about central collisions. It has been proposed that off-center collision thermalization could be studied with Myers-Perry black holes, which are a generalization of the familiar Kerr black holes. See *e.g.* Ref. [342] and references therein.

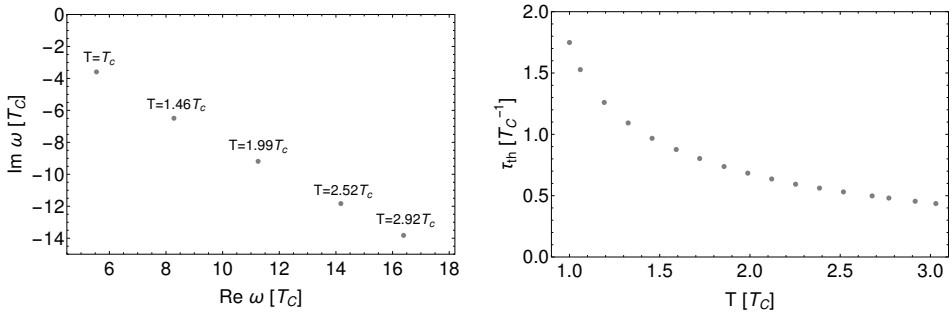

Figure 5.3: Left: location of the lowest quasinormal mode ω shown for five different temperatures. Right: thermalization time $\tau_{\rm th}$ in units of T_c^{-1} versus the temperature in units of T_c, T_c being the critical temperature.

with the dot denoting a derivative with respect to r. We can further mold this equation into a Scrödinger-type form by introducing the variable

$$u = \int_0^r \frac{dr'}{f(r')}\,, \tag{5.4}$$

and defining $\psi(u) \equiv \sqrt{b^3}\phi(u)$, giving us

$$-\psi''(u) + V_{\rm Sch}(u; z_h)\psi(u) = \omega^2\psi(u), \tag{5.5}$$

$$V_{\rm Sch}(u, z_h) = f^2\left[\frac{2\ddot{b}}{2b} + \frac{3\dot{b}^2}{4b^2} + \frac{3\dot{f}\dot{b}}{2fb}\right]_{z=z(u)}\,, \tag{5.6}$$

where the dash denotes a derivative with respect to u.

We require for the solution to be ingoing at the horizon, *i.e.* $\psi \propto e^{+i\omega u}$ at large u. To obtain the QNMs, we need to determine those eigenvalues ω, for which the solutions that satisfy this boundary condition are normalizable when $u \to 0$. To implement these boundary conditions simultaneously in the numerical computation, it is convenient to find the solution in the infrared analytically and match it with the numerically determined ultraviolet solution.

The Heuristic Method

Here we will shortly elaborate on the numerical method, first introduced in Ref. [232], that we used to finding the QNM spectra in article **II**. Most of the other technical details, alongside the results, are presented in the article, so we will not dwell on them too much here.

Eq. (5.5) is linear, so one would be tempted to think that finding the eigenvalues ω would be quite simple using the standard spectral methods, such as Chebyshev expansions together with a Lobatto grid. However, these methods rely on the solution being regular in the boundary, *i.e.* to be expanded in a power series, but in our bulk model the expansions contain logarithmic corrections, foiling the plans of using spectral methods. Therefore, we need to find other ways of numerically solving the equation.

From a numerical point of view, we do not expect any ω to be exactly at a QNM. It is therefore reasonable to expect that the corresponding solution ψ contains a part of the non-normalizable solution $\phi(u=0)=1$, meaning that $\psi(u) \to u^{-3/2}$, and diverges. For ω close to a QNM, we expect that the normalizable solution is dominant for closer to $u=0$, and the divergence only occurs when u is very small.

If one accepts this heuristic (which has been tested with known spectra), one can compute the QNM spectrum by taking a trial value of ω, then numerically finding the smallest local minimum of $|\psi(u)|$, which we denote by $u=u_{\min}$. Computing this on a grid over the complex ω-plane, we get $u_{\min}(\omega)$, and the QNM spectrum is approximately given by the values of ω which minimize $u_{\min}(\omega)$.

Results

Using the above method we get the lowest QNMs as a function of temperature, presented in the left panel in Fig. 5.3 for temperatures ranging from T_c to $3T_c$. As mentioned above, it is argued in Ref. [348] that the thermalization time is inversely proportional to the imaginary part of the lowest-lying QNM. The thermalization time $\tau_{\rm th}$, presented in the right panel in Fig. 5.3 as a function of temperature, is obtained for from the corresponding lowest mode via the relation [348]

$$\tau_{\rm th} = -\frac{2\pi}{\operatorname{Im}\omega}\,. \tag{5.7}$$

The curve for $\tau_{\rm th}(T)$ decreases slightly faster than $1/T$, with the scale being of order $\tau_{\rm th} \simeq 0.5/T_c \approx 0.5$ fm/c.

There is an interesting observation to be made about the behavior of higher QNMs as a function of temperature. When computing a spectrum for a given temperature, we found clearly separated, individual QNMs, which then terminate at an extended structure at a constant $\operatorname{Im}\omega$, with the number of accessible separate QNMs decreasing with increasing T. One is tempted to interpret this structure as a branch cut in the complex ω-plane, as nearly similar behavior is seen in other studies of QNM spectra (see *e.g.* Ref. [234]), but any certain statements cannot yet be made. This behavior is discussed in some more detail in the article with examples of the spectra.

To relate our holographic results back to the context of heavy-ion phenomenology; we have seen in Sections 4.2.1 and 4.3 that the finite temperature phase diagram of the holographic model we employ agrees quantitatively very well with lattice results. We have furthermore demonstrated that the model is also consistent with early thermalization dynamics. While both interesting for the building of the holographic model, our results also give further support for the applicability of hydrodynamics of a strongly coupled, rapidly equilibrating fluid, consisting of collectively free quarks and gluons, as a model of the initial stages of the system created in ultrarelativistic heavy-ion collisions.

Chapter 6

Neutron Stars and Holography

In the previous chapter, we established further confidence on the applicability of the holographic model we set up in Chapter 4, the use of which in the study of quark-gluon plasma is already bolstered to some extent by the preceding accomplishments of holographic methods concerning the subject. Now, to further map the possibilities in the utilizing the model, we shall explore the low-temperature, high-density regime of the QCD phase diagram realized in neutron stars.

The application of holographic methods in the study of neutron stars is a relatively young field, emerging in recent years in concurrence with the breakthrough in gravitational wave astronomy and more accurate astrophysical measurements of neutron star properties. These advances have already allowed for constraining the QCD equation of state (EoS) in the low-temperature regime, prompting a new era in the study of dense QCD. However, the densities reached in the cores of neutron stars are currently out of reach of lattice simulations due to the sign problem, and we thus need to find another first-principles approach to account for the sharpening picture we have of the QCD EoS. On the grounds of the regime in question being strongly coupled, this seems to accommodate the application of holographic methods.

In this chapter, we will first briefly review some information currently known about neutron stars, with a focus on the constraints applied in articles **I** and **III**. Subsequently, we will discuss the current state of theoretical knowledge as it relates to the microphysics of neutron stars. Then we consider the content of articles **I** and **III**, with a focus on the latter, as it builds on the work started in the former. We will look into how we use the existing effective models to complement the holographic approach. We will then subject these hybrid EoSs to the astrophysical constraints obtained from the study of neutron stars, discussing some of the implications and findings from this procedure.

6.1 Neutron Stars

Neutron stars are the densest observed objects in the universe besides black holes. They are created as remnants in supernova explosions of massive ($M \gtrsim 8M_\odot$, where $M_\odot \approx 1.989 \times 10^{30}$ kg is the mass of the Sun) main-sequence stars. These events ensue as the stars burn through their

fuel up to iron-group elements, which start accumulating in the center of the star, leading to the gravitational collapse of the core as its mass surpasses the Chandrasekhar limit of around $1.4M_\odot$ [358–360], *i.e.* when the electron degeneracy pressure within the core is lower than the gravitational pressure compressing it. Through many complex stages, this core collapse supernova event leads to the birth of a black hole, or of a neutron star[1].

These compact stars, while initially hot, rapidly cool down. Quiescent neutron stars have a temperature below 100 eV [361], which, even though translating to approximately 10^6 kelvins, is small compared to the QCD scale. Thus neutron stars can be considered low-temperature objects for our purposes. In the following, we will discuss the properties of these objects in this dormant state.

6.1.1 Neutron Star Observations

Since the discovery of pulsars[2] in 1967 [363], thousands of neutron stars have been observed [364], and we have accrued some amount of data on them with some accuracy. Recent years have seen a flood of new data thanks to progress in observational technology and the dawning of the era of multimessenger astronomy, heralded by the LIGO/Virgo gravitational wave detection of a neutron star binary merger [4, 5] in concert with the observation of its electromagnetic counterpart [6].

In this section, we will briefly go through some of the key observables, some of which we have utilized in articles **I** and **III** to constrain the holographic potentials.

Mass Measurements

The most accurate measurements currently available on neutron star masses are from observing millisecond pulsars. The period at which these pulsars rotate is extraordinarily stable, allowing for precise measurements of the properties of the system when bound in binaries. The total mass of the system, along with the orbital size can be inferred from the Doppler shift. One can further measure the Shapiro delay [365] in binaries with highly inclined orbits to deduce the mass of the companion as the radiation from the pulsar is further delayed by the gravity of the companion when the beam passes near it.

The most massive neutron stars observed by this method are PSR J1614-2230 with a mass of $M = 1.97 \pm 0.04M_\odot$ [366], PSR J0348+0432 with $M = 2.01 \pm 0.04M_\odot$ [367], and MSP J0740+6620 with $M = 2.14^{+0.10}_{-0.09}M_\odot$ [368], all with 1-σ confidence intervals.

Together with Low-Mass X-Ray Binary (LMXB) measurements (see *e.g.* Refs. [369, 370]), these measurements provide convincing evidence for the existence of a neutron star with $M \approx 2M_\odot$, providing us with a stringent lower bound for the maximum mass of a neutron star.

[1] There are also other speculated possibilities, such as quark and twin stars, none of which have yet been confirmed by observations.

[2] Quickly rotating compact stars [362], which emit electromagnetic radiation. The beam that the pulsar emits is usually misaligned with the spin axis, making it seem to pulse when observed from Earth.

There are no widely accepted observational upper bounds for the maximum mass of a neutron star. However, the electromagnetic signal from the kilonova counterpart to GW170817 (which we will discuss shortly) suggests that the remnant of the neutron star merger collapsed into a black hole. This would set an upper bound for a mass of a non-rotating neutron star, with the estimates being around $2.2M_\odot$ [371–373].

Radius Measurements

Radius measurements of neutron stars have proven extremely difficult due to the small size of, and large distance to the objects in question. However, the measurements have been getting increasingly better in the past years, with multiple different strategies being developed.

Some interesting developments include the publication of the results by the *NICER* collaboration [374, 375], which studied the energy-dependent X-ray pulse waveform data from the isolated millisecond pulsar PSR J0030+0451. They had two independent teams develop codes to determine the pulse waveforms, using different models for the X-ray emitting spots on the surface of the pulsar as well as for the instrumental response. The teams arrived at consistent estimates for the mass and radius of the pulsar, with the 1-σ results being indicated in Fig. 6.1, with the data by Riley *et al.* in black and Miller *et al.* in blue.

Further promising results are achieved by applying state-of-the art atmospheric models to data for the time-evolving type-I X-ray burst cooling tail spectra from LMXBs. The thermonuclear bursts originate from the matter from the accretion hitting the surface and sinking into the star until the pressure is high enough to fuse the nuclei together, starting a chain reaction that engulfs the surface of the star, releasing a burst of X-rays, until all the new fuel is exhausted. From observing the cooling tails of these bursts, one can infer properties such as the radius of the star, assuming one knows the composition of the neutron star atmosphere. In Fig. 6.1, we indicate some of these results; LMXB 4U 1702-429 (in dark cyan) from Ref. [376], 4U 1724-307 (in magenta), and SAX J1810.8-2609 (in light green) from Ref. [377]

Tidal Deformability Measurements from Neutron Star Mergers

The recent gravitational wave detection of a neutron star merger [6] has unlocked new possibilities in probing neutron star properties. For our interests here, the most relevant parameter that can be inferred from the data is the tidal deformability Λ, which quantifies the effect of an external tidal field on the induced quadrupole moment of the star [378, 379]. This deformation enhances gravitational wave emission, accelerating the decay of the inspiral, and thus affecting the signal [378].

The parameter Λ is given by the equation [378, 379]

$$\Lambda = \frac{2}{3} k_2 \left(\frac{c^2}{G} \frac{R}{M} \right)^5 , \tag{6.1}$$

where R is the radius of the star, M is its mass and the parameter k_2 is called the second Love

number, the definition of which can be found in Ref. [379]. To determine k_2 for a given star, one needs to know its mass and the EoS, making the determination of the tidal deformability a subtle question.

In Ref. [5], the authors used Bayesian analysis to determine Λ based on the gravitational wave observation from the inspiral. They sampled different equations of state[3], requiring the EoS to be causal, thermodynamically stable and internally and observationally consistent, and assuming that both of the infalling bodies were slowly spinning neutron stars described by the same EoS, they generated pairs of tidal deformabilities which were then used to compute waveform templates for the merger events.

In this manner the tidal deformability for a $M = 1.4M_\odot$ star was constrained with low-spin priors to [5]

$$70 \leq \Lambda(1.4M_\odot) \leq 580\,, \tag{6.2}$$

which provides a tighter constraint on Λ compared to the initial analysis in Ref. [4], where they provided an upper limit $\Lambda < 800$ for the value. This is due to the assumption made in the later analysis that both bodies involved in the merger were neutron stars described by the same EoS, and have spins within the range of observed Galactic binary neutron stars.

The discussion of the exact dynamics of the merging system after the neutron stars touch is beyond the scope of this thesis. The merger process has been recently reviewed in Ref. [380]. However, suffice to say that with some caution we can relate some of the characteristic frequencies of the gravitational wave signal – including peak frequencies of the power spectral density of the postmerger phase and the instantaneous frequency at the time of the merging of the stars – back to observables computable from the EoS by universal relations based on hydrodynamics and general relativity simulations [381–385].

6.1.2 Equation of State and the Structure of a Neutron Star

Although the first observations of neutron stars were made in 1967, their existence was already proposed on a theoretical basis by Baade and Zwicky in 1934 [4] [388]. The theoretical interest in neutron stars has increased in recent years because of the tantalizing prospects the observations discussed above present. Due to their enormous density, neutron stars provide us with an extraterrestrial laboratory to study the properties of QCD in extreme conditions differing from the one studied in heavy-ion collisions, where the baryon densities are meager due to the presence of antiparticles, but which probe considerably higher temperatures than are reached inside neutron stars.

The connection between the thermodynamic properties of QCD at high densities (*i.e.* the EoS) and the measurable macroscopic characteristics of quiescent neutron stars is provided

[3] The parametrization itself is model dependent, as it assumed that the logarithm of the adiabatic index $\gamma = \mathrm{d}\ln p/\mathrm{d}\ln\varepsilon$ can be expressed as a polynomial of the pressure.

[4] Arguably Landau anticipated the existence of neutron star-like objects, comparable to big nuclei, already in 1931 [386, 387].

by the Tolman-Oppenheimer-Volkoff (TOV) equations [389, 390]. These equations allow us to determine the mass and the radius of a self-gravitating, non-rotating[5], spherically symmetric body in hydrostatic equilibrium, given an EoS and the central pressure of the star. Examples of $M - R$ curves can be seen in Fig. 6.1.

For an isotropic, spherically symmetric star with the ideal fluid energy-momentum tensor $T^{\mu\nu} = \mathrm{diag}(\varepsilon, p, p, p)$, the TOV equations can be written as

$$\frac{\mathrm{d}p}{\mathrm{d}r} = -\frac{G}{c^2}\frac{(\varepsilon + p/c^2)(m + 4\pi r^3 p/c^2)}{r(r - 2Gm/c^2)}\,, \tag{6.3}$$

$$\frac{\mathrm{d}m}{\mathrm{d}r} = 4\pi r^2 \frac{\varepsilon}{c^2}\,, \tag{6.4}$$

where m is the gravitational mass enclosed within distance r from the center, p is pressure and ε is energy density. For a neutron star with total mass of M and a radius of R, the boundary conditions in the center are $m(r = 0) = 0$ and $p(0) = p_c$ and $\varepsilon(0) = \varepsilon_c$, while at the surface $m(r = R) = M$, $p(R) = 0$ and $\varepsilon(R) = 0$. Using these equations, we could determine the exact $M - R$ curve that encompasses all neutron stars fulfilling the above conditions, if we would just know the exact EoS.

As was foreshadowed in Section 2.6, the dense, zero-temperature EoS is known to certain extent for beta-equilibrated, strongly coupled matter in two opposing limits. In the low-density limit, we can use both established nuclear physics models (see *e.g.* Ref. [395] and references therein), and Chiral Effective Theory (CET) [137–139], to build the EoS. These various nuclear matter models are constructed in the small density regime, where the physics is well understood, and are then extrapolated to higher densities. There is a limit to their applicability – namely, relying on the interactions between the nucleons being weak – causing the extrapolations to eventually break down. CET, which is the state-of-the-art effective theory for neutron matter, is expected to be more or less valid up until the baryon number density n_B is between $1n_s$ to $2n_s$, where $n_s = 0.16/\mathrm{fm}^3$ is called the nuclear saturation density. Beyond this point, non-perturbative effects are expected to lead to large differences in the equation of state [396–398].

At very high densities, asymptotic freedom ensures that eventually the coupling constant admits perturbative computations [140, 399, 400]. The perturbative computations have uncertainties in the EoS comparable to the CET calculations around $n_B = 40n_s$ [400, 401], where n_B is the baryon number density. Between these two regimes, there is a gap in our knowledge, as the established methods are not suited to deal with intermediate chemical potentials.

The cores of heavier neutron stars are expected to have a density of around $n_B \sim 5 - 10n_s$, meaning that the densities of neutron star cores fall well within this intermediate theoretical nether-realm. However, various nuclear matter models are still applicable to study the (surface) structure of neutron stars with some certainty.

[5]For slowly rotating stars, a set of equations can be found in *e.g.* Refs. [391, 392]. The discussion for rapidly rotating stars is more involved, and can be found in *e.g.* Refs. [393, 394]

The Structure of Neutron Stars

Based on the models discussed above, the structure of a neutron star can be roughly divided into three regions: the core, the crust and the atmosphere. Of these, the atmosphere consists of the familiar, non-degenerate matter: electrons, ions, atoms and even molecules, but the thickness of the layer is only $\mathcal{O}(\text{cm})$ [402]. While the atmosphere does not significantly contribute to the mass of the star, it is a key factor in determining the spectrum of the electromagnetic radiation coming from the surface of the star, as was pointed out earlier in this chapter when we discussed the radius measurements.

Beneath the atmosphere is the $\mathcal{O}(\text{km})$ thick crust comprising of different sub-layers, which may differ depending on the formation and the magnetic field of the star. The outermost layer consists of a solid Coulomb crystal of charged particles, such as iron nuclei. As one goes deeper in the crust, the fraction of free neutrons grows as the neutrons drip out of the nuclei, forming a gas of neutrons in which the nuclei are embedded in the inner crust. Eventually, the matter becomes so neutron-rich and the pressure so high that the matter forms a uniform liquid of nucleons and electrons, with neutrons making the bulk of this strongly interacting Fermi liquid. Below this layer the so called "pasta" layer, which forms as the nucleons pack close enough together to arrange themselves into various exotic configurations, is believed to exist. In the familiar picture, this is usually taken to be the bottom-most layer before the crust-core interface, the exact location of which depends on the EoS, but is generally at around $n_B \sim n_s$, as beyond that point the nucleons begin to overlap, forming uniform nuclear matter. The structure of the crust is reviewed in detail in *e.g.* Ref. [403].

The exact nature of the core, which is multiple kilometers thick and makes up a substantial fraction of the total mass of the star, remains an open question. We have some certainty with regards to the outer part of the core, which consists of nuclear matter, together with electrons and possibly muons, with the physics being determined by beta equilibrium and many-body nuclear interactions, as depicted by *ab-initio* methods. Below this layer, the results are heavily model dependent, and the uncertainties in the EoSs grow significant, with various possibilities in even the particle composition of the core being open.

Even if we have no tractable first-principles description of the core, its existence provides us with an opportunity to study and constrain the QCD EoS in the intermediate regime of $n_s < n_B < 40n_s$ by the use of astrophysical observations. Recent years have seen a lot of work in this strain (see *e.g.* Refs. [401, 404–406] and references therein), and they usually include some sort of interpolation between the two known realms, with some physical limitations, such as causality and thermodynamic stability, being imposed on the interpolating functions. These interpolating EoSs are then put through the TOV equations, and the astrophysical constraints are imposed on the resulting $M - R$ curves and tidal deformabilities, allowing one to also constrain the space of possible interpolating functions.

6.2 Neutron Stars in V-QCD

One cannot *a priori* know for certain, how well applicable holographic methods are in the study of neutron stars. However, the success of holography in describing hot QGP might embolden us to at least ponder whether it could also teach us something at finite baryon density. The ability of holography to do so is not at all obvious at a glance, as the physics of matter at finite density depend on N_c, whereas the gravity limit within the bulk dual framework relies heavily on $N_c \to \infty$. However, as we have discussed in the text above, we now are able to include backreacted fundamental flavor in the holographic description, along with describing finite chemical potential. Together with recent studies on both finite density quark matter and neutron star physics (see *e.g.* Refs. [219, 407–412]) using holographic methods give us a reason for optimism.

In articles **I** and **III**, we applied V-QCD to the study of the dense, cold QCD matter. In **I**, we were using polytropic interpolations similar to the ones in Ref. [405] to quantify our ignorance of the nuclear matter phase as we were describing the quark matter phase using holography. In **III**, we expanded on this work, doing away with the interpolations and including baryons in the homogeneous approximation in our description of the nuclear matter phase. As the later work in article **III** complements and furthers the analysis that begun in article **I**, and the unique content of article **I** – the fitting of the flavor potentials – was already discussed in Section 4.2.2, we will not describe the results of **I** concerning neutrons stars here in detail.

As was mentioned in Section 4.1.2, the homogeneous approximation can only be expected to be accurate when the interactions between the nucleons making up the nuclear matter are strong and the baryon density is high. To complement this strongly coupled approach and in an effort to quantify our ignorance of the correct weakly-coupled holographic nuclear matter EoS, we employed the use of various nuclear matter models, the use of which we will discuss next. From the point of view of the nuclear matter models, the holographic approach also complements them, as they are reliable only up to around two times the nuclear saturation density, which is much smaller than the transition density to quark matter.

6.2.1 Hybrid Equations of State

To combine the holographic and weakly coupled nuclear matter EoSs, we need to make the transition as smooth as possible, since the two models are supposed to be different descriptions of the same matter. In practice, we can only make the transition a second order one, as we have two unfixed parameters in the holographic nuclear matter phase: c_b, which acts as a normalization of the pressure in the holographic model; and b, which controls the location of the instanton in the bulk and its coupling to the tachyon, as was discussed in Section 4.1.2.

Using these two parameters, we can join a given nuclear matter model with the V-QCD model together at a given matching density $n_{\rm tr}$ by requiring that both the pressure and its first derivative with respect to the chemical potential are equal in both descriptions in that point.

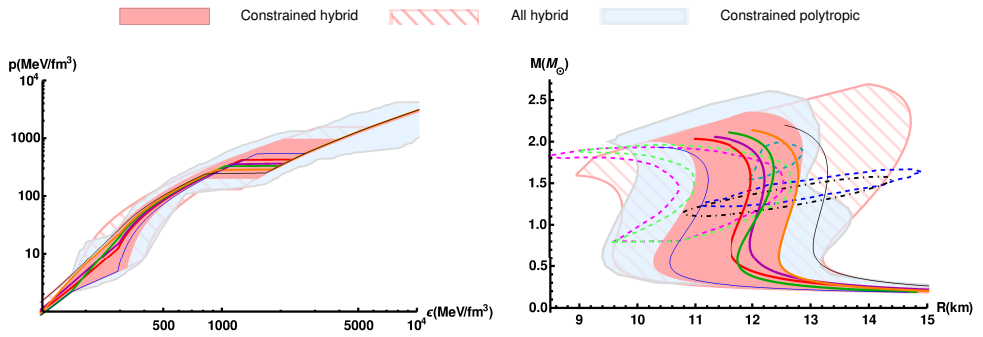

Figure 6.1: (Left) The EoS cloud spanned by the hybrid EoSs. On the vertical axis is pressure p and on the horizontal axis is energy density ϵ. The EoSs satisfying both the maximum mass and the tidal deformability constraints span the light red band, whereas the excluded EoSs span the striped band. Also presented is the cloud spanned by the polytropic interpolations between the nuclear matter and the pQCD EoSs, which also satisfy both the astrophysical constraints. Along with the bands, we present some examples of hybrid EoSs for the different nuclear matter models used, combined with potential **7a** at $n_{\rm tr}/n_s = 1.9$, with a thick curve indicating that the EoS satisfies the constraints.
(Right) The mass-radius cloud spanned by the hybrid EoSs. Also indicated are the 1-σ results discussed in Section 6.1.1, with the *NICER* analysis on PSR J0030+0451 from Ref. [374] being marked by the dashed blue line and from Ref. [375] with the dashed black line, along with the fits for the time-evolving X-ray burst spectra for 4U 1702-429 (dark cyan) from Ref. [376], 4U 1724-307 (magenta) and SAX J1810.8-2609 (light green), both from Ref. [377].

This gives us a family of EoSs which are parametrized by the matching density $n_{\rm tr}$ between the two parts. We choose to examine the values lying within the range $1.2n_s \leq n_{\rm tr} \leq 2.6n_s$, which, as we will see shortly, is sufficient considering the constraints. This allows us to compute the EoS varying $n_{\rm tr}$. We can then compute the astrophysical observables for these EoSs and apply astrophysical constraints to limit our choice of $n_{\rm tr}$.

The matching density is not the only unknown parameter, however. As was discussed in Section 4.2.2, the fitting of the flavor sector of V-QCD allows for different choices of parameters that all result in excellent fits to the $\mu_B = 0$ lattice data. To represent the different possible choices we analyzed in article **I**, we chose to work with three of the potentials in article **III**, specifically potentials **5b**, **7a**, and **8b**, ordered here from the softest to the stiffest[6]. It bears repeating that for any given potential, the model describes both the dense nuclear matter phase and the quark matter phase, with a first order transition between them. The strength of this transition depends on the choices of the parameters c_b and b, which will be determined by constraining $n_{\rm tr}$.

To allow for generic predictions to be made from our construction, and to properly parametrize the uncertainty that is involved with models of nuclear matter at finite densities, we also

[6]The stiffer the EoS, the larger the pressure for a given density. A consistently stiffer EoS means that the matter resists compression, leading to a larger radius for a given mass.

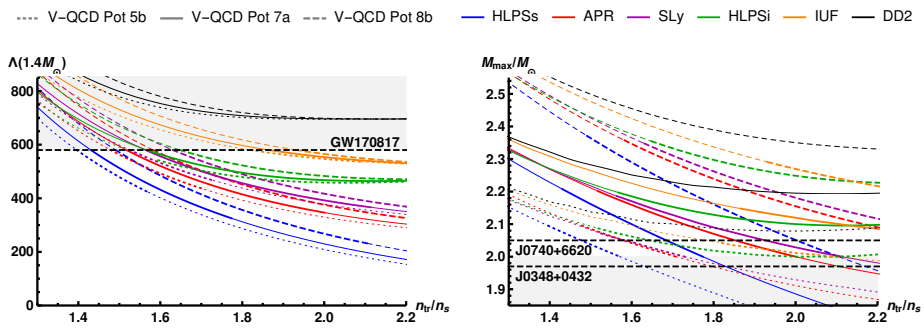

Figure 6.2: The tidal deformability $\Lambda(1.4M_\odot)$ (left) and the maximum mass (right) constraints on the hybrid equations of state. The different colors indicate the nuclear matter model used, as explained by the label, and the dotted, solid and dashed curves correspond with different choices of potentials in V-QCD, the parametrizations of which are explained in Appendix A in article **III**.

considered a wide range of different nuclear matter models, as mentioned earlier. Varying from soft to stiff, the models were the Hebeler-Lattimer-Petchick-Schwenk (HLPS) soft [138], Akmal-Pandharipande-Ravenhall (APR) [413], Skyrme-Lyon (SLy) [414, 415], HLPS intermediate, IUF [416, 417] and DD2 [418]. For our purposes, we need not consider EoSs that are stiffer than DD2, as it is already too stiff to pass the astrophysical constraints, as we will see.

To summarize the construction, the hybrid EoSs effectively describe three regions:

- Weakly coupled nuclear matter, described by one of the nuclear matter models

  $\updownarrow$ 2^{nd} order transition at $n = n_{\text{tr}}$

- Dense nuclear matter described by V-QCD

  $\updownarrow$ 1^{st} order transition at $n = n_b$

- Quark matter described by V-QCD

Having constructed the hybrid EoSs, we can compute the associated $M - R$ curves and the tidal deformabilities and impose constraints on them based on the maximum observed mass (which we take to be $2M_\odot$) and the tidal deformability of a $1.4M_\odot$ neutron star. The cloud of EoSs and $M - R$ curves spanned by the hybrid EoS is presented in Fig. 6.1. Both M_{max} and $\Lambda(1.4M_\odot)$ are presented in Fig. 6.2 as a function of the matching density n_{tr}.

The zones excluded by the constraints are indicated in the plots in Fig. 6.2 by the gray regions, and the thick curves indicate the EoSs which pass both constraints. Different models of nuclear matter are indicated by different colors, whereas the different dashings correspond to different choices of V-QCD potentials. Also shown are the 1-σ lower bounds for the mass measurements for both J0348+0432 and J0740+6620 discussed previously in the chapter. One can immediately note that the astrophysical constraints rule out the hybrid EoSs with DD2, effectively determining

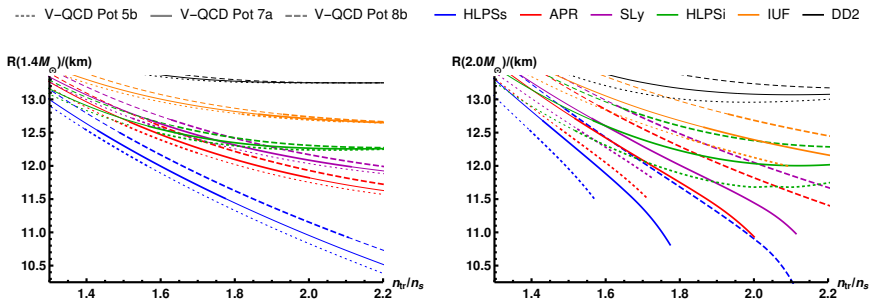

Figure 6.3: Radius of a 1.4 solar mass (left) and 2.0 solar mass (right) neutron star as a function of the matching density $n_{\rm tr}$. The thick curves satisfy the imposed astrophysical constraints.

an upper limit to the stiffness of the weakly coupled part of the nuclear matter EoS.

Because both curves are monotonically descending, the upper limit for $\Lambda(1.4M_\odot)$ acts as a lower limit for $n_{\rm tr}$, and the lower limit for $M_{\rm max}$ acts as an upper limit for $n_{\rm tr}$, bracketing the permissible values for $n_{\rm tr}$.

6.2.2 Some Key Results

In article **III**, we discussed the results for a multitude of different observables from the analysis of the hybrid EoSs. Here we will only focus on a few of them that seem especially relevant for the preceding discussion.

The hybrid EoSs favor relatively large neutron star radii. The smallest of these radii are achieved using HLPS soft together with the (generically considerably stiff) V-QCD EoS. This large change in the stiffness of the EoS causes a considerable jump in the speed of sound at the matching density. The EoSs more regular in the speed of sound favor larger radii. The radii at both $1.4M_\odot$ and at $2M_\odot$ are presented in Fig. 6.3 as functions of the transition density. Considered *en masse*, the hybrid EoSs satisfying the astrophysical constraints predict that the radius of a 1.4 solar mass star is within the range

$$10.9\ \text{km} \lesssim R(1.4M_\odot) \lesssim 12.8\ \text{km}\,. \tag{6.5}$$

Similarly, due to the stiffness of the EoSs, the produced tidal deformabilities are on the larger side, with all constrained EoSs having

$$\Lambda(1.4M_\odot) \gtrsim 230\,. \tag{6.6}$$

We should also note that for the hybrid EoSs satisfying the astrophysical constraints, the deconfinement transition is strongly first order, with the latent heat $\Delta\epsilon \gtrsim 700\ \text{MeV/fm}^3$. This, together with the fact that for central pressures that could support quark matter the TOV equations prove unstable (*i.e.* $\mathrm{d}M/\,\mathrm{d}r > 0$), makes quark matter cores in cold, quiescent neutron stars unstable. We also came to the same conclusion in article **I**, where we used the V-QCD

EoS for quark matter and combined it with quardutropes for nuclear matter. This does not however mean that quasistable quark matter cores could not exist in mergers, as the latent heat is expected to decrease with increasing temperature [419].

This finding is in stark contrast with analysis of *e.g.* Annala *et al.* [401], who claim that massive neutron stars most likely contain massive quark matter cores. Their analysis was based on multiple different kinds of interpolating functions – piecewise polytropic interpolations of the pressure as a function of baryon density, spectral interpolations of the adiabatic index, and piecewise linear interpolations of the speed of sound c_s^2 – between the two well-controlled regimes, and imposing astrophysical constraints similar to ours.

This disparity between the two approaches raises interesting questions, which have not yet been fully explained, but to some extent they could be reflective of the assumptions Annala *et al.* make about the adiabatic index $\gamma = \frac{\mathrm{d}\ln p}{\mathrm{d}\ln \varepsilon}$ in the quark matter phase, namely that if $\gamma < 1.75$, the EoS is describing a quark matter phase. However, for the hybrid EoSs, almost all models show a high peak in γ just above the matching density n_{tr}, after which the index decreases fast, reaching values near 1.5 in the nuclear matter phase. Because this kind of behavior does not seem common in other models of nuclear matter, this might provide smoking gun evidence for holography in dense stars.

Chapter 7

Summary

In this thesis, we have discussed the application of holographic methods to probe the QCD phase diagram, studying both out-of-equilibrium processes in the high-temperature, low-baryon density region, and in the high-density, low-temperature regime of neutron stars.

The motivation for using holography to study QCD is founded on the theory being strongly coupled at low energies, which has provided researchers with theoretical challenges for decades. To combat this, frameworks such as lattice QCD have been developed, but they too have their shortcomings, namely reproducing real-time dynamics and finite chemical potentials.

The need for new methods to tackle strongly coupled systems has been accentuated, as both the high-temperature and high density realms of the QCD phase diagram have become under newfound empirical scrutiny. This has been made possible by both the collider experiments probing the properties of hot QCD matter resulting from heavy-ion collisions, as well as the recent gravitational wave detection of a neutron star merger, which has allowed us an access to high-density laboratories out of reach for Earth-bound colliders.

Holography has arisen as a tool – if one wishes to view it as such – to study strongly coupled gauge theories by providing a link between said theories and weakly coupled gravity theories living in a higher-dimensional spacetime. However, there is still no known gravity dual for QCD, and so to study it, one needs to resort to modeling. The different holographic models have already had a lot of success in describing the dynamics of quark gluon plasma, its properties and hydrodynamization.

In Chapter 4, we presented the model that is in the heart of the articles that form this thesis. We considered the construction of the model, motivations behind choosing the action and the fusing together of the string-inspired gluonic action and the tachyonic Dirac-Born-Infeld flavor action, which are fully backreacted in the Veneziano limit. We also reviewed the recently introduced homogeneous approximation of baryons within the V-QCD framework that allows us to include a description of nuclear matter in the description of the QCD phase diagram, a holographic version of which was also provided later on in the chapter. We also discussed the effective potentials, and how their asymptotics are determined so as to reproduce qualitative properties of QCD, such as confinement and the logarithmic running of the coupling, and we

then used both the running coupling and lattice QCD results to fix parameters. The resulting fits were stiff, and for the flavor potential, multiple different sets of parameter choices produce equally good fits, thus calling for further constraints on the model, as was found in article **I**.

However, we first discussed the phenomenology associated with heavy-ion collisions, and discussed the work done in article **II**, where we considered the quasinormal mode spectrum of a scalar field for a range of temperatures from T_c up to $3T_c$ in the gluonic part of V-QCD, Improved Holographic QCD. The quasinormal mode spectrum of the gravity dual is connected to the equilibration of the boundary theory, and therefore we could make predictions on the thermalization timescale associated with the out-of-equilibrium plasma that is created in heavy-ion collisions. We obtained a very phenomenologically reasonable estimate for the thermalization time of the correlator. Moreover, we found qualitatively interesting behavior associated with the quasinormal mode spectrum: instead of a clean spectrum of individual modes, there emerged an additional a linear structure parallel to the real axis of the complex frequency plane, the existence of which might be interpreted to suggest the presence of a branch cut. Similar behavior of has been observed in both kinetic theory [420] and some holographic models at finite coupling [234, 421].

After that, we moved to discuss neutron stars, both from the point of view of astronomical observations as well as particle physics. This, in the dual purpose of constraining the effective potentials – including the description of strongly coupled nuclear matter as in article **III** – by the use of astrophysical constraints, and also to see if we could already make some predictions on the structure and properties of neutron stars. We found that V-QCD, combined with nuclear models in the weakly coupled regime in an effort to parametrize our ignorance on the weakly coupled nuclear matter description, provides viable equations of state which satisfy the current astrophysical bounds. The model has strong predictive power, with the qualitative features of the models being similar with different parameter choices. The constructed hybrid equations of state were generically stiff, producing stars with larger radii, tidal deformabilities and speeds of sound. The model does not support the existence of stable quark matter cores within quiescent neutron stars.

In the future, both of these lines of research could be furthered in many ways. In the study of the quasinormal mode spectrum, it would be interesting to use the full V-QCD machinery by including dynamical quarks, and to further study the emerging linear structure in the complex frequency plane and include $\mathbf{q} \neq 0$ into the fluctuation equations. Whereas in the case of neutron stars, one could improve on the description of the nuclear matter phase and include non-zero or even flavor-dependent quark masses. Also, if one wishes to fully study neutron star mergers within the model, the finite temperature effects cannot be ignored. Most of these improvements are quite realistically implemented soon, and we will hopefully get an even more vivid picture of the possibilities that holography provides for the study of QCD.

References

[**I**] N. Jokela, M. Järvinen, and J. Remes: "Holographic QCD in the Veneziano limit and neutron stars". *JHEP* **03** (2019), 041. arXiv: 1809.07770 [hep-ph].

[**II**] T. Alho, J. Remes, K. Tuominen, and A. Vuorinen: "Quasinormal modes and thermalization in Improved Holographic QCD". *Phys. Rev. D* **101**.10 (2020), 106025. arXiv: 2002.09544 [hep-ph].

[**III**] N. Jokela, M. Järvinen, G. Nijs, and J. Remes: "Unified weak/strong coupling framework for nuclear matter and neutron stars" (June 2020). arXiv: 2006.01141 [hep-ph].

[1] T. Kuhn: *The Structure of Scientific Revolutions*. 1st ed. The University of Chigago Press, 1962. ISBN: 9780226458113.

[2] P. de Forcrand: "Simulating QCD at finite density". *PoS* **LAT2009** (2009). Ed. by C. Liu and Y. Zhu, 010. arXiv: 1005.0539 [hep-lat].

[3] J. Berges, S. Borsanyi, D. Sexty, and I.-O. Stamatescu: "Lattice simulations of real-time quantum fields". *Phys. Rev. D* **75** (2007), 045007. arXiv: hep-lat/0609058.

[4] B. Abbott et al.: "GW170817: Observation of Gravitational Waves from a Binary Neutron Star Inspiral". *Phys. Rev. Lett.* **119**.16 (2017), 161101. arXiv: 1710.05832 [gr-qc].

[5] B. Abbott et al. LIGO Scientific, Virgo: "GW170817: Measurements of neutron star radii and equation of state". *Phys. Rev. Lett.* **121**.16 (2018), 161101. arXiv: 1805.11581 [gr-qc].

[6] B. Abbott et al.: "Multi-messenger Observations of a Binary Neutron Star Merger". *Astrophys. J. Lett.* **848**.2 (2017), L12. arXiv: 1710.05833 [astro-ph.HE].

[7] J. M. Maldacena: "The Large N limit of superconformal field theories and supergravity". *Adv.Theor.Math.Phys.* **2** (1998), 231–252. arXiv: hep-th/9711200.

[8] G. Policastro, D. T. Son, and A. O. Starinets: "The Shear viscosity of strongly coupled N=4 supersymmetric Yang-Mills plasma". *Phys. Rev. Lett.* **87** (2001), 081601. arXiv: hep-th/0104066 [hep-th].

[9] J. Casalderrey-Solana, H. Liu, D. Mateos, K. Rajagopal, and U. A. Wiedemann: "Gauge/String Duality, Hot QCD and Heavy Ion Collisions" (2011). arXiv: 1101.0618 [hep-th].

[10] W. Ochs: "The Status of Glueballs". *J. Phys. G* **40** (2013), 043001. arXiv: 1301.5183 [hep-ph].

[11] C. J. Morningstar and M. J. Peardon: "The Glueball spectrum from an anisotropic lattice study". *Phys. Rev. D* **60** (1999), 034509. arXiv: hep-lat/9901004.

[12] N. Brambilla et al.: "QCD and Strongly Coupled Gauge Theories: Challenges and Perspectives". *Eur. Phys. J. C* **74**.10 (2014), 2981. arXiv: 1404.3723 [hep-ph].

[13] C. A. Baker et al.: "Improved Experimental Limit on the Electric Dipole Moment of the Neutron". *Physical Review Letters* **97**.13 (2006). ISSN: 1079-7114.

[14] J. M. Pendlebury et al.: "Revised experimental upper limit on the electric dipole moment of the neutron". *Phys. Rev. D* **92**.9 (2015), 092003. arXiv: 1509.04411 [hep-ex].

[15] B. Graner, Y. Chen, E. Lindahl, and B. Heckel: "Reduced Limit on the Permanent Electric Dipole Moment ofHg199". *Physical Review Letters* **116**.16 (2016). ISSN: 1079-7114.

[16] J. E. Kim and G. Carosi: "Axions and the Strong CP Problem". *Rev. Mod. Phys.* **82** (2010). [Erratum: Rev.Mod.Phys. 91, 049902 (2019)], 557–602. arXiv: 0807.3125 [hep-ph].

[17] M. Tanabashi et al. Particle Data Group: "Review of Particle Physics". *Phys. Rev. D* **98**.3 (2018), 030001.

[18] L. Faddeev and V. Popov: "Feynman Diagrams for the Yang-Mills Field". *Phys. Lett. B* **25** (1967). Ed. by J.-P. Hsu and D. Fine, 29–30.

[19] J. Donoghue, E. Golowich, and B. R. Holstein: *Dynamics of the standard model*. **2**. Cambridge University Press, 1992. ISBN: 0-521-36288-1.

[20] D. J. Gross and F. Wilczek: "Ultraviolet Behavior of Nonabelian Gauge Theories". *Phys.Rev.Lett.* **30** (1973), 1343–1346.

[21] H. D. Politzer: "Reliable Perturbative Results for Strong Interactions?" *Phys.Rev.Lett.* **30** (1973), 1346–1349.

[22] T. van Ritbergen, J. Vermaseren, and S. Larin: "The Four loop beta function in quantum chromodynamics". *Phys. Lett. B* **400** (1997), 379–384. arXiv: hep-ph/9701390.

[23] W. A. Bardeen, A. Buras, D. Duke, and T. Muta: "Deep Inelastic Scattering Beyond the Leading Order in Asymptotically Free Gauge Theories". *Phys. Rev. D* **18** (1978), 3998.

[24] E. D. Bloom et al.: "High-Energy Inelastic $e - p$ Scattering at 6° and 10°". *Phys. Rev. Lett.* **23** (16 1969), 930–934.

[25] F. Herzog, B. Ruijl, T. Ueda, J. Vermaseren, and A. Vogt: "The five-loop beta function of Yang-Mills theory with fermions". *JHEP* **02** (2017), 090. arXiv: 1701.01404 [hep-ph].

[26] M. Göckeler, R. Horsley, V. Linke, P. E. Rakow, G. Schierholz, and H. Stuben: "Is there a Landau pole problem in QED?" *Phys. Rev. Lett.* **80** (1998), 4119–4122. arXiv: hep-th/9712244.

[27] G. 't Hooft: "A Planar Diagram Theory for Strong Interactions". *Nucl. Phys. B* **72** (1974). Ed. by J. Taylor, 461.

[28] A. V. Manohar: "Large N QCD". *Les Houches Summer School in Theoretical Physics, Session 68: Probing the Standard Model of Particle Interactions*. Feb. 1998, 1091–1169. arXiv: `hep-ph/9802419`.

[29] E. Witten: "Baryons in the 1/n Expansion". *Nucl. Phys. B* **160** (1979), 57–115.

[30] S. Bethke: "The 2009 World Average of $\alpha(s)$". *Eur.Phys.J.* **C64** (2009), 689–703. arXiv: `0908.1135 [hep-ph]`.

[31] K. G. Wilson: "Confinement of Quarks". *Phys.Rev.* **D10** (1974), 2445–2459.

[32] G. 't Hooft: "On the Phase Transition Towards Permanent Quark Confinement". *Nucl. Phys. B* **138** (1978), 1–25.

[33] G. 't Hooft: "A Property of Electric and Magnetic Flux in Nonabelian Gauge Theories". *Nucl. Phys. B* **153** (1979), 141–160.

[34] G. 't Hooft: "Topology of the Gauge Condition and New Confinement Phases in Nonabelian Gauge Theories". *Nucl. Phys. B* **190** (1981), 455–478.

[35] A. Manohar and H. Georgi: "Chiral Quarks and the Nonrelativistic Quark Model". *Nucl. Phys. B* **234** (1984), 189–212.

[36] L. Gribov, E. Levin, and M. Ryskin: "Semihard Processes in QCD". *Phys. Rept.* **100** (1983), 1–150.

[37] A. Chodos, R. Jaffe, K. Johnson, C. B. Thorn, and V. Weisskopf: "A New Extended Model of Hadrons". *Phys. Rev. D* **9** (1974), 3471–3495.

[38] P. Hasenfratz: "Nonperturbative Methods in Quantum Field Theory". *23rd International Conference on High-Energy Physics*. July 1986.

[39] M. Fukugita: "Present Status od Numerical Quantum Chromodynamics". *CCAST (China Center for Advanced Study and Technology) (World Laboratory) Symposium/Workshop: Lattice gauge theory using parallel processors*. June 1987.

[40] B. Ioffe: "Axial anomaly: The Modern status". *Int. J. Mod. Phys. A* **21** (2006), 6249–6266. arXiv: `hep-ph/0611026`.

[41] Y. Nambu and G. Jona-Lasinio: "Dynamical Model of Elementary Particles Based on an Analogy with Superconductivity. 1." *Phys. Rev.* **122** (1961). Ed. by T. Eguchi, 345–358.

[42] M. E. Peskin and D. V. Schroeder: *An Introduction to quantum field theory*. Advanced book program. Westview Press Reading (Mass.), 1995. ISBN: 0-201-50934-2.

[43] M. E. Peskin: "Chiral Symmetry and Chiral Symmetry Breaking". *Les Houches Summer School in Theoretical Physics: Recent Advances in Field Theory and Statistical Mechanics*. Dec. 1982.

[44] C. W. Bernard, T. Blum, C. E. Detar, S. A. Gottlieb, U. M. Heller, J. E. Hetrick, K. Rummukainen, R. Sugar, D. Toussaint, and M. Wingate: "Which chiral symmetry is restored in high temperature QCD?" *Phys. Rev. Lett.* **78** (1997), 598–601. arXiv: `hep-lat/9611031`.

[45] R. Rapp and J. Wambach: "Chiral symmetry restoration and dileptons in relativistic heavy ion collisions". *Adv. Nucl. Phys.* **25** (2000), 1. arXiv: `hep-ph/9909229`.

[46] A. Bazavov et al.: "Chiral crossover in QCD at zero and non-zero chemical potentials". *Phys. Lett. B* **795** (2019), 15–21. arXiv: `1812.08235 [hep-lat]`.

[47] F. R. Brown, F. P. Butler, H. Chen, N. H. Christ, Z.-h. Dong, W. Schaffer, L. I. Unger, and A. Vaccarino: "On the existence of a phase transition for QCD with three light quarks". *Phys. Rev. Lett.* **65** (1990), 2491–2494.

[48] H. Georgi: "Effective field theory". *Ann. Rev. Nucl. Part. Sci.* **43** (1993), 209–252.

[49] S. Glashow and S. Weinberg: "Breaking chiral symmetry". *Phys. Rev. Lett.* **20** (1968), 224–227.

[50] S. Weinberg: "Nonlinear realizations of chiral symmetry". *Phys. Rev.* **166** (1968), 1568–1577.

[51] S. R. Coleman, J. Wess, and B. Zumino: "Structure of phenomenological Lagrangians. 1." *Phys. Rev.* **177** (1969), 2239–2247.

[52] J. Callan Curtis G., S. R. Coleman, J. Wess, and B. Zumino: "Structure of phenomenological Lagrangians. 2." *Phys. Rev.* **177** (1969), 2247–2250.

[53] E. Epelbaum, H.-W. Hammer, and U.-G. Meißner: "Modern Theory of Nuclear Forces". *Rev. Mod. Phys.* **81** (2009), 1773–1825. arXiv: `0811.1338 [nucl-th]`.

[54] S. Weinberg: "Three body interactions among nucleons and pions". *Phys. Lett. B* **295** (1992), 114–121. arXiv: `hep-ph/9209257`.

[55] U. van Kolck: "Few nucleon forces from chiral Lagrangians". *Phys. Rev. C* **49** (1994), 2932–2941.

[56] L. Coraggio, A. Covello, A. Gargano, and N. Itaco: "Shell-model calculations for neutron-rich carbon isotopes with a chiral nucleon-nucleon potential". *Phys. Rev. C* **81** (2010), 064303. arXiv: `1005.2896 [nucl-th]`.

[57] S. Fujii, R. Okamoto, and K. Suzuki: "Ground-state and single-particle energies of nuclei around O-16, Ca-40, and Ni-56 from realistic nucleon-nucleon forces". *Phys. Rev. Lett.* **103** (2009), 182501. arXiv: `0908.3376 [nucl-th]`.

[58] G. Hagen, T. Papenbrock, D. Dean, and M. Hjorth-Jensen: "Ab initio coupled-cluster approach to nuclear structure with modern nucleon-nucleon interactions". *Phys. Rev. C* **82** (2010), 034330. arXiv: `1005.2627 [nucl-th]`.

[59] C. Forssen, P. Navratil, W. Ormand, and E. Caurier: "Large basis ab initio shell model investigation of Be-9 and Be-11". *Phys. Rev. C* **71** (2005), 044312. arXiv: `nucl-th/0412049`.

[60] P. H. Ginsparg: "Applied Conformal Field Theory". *Les Houches Summer School in Theoretical Physics: Fields, Strings, Critical Phenomena*. Sept. 1988, 1–168. arXiv: `hep-th/9108028`.

[61] P. Di Francesco, P. Mathieu, and D. Senechal: *Conformal Field Theory*. Graduate Texts in Contemporary Physics. New York: Springer-Verlag, 1997. ISBN: 978-0-387-94785-3, 978-1-4612-7475-9.

[62] G. Parisi: "Conformal invariance in perturbation theory". *Phys. Lett. B* **39** (1972), 643–645.

[63] W. E. Caswell: "Asymptotic Behavior of Nonabelian Gauge Theories to Two Loop Order". *Phys. Rev. Lett.* **33** (1974), 244.

[64] T. Banks and A. Zaks: "On the Phase Structure of Vector-Like Gauge Theories with Massless Fermions". *Nucl. Phys.* **B196** (1982), 189–204.

[65] R. Alkofer, C. S. Fischer, and F. J. Llanes-Estrada: "Vertex functions and infrared fixed point in Landau gauge SU(N) Yang-Mills theory". *Phys. Lett. B* **611** (2005). [Erratum: Phys.Lett.B 670, 460–461 (2009)], 279–288. arXiv: `hep-th/0412330`.

[66] S. J. Brodsky, S. Menke, C. Merino, and J. Rathsman: "On the behavior of the effective QCD coupling alpha(tau)(s) at low scales". *Phys. Rev. D* **67** (2003), 055008. arXiv: `hep-ph/0212078`.

[67] G. Aarts: "Introductory lectures on lattice QCD at nonzero baryon number". *J. Phys. Conf. Ser.* **706**.2 (2016), 022004. arXiv: `1512.05145 [hep-lat]`.

[68] T. Pichler, M. Dalmonte, E. Rico, P. Zoller, and S. Montangero: "Real-time Dynamics in U(1) Lattice Gauge Theories with Tensor Networks". *Phys. Rev. X* **6**.1 (2016), 011023. arXiv: `1505.04440 [cond-mat.quant-gas]`.

[69] J. B. Kogut: "An Introduction to Lattice Gauge Theory and Spin Systems". *Rev. Mod. Phys.* **51** (1979), 659.

[70] J. B. Kogut: "A Review of the Lattice Gauge Theory Approach to Quantum Chromodynamics". *Rev. Mod. Phys.* **55** (1983), 775.

[71] Z. Fodor and C. Hoelbling: "Light Hadron Masses from Lattice QCD". *Rev. Mod. Phys.* **84** (2012), 449. arXiv: `1203.4789 [hep-lat]`.

[72] H. B. Nielsen and M. Ninomiya: "Absence of Neutrinos on a Lattice. 1. Proof by Homotopy Theory" (Nov. 1980). Ed. by J. Julve and M. Ramón-Medrano. [Erratum: Nucl.Phys.B 195, 541 (1982)], 533–555.

[73] H. B. Nielsen and M. Ninomiya: "Absence of Neutrinos on a Lattice. 2. Intuitive Topological Proof". *Nucl. Phys. B* **193** (1981), 173–194.

[74] B. Sheikholeslami and R. Wohlert: "Improved Continuum Limit Lattice Action for QCD with Wilson Fermions". *Nucl. Phys. B* **259** (1985), 572.

[75] K. Jansen, C. Liu, M. Luscher, H. Simma, S. Sint, R. Sommer, P. Weisz, and U. Wolff: "Nonperturbative renormalization of lattice QCD at all scales". *Phys. Lett. B* **372** (1996), 275–282. arXiv: `hep-lat/9512009`.

[76] E. Follana, Q. Mason, C. Davies, K. Hornbostel, G. Lepage, J. Shigemitsu, H. Trottier, and K. Wong HPQCD, UKQCD: "Highly improved staggered quarks on the lattice, with applications to charm physics". *Phys. Rev. D* **75** (2007), 054502. arXiv: `hep-lat/0610092`.

[77] P. Hasenfratz and F. Karsch: "Chemical Potential on the Lattice". *Phys. Lett. B* **125** (1983), 308–310.

[78] Z.-X. Li, Y.-F. Jiang, and H. Yao: "Majorana-time-reversal symmetries: a fundamental principle for sign-problem-free quantum Monte Carlo simulations". *Phys. Rev. Lett.* **117**.26 (2016), 267002. arXiv: `1601.05780 [cond-mat.str-el]`.

[79] M. Cristoforetti, F. Di Renzo, and L. Scorzato AuroraScience: "New approach to the sign problem in quantum field theories: High density QCD on a Lefschetz thimble". *Phys. Rev. D* **86** (2012), 074506. arXiv: `1205.3996 [hep-lat]`.

[80] G. Aarts: "Can stochastic quantization evade the sign problem? The relativistic Bose gas at finite chemical potential". *Phys. Rev. Lett.* **102** (2009), 131601. arXiv: `0810.2089 [hep-lat]`.

[81] C. Allton, S. Ejiri, S. Hands, O. Kaczmarek, F. Karsch, E. Laermann, C. Schmidt, and L. Scorzato: "The QCD thermal phase transition in the presence of a small chemical potential". *Phys. Rev. D* **66** (2002), 074507. arXiv: `hep-lat/0204010`.

[82] S. Chandrasekharan and U.-J. Wiese: "Meron cluster solution of a fermion sign problem". *Phys. Rev. Lett.* **83** (1999), 3116–3119. arXiv: `cond-mat/9902128`.

[83] P. de Forcrand and O. Philipsen: "The QCD phase diagram for small densities from imaginary chemical potential". *Nucl. Phys. B* **642** (2002), 290–306. arXiv: `hep-lat/0205016`.

[84] M. D'Elia and M.-P. Lombardo: "Finite density QCD via imaginary chemical potential". *Phys. Rev. D* **67** (2003), 014505. arXiv: `hep-lat/0209146`.

[85] M. G. Alford, A. Kapustin, and F. Wilczek: "Imaginary chemical potential and finite fermion density on the lattice". *Phys. Rev. D* **59** (1999), 054502. arXiv: `hep-lat/9807039`.

[86] J. Kogut and D. Sinclair: "Lattice QCD at finite isospin density at zero and finite temperature". *Phys. Rev. D* **66** (2002), 034505. arXiv: `hep-lat/0202028`.

[87] P. de Forcrand, M. A. Stephanov, and U. Wenger: "On the phase diagram of QCD at finite isospin density". *PoS* **LATTICE2007** (2007). Ed. by G. Bali, V. Braun, C. Gattringer, M. Gockeler, A. Schafer, P. Weisz, and T. Wettig, 237. arXiv: 0711.0023 [hep-lat].

[88] P. Cea, L. Cosmai, M. D'Elia, A. Papa, and F. Sanfilippo: "Two-flavor QCD at finite quark or isospin density". *PoS* **LATTICE2012** (2012). Ed. by D. Leinweber, W. Kamleh, S. Mahbub, H. Matevosyan, A. Thomas, A. G. Williams, R. Young, and J. Zanotti, 067. arXiv: 1210.5896 [hep-lat].

[89] A. S. Kronfeld: "Twenty-first Century Lattice Gauge Theory: Results from the QCD Lagrangian". *Ann. Rev. Nucl. Part. Sci.* **62** (2012), 265–284. arXiv: 1203.1204 [hep-lat].

[90] R. A. Briceno, J. J. Dudek, and R. D. Young: "Scattering processes and resonances from lattice QCD". *Rev. Mod. Phys.* **90**.2 (2018), 025001. arXiv: 1706.06223 [hep-lat].

[91] C. Alexandrou and C. Kallidonis: "Low-lying baryon masses using $N_f = 2$ twisted mass clover-improved fermions directly at the physical pion mass". *Phys. Rev. D* **96**.3 (2017), 034511. arXiv: 1704.02647 [hep-lat].

[92] S. Olausen and V. Kaspi: "The McGill Magnetar Catalog". *Astrophys. J. Suppl.* **212** (2014), 6. arXiv: 1309.4167 [astro-ph.HE].

[93] G. Bali, F. Bruckmann, G. Endrődi, Z. Fodor, S. Katz, S. Krieg, A. Schafer, and K. Szabo: "The QCD phase diagram for external magnetic fields". *JHEP* **02** (2012), 044. arXiv: 1111.4956 [hep-lat].

[94] S. Godfrey and N. Isgur: "Mesons in a Relativized Quark Model with Chromodynamics". *Phys. Rev. D* **32** (1985), 189–231.

[95] S. Capstick and N. Isgur: "Baryons in a Relativized Quark Model with Chromodynamics". *AIP Conf. Proc.* **132** (1985). Ed. by S. Oneda, 267–271.

[96] F. Karsch, K. Redlich, and A. Tawfik: "Hadron resonance mass spectrum and lattice QCD thermodynamics". *Eur. Phys. J. C* **29** (2003), 549–556. arXiv: hep-ph/0303108.

[97] S. Chatterjee, D. Mishra, B. Mohanty, and S. Samanta: "Freezeout systematics due to the hadron spectrum". *Phys. Rev. C* **96**.5 (2017), 054907. arXiv: 1708.08152 [nucl-th].

[98] S. Borsanyi, Z. Fodor, S. D. Katz, S. Krieg, C. Ratti, and K. Szabo: "Fluctuations of conserved charges at finite temperature from lattice QCD". *JHEP* **01** (2012), 138. arXiv: 1112.4416 [hep-lat].

[99] A. Vuorinen: "The Pressure of QCD at finite temperatures and chemical potentials". *Phys. Rev. D* **68** (2003), 054017. arXiv: hep-ph/0305183.

[100] U. W. Heinz and M. Jacob: "Evidence for a new state of matter: An Assessment of the results from the CERN lead beam program" (Jan. 2000). arXiv: nucl-th/0002042.

[101] I. Arsene et al. BRAHMS: "Quark gluon plasma and color glass condensate at RHIC? The Perspective from the BRAHMS experiment". *Nucl. Phys.* **A757** (2005), 1–27. arXiv: nucl-ex/0410020 [nucl-ex].

[102] B. B. Back et al.: "The PHOBOS perspective on discoveries at RHIC". *Nucl. Phys.* **A757** (2005), 28–101. arXiv: nucl-ex/0410022 [nucl-ex].

[103] J. Adams et al. STAR: "Experimental and theoretical challenges in the search for the quark gluon plasma: The STAR Collaboration's critical assessment of the evidence from RHIC collisions". *Nucl. Phys.* **A757** (2005), 102–183. arXiv: nucl-ex/0501009 [nucl-ex].

[104] K. Adcox et al. PHENIX: "Formation of dense partonic matter in relativistic nucleus-nucleus collisions at RHIC: Experimental evaluation by the PHENIX collaboration". *Nucl. Phys.* **A757** (2005), 184–283. arXiv: nucl-ex/0410003 [nucl-ex].

[105] B. Müller, J. Schukraft, and B. Wyslouch: "First Results from Pb+Pb collisions at the LHC". *Ann. Rev. Nucl. Part. Sci.* **62** (2012), 361–386. arXiv: 1202.3233 [hep-ex].

[106] P. Jacobs and X.-N. Wang: "Matter in extremis: Ultrarelativistic nuclear collisions at RHIC". *Prog. Part. Nucl. Phys.* **54** (2005), 443–534. arXiv: hep-ph/0405125.

[107] B. Müller and J. L. Nagle: "Results from the relativistic heavy ion collider". *Ann. Rev. Nucl. Part. Sci.* **56** (2006), 93–135. arXiv: nucl-th/0602029.

[108] D. Teaney: "The Effects of viscosity on spectra, elliptic flow, and HBT radii". *Phys. Rev. C* **68** (2003), 034913. arXiv: nucl-th/0301099.

[109] H. Song and U. W. Heinz: "Causal viscous hydrodynamics in 2+1 dimensions for relativistic heavy-ion collisions". *Phys. Rev. C* **77** (2008), 064901. arXiv: 0712.3715 [nucl-th].

[110] D. Steineder, S. A. Stricker, and A. Vuorinen: "Probing the pattern of holographic thermalization with photons". *JHEP* **07** (2013), 014. arXiv: 1304.3404 [hep-ph].

[111] S. A. Stricker: "Holographic thermalization in N=4 Super Yang-Mills theory at finite coupling". *Eur. Phys. J. C* **74**.2 (2014), 2727. arXiv: 1307.2736 [hep-th].

[112] P. B. Arnold, G. D. Moore, and L. G. Yaffe: "Transport coefficients in high temperature gauge theories. 2. Beyond leading log". *JHEP* **05** (2003), 051. arXiv: hep-ph/0302165.

[113] J. Blaizot, E. Iancu, and A. Rebhan: "The Entropy of the QCD plasma". *Phys. Rev. Lett.* **83** (1999), 2906–2909. arXiv: hep-ph/9906340.

[114] A. Nakamura and S. Sakai: "Transport coefficients of gluon plasma". *Phys. Rev. Lett.* **94** (2005), 072305. arXiv: hep-lat/0406009.

[115] T. Lee and G. Wick: "Vacuum Stability and Vacuum Excitation in a Spin 0 Field Theory". *Phys. Rev. D* **9** (1974), 2291–2316.

[116] J. C. Collins and M. Perry: "Superdense Matter: Neutrons Or Asymptotically Free Quarks?" *Phys. Rev. Lett.* **34** (1975), 1353.

[117] E. V. Shuryak: "Quark-Gluon Plasma and Hadronic Production of Leptons, Photons and Psions". *Sov. J. Nucl. Phys.* **28** (1978), 408.

[118] T. Banks and A. Casher: "Chiral Symmetry Breaking in Confining Theories". *Nucl. Phys. B* **169** (1980), 103–125.

[119] S. Borsanyi, Z. Fodor, J. N. Guenther, R. Kara, S. D. Katz, P. Parotto, A. Pasztor, C. Ratti, and K. K. Szabo: "The QCD crossover at finite chemical potential from lattice simulations" (Feb. 2020). arXiv: 2002.02821 [hep-lat].

[120] S. Klevansky: "The Nambu-Jona-Lasinio model of quantum chromodynamics". *Rev. Mod. Phys.* **64** (1992), 649–708.

[121] A. Barducci, R. Casalbuoni, G. Pettini, and R. Gatto: "Chiral phases of QCD at finite density and temperature". *Phys. Rev. D* **49** (1994), 426–436.

[122] J. Berges and K. Rajagopal: "Color superconductivity and chiral symmetry restoration at nonzero baryon density and temperature". *Nucl. Phys. B* **538** (1999), 215–232. arXiv: hep-ph/9804233.

[123] A. M. Halasz, A. Jackson, R. Shrock, M. A. Stephanov, and J. Verbaarschot: "On the phase diagram of QCD". *Phys. Rev. D* **58** (1998), 096007. arXiv: hep-ph/9804290.

[124] M. G. Alford, K. Rajagopal, and F. Wilczek: "QCD at finite baryon density: Nucleon droplets and color superconductivity". *Phys. Lett. B* **422** (1998), 247–256. arXiv: hep-ph/9711395.

[125] R. Rapp, T. Schäfer, E. V. Shuryak, and M. Velkovsky: "Diquark Bose condensates in high density matter and instantons". *Phys. Rev. Lett.* **81** (1998), 53–56. arXiv: hep-ph/9711396.

[126] M. Kitazawa, T. Koide, T. Kunihiro, and Y. Nemoto: "Chiral and color superconducting phase transitions with vector interaction in a simple model". *Prog. Theor. Phys.* **108**.5 (2002). [Erratum: Prog.Theor.Phys. 110, 185–186 (2003)], 929–951. arXiv: hep-ph/0207255.

[127] C. Sasaki, B. Friman, and K. Redlich: "Quark Number Fluctuations in a Chiral Model at Finite Baryon Chemical Potential". *Phys. Rev. D* **75** (2007), 054026. arXiv: hep-ph/0611143.

[128] K. Fukushima: "Critical surface in hot and dense QCD with the vector interaction". *Phys. Rev. D* **78** (2008), 114019. arXiv: 0809.3080 [hep-ph].

[129] X. Luo and N. Xu: "Search for the QCD Critical Point with Fluctuations of Conserved Quantities in Relativistic Heavy-Ion Collisions at RHIC : An Overview". *Nucl. Sci. Tech.* **28**.8 (2017), 112. arXiv: 1701.02105 [nucl-ex].

[130] G. Endrődi, Z. Fodor, S. Katz, and K. Szabo: "The QCD phase diagram at nonzero quark density". *JHEP* **04** (2011), 001. arXiv: 1102.1356 [hep-lat].

[131] C. S. Fischer: "QCD at finite temperature and chemical potential from Dyson–Schwinger equations". *Prog. Part. Nucl. Phys.* **105** (2019), 1–60. arXiv: 1810.12938 [hep-ph].

[132] W.-j. Fu, J. M. Pawlowski, and F. Rennecke: "QCD phase structure at finite temperature and density". *Phys. Rev. D* **101**.5 (2020), 054032. arXiv: 1909.02991 [hep-ph].

[133] G. Odyniec: "Beam Energy Scan Program at RHIC (BES I and BES II) – Probing QCD Phase Diagram with Heavy-Ion Collisions". *PoS* **CORFU2018** (2019). Ed. by K. Anagnostopoulos et al., 151.

[134] P. Chomaz: "The nuclear liquid gas phase transition and phase coexistence". *AIP Conf. Proc.* **610**.1 (2002). Ed. by E. Norman, L. Schroeder, and G. Wozniak, 167. arXiv: nucl-ex/0410024.

[135] H. Jaqaman, A. Mekjian, and L. Zamick: "Liquid-gas phase transitions in finite nuclear matter". *Phys. Rev. C* **29** (1984), 2067–2074.

[136] R.-K. Su and F.-M. Lin: "Liquid-gas and superconducting phase transitions in finite symmetric nuclear matter". *Phys. Rev. C* **39** (1989), 2438–2444.

[137] I. Tews, T. Krüger, K. Hebeler, and A. Schwenk: "Neutron matter at next-to-next-to-next-to-leading order in chiral effective field theory". *Phys. Rev. Lett.* **110**.3 (2013), 032504. arXiv: 1206.0025 [nucl-th].

[138] K. Hebeler, J. Lattimer, C. Pethick, and A. Schwenk: "Equation of state and neutron star properties constrained by nuclear physics and observation". *Astrophys. J.* **773** (2013), 11. arXiv: 1303.4662 [astro-ph.SR].

[139] T. Krüger, I. Tews, K. Hebeler, and A. Schwenk: "Neutron matter from chiral effective field theory interactions". *Phys. Rev. C* **88** (2013), 025802. arXiv: 1304.2212 [nucl-th].

[140] A. Kurkela, P. Romatschke, and A. Vuorinen: "Cold Quark Matter". *Phys. Rev. D* **81** (2010), 105021. arXiv: 0912.1856 [hep-ph].

[141] B. C. Barrois: "Superconducting Quark Matter". *Nucl. Phys. B* **129** (1977), 390–396.

[142] S. C. Frautschi: "Asymptotic Freedom And Color Superconductivity In Dense Quark Matter". *Workshop on Theoretical Physics: Hadronic Matter at Extreme Energy Density.* Oct. 1978, 18.

[143] D. Bailin and A. Love: "Superfluid Quark Matter". *J. Phys. A* **12** (1979), L283.

[144] D. Bailin and A. Love: "Superfluidity and Superconductivity in Relativistic Fermion Systems". *Phys. Rept.* **107** (1984), 325.

[145] M. Iwasaki and T. Iwado: "Superconductivity in the quark matter". *Phys. Lett. B* **350** (1995), 163–168.

[146] M. G. Alford, K. Rajagopal, and F. Wilczek: "Color flavor locking and chiral symmetry breaking in high density QCD". *Nucl. Phys. B* **537** (1999), 443–458. arXiv: hep-ph/9804403.

[147] A. W. Steiner, S. Reddy, and M. Prakash: "Color neutral superconducting quark matter". *Phys. Rev. D* **66** (2002), 094007. arXiv: hep-ph/0205201.

[148] H. Abuki and T. Kunihiro: "Extensive study of phase diagram for charge neutral homogeneous quark matter affected by dynamical chiral condensation: Unified picture for thermal unpairing transitions from weak to strong coupling". *Nucl. Phys. A* **768** (2006), 118–159. arXiv: hep-ph/0509172.

[149] D. H. Rischke: "Debye screening and Meissner effect in a three flavor color superconductor". *Phys. Rev. D* **62** (2000), 054017. arXiv: nucl-th/0003063.

[150] H. Abuki, T. Hatsuda, and K. Itakura: "Structural change of Cooper pairs and momentum dependent gap in color superconductivity". *Phys. Rev. D* **65** (2002), 074014. arXiv: hep-ph/0109013.

[151] K. Fukushima and K. Iida: "Collective excitations in a superfluid of color-flavor locked quark matter". *Phys. Rev. D* **71** (2005), 074011. arXiv: hep-ph/0501276.

[152] T. Hatsuda, M. Tachibana, N. Yamamoto, and G. Baym: "New critical point induced by the axial anomaly in dense QCD". *Phys. Rev. Lett.* **97** (2006), 122001. arXiv: hep-ph/0605018.

[153] M. Kitazawa, T. Koide, T. Kunihiro, and Y. Nemoto: "Precursor of color superconductivity in hot quark matter". *Phys. Rev. D* **65** (2002), 091504. arXiv: nucl-th/0111022.

[154] M. Kitazawa, T. Koide, T. Kunihiro, and Y. Nemoto: "Pseudogap of color superconductivity in heated quark matter". *Phys. Rev. D* **70** (2004), 056003. arXiv: hep-ph/0309026.

[155] M. Kitazawa, T. Kunihiro, and Y. Nemoto: "Non-Fermi liquid behavior induced by resonant diquark-pair scattering in heated quark matter". *Phys. Lett. B* **631** (2005), 157–163. arXiv: hep-ph/0505070.

[156] M. Kitazawa, T. Koide, T. Kunihiro, and Y. Nemoto: "Pre-critical phenomena of two-flavor color superconductivity in heated quark matter: Diquark-pair fluctuations and non-Fermi liquid behavior". *Prog. Theor. Phys.* **114** (2005), 117–155. arXiv: hep-ph/0502035.

[157] M. Kitazawa, D. H. Rischke, and I. A. Shovkovy: "Bound diquarks and their Bose-Einstein condensation in strongly coupled quark matter". *Phys. Lett. B* **663** (2008), 228–233. arXiv: 0709.2235 [hep-ph].

[158] D. Voskresensky: "Fluctuations of the color-superconducting gap in hot and dense quark matter". *Phys. Rev. C* **69** (2004), 065209.

[159] N. Yamamoto, M. Tachibana, T. Hatsuda, and G. Baym: "Phase structure, collective modes, and the axial anomaly in dense QCD". *Phys. Rev. D* **76** (2007), 074001. arXiv: 0704.2654 [hep-ph].

[160] M. G. Alford, J. A. Bowers, and K. Rajagopal: "Crystalline color superconductivity". *Phys. Rev. D* **63** (2001), 074016. arXiv: hep-ph/0008208.

[161] M. G. Alford, A. Schmitt, K. Rajagopal, and T. Schäfer: "Color superconductivity in dense quark matter". *Rev. Mod. Phys.* **80** (2008), 1455–1515. arXiv: 0709.4635 [hep-ph].

[162] R. Anglani, R. Casalbuoni, M. Ciminale, N. Ippolito, R. Gatto, M. Mannarelli, and M. Ruggieri: "Crystalline color superconductors". *Rev. Mod. Phys.* **86** (2014), 509–561. arXiv: 1302.4264 [hep-ph].

[163] P. Basu, F. Nogueira, M. Rozali, J. B. Stang, and M. Van Raamsdonk: "Towards A Holographic Model of Color Superconductivity". *New J. Phys.* **13** (2011), 055001. arXiv: 1101.4042 [hep-th].

[164] G. 't Hooft: "Dimensional reduction in quantum gravity" (1993). arXiv: gr-qc/9310026.

[165] L. Susskind: "The World as a hologram". *J.Math.Phys.* **36** (1995), 6377–6396. arXiv: hep-th/9409089.

[166] J. D. Brown and M. Henneaux: "Central Charges in the Canonical Realization of Asymptotic Symmetries: An Example from Three-Dimensional Gravity". *Commun. Math. Phys.* **104** (1986), 207–226.

[167] H. Năstase: "Introduction to AdS-CFT" (2007). arXiv: 0712.0689 [hep-th].

[168] A. V. Ramallo: "Introduction to the AdS/CFT correspondence". *Springer Proc. Phys.* **161** (2015). Ed. by C. Merino, 411–474. arXiv: 1310.4319 [hep-th].

[169] E. Kiritsis: *String theory in a nutshell*. USA: Princeton University Press, 2019. ISBN: 978-0-691-15579-1, 978-0-691-18896-6.

[170] J. Dai, R. Leigh, and J. Polchinski: "New Connections Between String Theories". *Mod. Phys. Lett. A* **4** (1989), 2073–2083.

[171] R. Leigh: "Dirac-Born-Infeld Action from Dirichlet Sigma Model". *Mod. Phys. Lett. A* **4** (1989), 2767.

[172] H. P. Nilles: "Supersymmetry, Supergravity and Particle Physics". *Phys. Rept.* **110** (1984), 1–162.

[173] O. Aharony, S. S. Gubser, J. M. Maldacena, H. Ooguri, and Y. Oz: "Large N field theories, string theory and gravity". *Phys.Rept.* **323** (2000), 183–386. arXiv: hep-th/9905111.

[174] E. Witten: "Anti-de Sitter space and holography". *Adv.Theor.Math.Phys.* **2** (1998), 253–291. arXiv: hep-th/9802150.

[175] K. Skenderis: "Lecture notes on holographic renormalization". *Class. Quant. Grav.* **19** (2002), 5849–5876. arXiv: hep-th/0209067.

[176] M. Ammon and J. Erdmenger: *Gauge/gravity duality: Foundations and applications*. Cambridge: Cambridge University Press, Apr. 2015. ISBN: 978-1-107-01034-5, 978-1-316-23594-2.

[177] N. Beisert et al.: "Review of AdS/CFT Integrability: An Overview". *Lett. Math. Phys.* **99** (2012), 3–32. arXiv: 1012.3982 [hep-th].

[178] E. Witten: "Anti-de Sitter space, thermal phase transition, and confinement in gauge theories". *Adv. Theor. Math. Phys.* **2** (1998). Ed. by L. Bergstrom and U. Lindstrom, 505–532. arXiv: hep-th/9803131.

[179] S. Gubser, I. R. Klebanov, and A. M. Polyakov: "Gauge theory correlators from noncritical string theory". *Phys.Lett.* **B428** (1998), 105–114. arXiv: hep-th/9802109.

[180] S. Hawking and D. N. Page: "Thermodynamics of Black Holes in anti-De Sitter Space". *Commun. Math. Phys.* **87** (1983), 577.

[181] G. Gibbons and M. Perry: "Black Holes in Thermal Equilibrium". *Phys. Rev. Lett.* **36** (1976), 985.

[182] M. Laine and A. Vuorinen: *Basics of Thermal Field Theory*. **925**. Springer, 2016. arXiv: 1701.01554 [hep-ph].

[183] J. D. Bekenstein: "Black holes and entropy". *Phys.Rev.* **D7** (1973), 2333–2346.

[184] S. Hawking: "Particle Creation by Black Holes". *Commun. Math. Phys.* **43** (1975). Ed. by G. Gibbons and S. Hawking. [Erratum: Commun.Math.Phys. 46, 206 (1976)], 199–220.

[185] S. Gubser, I. R. Klebanov, and A. Peet: "Entropy and temperature of black 3-branes". *Phys. Rev. D* **54** (1996), 3915–3919. arXiv: hep-th/9602135.

[186] A. Karch and A. O'Bannon: "Holographic thermodynamics at finite baryon density: Some exact results". *JHEP* **11** (2007), 074. arXiv: 0709.0570 [hep-th].

[187] K. Ghoroku, M. Ishihara, and A. Nakamura: "D3/D7 holographic Gauge theory and Chemical potential". *Phys. Rev. D* **76** (2007), 124006. arXiv: 0708.3706 [hep-th].

[188] S. Kobayashi, D. Mateos, S. Matsuura, R. C. Myers, and R. M. Thomson: "Holographic phase transitions at finite baryon density". *JHEP* **02** (2007), 016. arXiv: hep-th/0611099.

[189] S. Nakamura, Y. Seo, S.-J. Sin, and K. Yogendran: "Baryon-charge Chemical Potential in AdS/CFT". *Prog. Theor. Phys.* **120** (2008), 51–76. arXiv: 0708.2818 [hep-th].

[190] J. D. Edelstein, J. P. Shock, and D. Zoakos: "The AdS/CFT Correspondence and Non-perturbative QCD". *AIP Conf. Proc.* **1116**.1 (2009), 265–284. arXiv: 0901.2534 [hep-ph].

[191] N. Seiberg and E. Witten: "Electric - magnetic duality, monopole condensation, and confinement in N=2 supersymmetric Yang-Mills theory". *Nucl. Phys. B* **426** (1994). [Erratum: Nucl.Phys.B 430, 485–486 (1994)], 19–52. arXiv: hep-th/9407087.

[192] O. Aharony, O. Bergman, D. L. Jafferis, and J. Maldacena: "N=6 superconformal Chern-Simons-matter theories, M2-branes and their gravity duals". *JHEP* **10** (2008), 091. arXiv: 0806.1218 [hep-th].

[193] N. Jokela and A. Pönni: "Towards precision holography" (June 2020). arXiv: 2007.00010 [hep-th].

[194] D. Harlow: "TASI Lectures on the Emergence of Bulk Physics in AdS/CFT". *PoS* **TASI2017** (2018), 002. arXiv: 1802.01040 [hep-th].

[195] D. Mateos: "String Theory and Quantum Chromodynamics". *Class. Quant. Grav.* **24** (2007). Ed. by J.-P. Derendinger, C. A. Scrucca, and A. M. Uranga, S713–S740. arXiv: 0709.1523 [hep-th].

[196] S. S. Gubser: "Einstein manifolds and conformal field theories". *Phys. Rev. D* **59** (1999), 025006. arXiv: hep-th/9807164.

[197] I. R. Klebanov and E. Witten: "Superconformal field theory on three-branes at a Calabi-Yau singularity". *Nucl. Phys. B* **536** (1998), 199–218. arXiv: hep-th/9807080.

[198] I. R. Klebanov and M. J. Strassler: "Supergravity and a confining gauge theory: Duality cascades and chi SB resolution of naked singularities". *JHEP* **08** (2000), 052. arXiv: hep-th/0007191.

[199] J. Polchinski and M. J. Strassler: "The String dual of a confining four-dimensional gauge theory" (Mar. 2000). arXiv: hep-th/0003136.

[200] J. Polchinski and M. J. Strassler: "Hard scattering and gauge / string duality". *Phys. Rev. Lett.* **88** (2002), 031601. arXiv: hep-th/0109174.

[201] J. Babington, J. Erdmenger, N. J. Evans, Z. Guralnik, and I. Kirsch: "Chiral symmetry breaking and pions in nonsupersymmetric gauge / gravity duals". *Phys. Rev. D* **69** (2004), 066007. arXiv: hep-th/0306018.

[202] A. Karch and E. Katz: "Adding flavor to AdS / CFT". *JHEP* **06** (2002), 043. arXiv: hep-th/0205236.

[203] J. T. Liu, D. Vaman, and W. Wen: "Bubbling 1/4 BPS solutions in type IIB and supergravity reductions on S**n x S**n". *Nucl. Phys. B* **739** (2006), 285–310. arXiv: hep-th/0412043.

[204] I. Kirsch and D. Vaman: "The D3 / D7 background and flavor dependence of Regge trajectories". *Phys. Rev. D* **72** (2005), 026007. arXiv: hep-th/0505164.

[205] P. Ouyang: "Holomorphic D7 branes and flavored N=1 gauge theories". *Nucl. Phys. B* **699** (2004), 207–225. arXiv: hep-th/0311084.

[206] M. Mia, K. Dasgupta, C. Gale, and S. Jeon: "Five Easy Pieces: The Dynamics of Quarks in Strongly Coupled Plasmas". *Nucl. Phys. B* **839** (2010), 187–293. arXiv: 0902.1540 [hep-th].

[207] M. Mia, K. Dasgupta, C. Gale, and S. Jeon: "The Double Life of Thermal QCD". *J. Phys. Conf. Ser.* **462**.1 (2013). Ed. by S. R. Das and A. D. Shapere, 012009. arXiv: 0902.2216 [hep-th].

[208] C. Núñez, A. Paredes, and A. V. Ramallo: "Unquenched Flavor in the Gauge/Gravity Correspondence". *Adv. High Energy Phys.* **2010** (2010), 196714. arXiv: 1002.1088 [hep-th].

[209] E. Witten: "Baryons and branes in anti-de Sitter space". *JHEP* **9807** (1998), 006. arXiv: hep-th/9805112.

[210] T. Sakai and S. Sugimoto: "Low energy hadron physics in holographic QCD". *Prog. Theor. Phys.* **113** (2005), 843–882. arXiv: hep-th/0412141 [hep-th].

[211] T. Sakai and S. Sugimoto: "More on a holographic dual of QCD". *Prog. Theor. Phys.* **114** (2005), 1083–1118. arXiv: hep-th/0507073.

[212] M. Bertolini, P. Di Vecchia, M. Frau, A. Lerda, and R. Marotta: "N=2 gauge theories on systems of fractional D3/D7 branes". *Nucl. Phys. B* **621** (2002), 157–178. arXiv: hep-th/0107057.

[213] M. Kruczenski, D. Mateos, R. C. Myers, and D. J. Winters: "Meson spectroscopy in AdS / CFT with flavor". *JHEP* **07** (2003), 049. arXiv: hep-th/0304032.

[214] A. Rebhan: "The Witten-Sakai-Sugimoto model: A brief review and some recent results". *EPJ Web Conf.* **95** (2015), 02005. arXiv: 1410.8858 [hep-th].

[215] F. Bigazzi, A. L. Cotrone, and J. Tarrio: "Charged D3-D7 plasmas: novel solutions, extremality and stability issues". *JHEP* **07** (2013), 074. arXiv: 1304.4802 [hep-th].

[216] G. Policastro, D. T. Son, and A. O. Starinets: "From AdS / CFT correspondence to hydrodynamics". *JHEP* **09** (2002), 043. arXiv: hep-th/0205052.

[217] D. T. Son and A. O. Starinets: "Viscosity, Black Holes, and Quantum Field Theory". *Ann. Rev. Nucl. Part. Sci.* **57** (2007), 95–118. arXiv: 0704.0240 [hep-th].

[218] H. Liu, K. Rajagopal, and U. A. Wiedemann: "Calculating the jet quenching parameter from AdS/CFT". *Phys. Rev. Lett.* **97** (2006), 182301. arXiv: hep-ph/0605178.

[219] C. Hoyos, N. Jokela, M. Järvinen, J. G. Subils, J. Tarrio, and A. Vuorinen: "Transport in strongly coupled quark matter" (May 2020). arXiv: 2005.14205 [hep-th].

[220] J. Casalderrey-Solana, M. P. Heller, D. Mateos, and W. van der Schee: "From full stopping to transparency in a holographic model of heavy ion collisions". *Phys. Rev. Lett.* **111** (2013), 181601. arXiv: 1305.4919 [hep-th].

[221] J. Casalderrey-Solana, M. P. Heller, D. Mateos, and W. van der Schee: "Longitudinal Coherence in a Holographic Model of Asymmetric Collisions". *Phys. Rev. Lett.* **112**.22 (2014), 221602. arXiv: 1312.2956 [hep-th].

[222] P. M. Chesler and L. G. Yaffe: "Holography and colliding gravitational shock waves in asymptotically AdS_5 spacetime". *Phys. Rev. Lett.* **106** (2011), 021601. arXiv: 1011.3562 [hep-th].

[223] P. M. Chesler: "Colliding shock waves and hydrodynamics in small systems". *Phys. Rev. Lett.* **115**.24 (2015), 241602. arXiv: 1506.02209 [hep-th].

[224] J. Erlich, E. Katz, D. T. Son, and M. A. Stephanov: "QCD and a holographic model of hadrons". *Phys.Rev.Lett.* **95** (2005), 261602. arXiv: hep-ph/0501128.

[225] L. Da Rold and A. Pomarol: "Chiral symmetry breaking from five dimensional spaces". *Nucl.Phys.* **B721** (2005), 79–97. arXiv: hep-ph/0501218.

[226] A. Karch, E. Katz, D. T. Son, and M. A. Stephanov: "Linear confinement and AdS/QCD". *Phys. Rev. D* **74** (2006), 015005. arXiv: hep-ph/0602229.

[227] C. P. Herzog: "A Holographic Prediction of the Deconfinement Temperature". *Phys. Rev. Lett.* **98** (2007), 091601. arXiv: hep-th/0608151.

[228] P. Colangelo, F. De Fazio, F. Giannuzzi, F. Jugeau, and S. Nicotri: "Light scalar mesons in the soft-wall model of AdS/QCD". *Phys. Rev. D* **78** (2008), 055009. arXiv: 0807.1054 [hep-ph].

[229] T. Gherghetta, J. I. Kapusta, and T. M. Kelley: "Chiral symmetry breaking in the soft-wall AdS/QCD model". *Phys. Rev. D* **79** (2009), 076003. arXiv: 0902.1998 [hep-ph].

[230] B. Batell and T. Gherghetta: "Dynamical Soft-Wall AdS/QCD". *Phys. Rev. D* **78** (2008), 026002. arXiv: 0801.4383 [hep-ph].

[231] Y.-Q. Sui, Y.-L. Wu, Z.-F. Xie, and Y.-B. Yang: "Prediction for the Mass Spectra of Resonance Mesons in the Soft-Wall AdS/QCD with a Modified 5D Metric". *Phys. Rev. D* **81** (2010), 014024. arXiv: 0909.3887 [hep-ph].

[232] J. Alanen, T. Alho, K. Kajantie, and K. Tuominen: "Mass spectrum and thermodynamics of quasi-conformal gauge theories from gauge/gravity duality". *Phys. Rev.* **D84** (2011), 086007. arXiv: 1107.3362 [hep-th].

[233] R. A. Janik, J. Jankowski, and H. Soltanpanahi: "Quasinormal modes and the phase structure of strongly coupled matter". *JHEP* **06** (2016), 047. arXiv: 1603.05950 [hep-th].

[234] P. Betzios, U. Gürsoy, M. Järvinen, and G. Policastro: "Quasi-normal modes of a strongly coupled non-conformal plasma and approach to criticality" (2017). arXiv: 1708.02252 [hep-th].

[235] P. Betzios, U. Gürsoy, M. Järvinen, and G. Policastro: "Fluctuations in a nonconformal holographic plasma at criticality". *Phys. Rev. D* **101**.8 (2020), 086026. arXiv: 1807.01718 [hep-th].

[236] U. Gürsoy and E. Kiritsis: "Exploring improved holographic theories for QCD: Part I". *JHEP* **02** (2008), 032. arXiv: 0707.1324 [hep-th].

[237] U. Gürsoy, E. Kiritsis, and F. Nitti: "Exploring improved holographic theories for QCD: Part II". *JHEP* **02** (2008), 019. arXiv: 0707.1349 [hep-th].

[238] U. Gürsoy, E. Kiritsis, L. Mazzanti, and F. Nitti: "Deconfinement and Gluon Plasma Dynamics in Improved Holographic QCD". *Phys. Rev. Lett.* **101** (2008), 181601. arXiv: 0804.0899 [hep-th].

[239] U. Gürsoy, E. Kiritsis, L. Mazzanti, and F. Nitti: "Holography and Thermodynamics of 5D Dilaton-gravity". *JHEP* **05** (2009), 033. arXiv: 0812.0792 [hep-th].

[240] U. Gürsoy, E. Kiritsis, L. Mazzanti, and F. Nitti: "Improved Holographic Yang-Mills at Finite Temperature: Comparison with Data". *Nucl. Phys.* **B820** (2009), 148–177. arXiv: 0903.2859 [hep-th].

[241] S. S. Gubser and A. Nellore: "Mimicking the QCD equation of state with a dual black hole". *Phys. Rev.* **D78** (2008), 086007. arXiv: 0804.0434 [hep-th].

[242] I. R. Klebanov and J. M. Maldacena: "Superconformal gauge theories and non-critical superstrings". *Int. J. Mod. Phys. A* **19** (2004), 5003–5016. arXiv: hep-th/0409133.

[243] F. Bigazzi, R. Casero, A. L. Cotrone, E. Kiritsis, and A. Paredes: "Non-critical holography and four-dimensional CFT's with fundamentals". *JHEP* **10** (2005), 012. arXiv: hep-th/0505140 [hep-th].

[244] R. Casero, E. Kiritsis, and A. Paredes: "Chiral symmetry breaking as open string tachyon condensation". *Nucl. Phys.* **B787** (2007), 98–134. arXiv: hep-th/0702155 [HEP-TH].

[245] I. Iatrakis, E. Kiritsis, and A. Paredes: "An AdS/QCD model from Sen's tachyon action". *Phys. Rev. D* **81** (2010), 115004. arXiv: 1003.2377 [hep-ph].

[246] I. Iatrakis, E. Kiritsis, and A. Paredes: "An AdS/QCD model from tachyon condensation: II". *JHEP* **11** (2010), 123. arXiv: 1010.1364 [hep-ph].

[247] O. Bergman, S. Seki, and J. Sonnenschein: "Quark mass and condensate in HQCD". *JHEP* **12** (2007), 037. arXiv: 0708.2839 [hep-th].

[248] A. Dhar and P. Nag: "Sakai-Sugimoto model, Tachyon Condensation and Chiral symmetry Breaking". *JHEP* **01** (2008), 055. arXiv: 0708.3233 [hep-th].

[249] A. Dhar and P. Nag: "Tachyon condensation and quark mass in modified Sakai-Sugimoto model". *Phys. Rev. D* **78** (2008), 066021. arXiv: 0804.4807 [hep-th].

[250] N. Jokela, M. Järvinen, and S. Nowling: "Winding effects on brane/anti-brane pairs". *JHEP* **07** (2009), 085. arXiv: 0901.0281 [hep-th].

[251] M. Järvinen and E. Kiritsis: "Holographic Models for QCD in the Veneziano Limit". *JHEP* **03** (2012), 002. arXiv: 1112.1261 [hep-ph].

[252] G. Veneziano: "U(1) without instantons". *Nuclear Physics B* **159**.1 (1979), 213 –224. ISSN: 0550-3213.

[253] D. Areán, I. Iatrakis, M. Järvinen, and E. Kiritsis: "CP-odd sector and θ dynamics in holographic QCD". *Phys. Rev. D* **96**.2 (2017), 026001. arXiv: 1609.08922 [hep-ph].

[254] E. Kiritsis: "Dissecting the string theory dual of QCD". *Fortsch. Phys.* **57** (2009). Ed. by D. Lust and V. Dobrev, 396–417. arXiv: 0901.1772 [hep-th].

[255] G. Gibbons and S. Hawking: "Action Integrals and Partition Functions in Quantum Gravity". *Phys. Rev. D* **15** (1977), 2752–2756.

[256] A. Sen: "Dirac-Born-Infeld action on the tachyon kink and vortex". *Phys. Rev. D* **68** (2003), 066008. arXiv: hep-th/0303057.

[257] P. Kraus and F. Larsen: "Boundary string field theory of the D anti-D system". *Phys. Rev. D* **63** (2001), 106004. arXiv: hep-th/0012198.

[258] L. Del Debbio, L. Giusti, and C. Pica: "Topological susceptibility in the SU(3) gauge theory". *Phys. Rev. Lett.* **94** (2005), 032003. arXiv: hep-th/0407052.

[259] G. 't Hooft: "Symmetry Breaking Through Bell-Jackiw Anomalies". *Phys. Rev. Lett.* **37** (1976). Ed. by M. A. Shifman, 8–11.

[260] E. Witten: "Current Algebra Theorems for the U(1) Goldstone Boson". *Nucl. Phys. B* **156** (1979), 269–283.

[261] G. Veneziano: "U(1) Without Instantons". *Nucl. Phys. B* **159** (1979), 213–224.

[262] A. A. Tseytlin: "On nonAbelian generalization of Born-Infeld action in string theory". *Nucl. Phys. B* **501** (1997), 41–52. arXiv: hep-th/9701125.

[263] P. Koerber and A. Sevrin: "The NonAbelian D-brane effective action through order alpha-prime**4". *JHEP* **10** (2002), 046. arXiv: hep-th/0208044.

[264] M. Järvinen: "Massive holographic QCD in the Veneziano limit". *JHEP* **07** (2015), 033. arXiv: 1501.07272 [hep-ph].

[265] T. Ishii, M. Järvinen, and G. Nijs: "Cool baryon and quark matter in holographic QCD". *JHEP* **07** (2019), 003. arXiv: 1903.06169 [hep-ph].

[266] D. J. Gross and H. Ooguri: "Aspects of large N gauge theory dynamics as seen by string theory". *Phys. Rev. D* **58** (1998), 106002. arXiv: hep-th/9805129.

[267] D. K. Hong, M. Rho, H.-U. Yee, and P. Yi: "Chiral Dynamics of Baryons from String Theory". *Phys.Rev.* **D76** (2007), 061901. arXiv: hep-th/0701276.

[268] H. Hata, T. Sakai, S. Sugimoto, and S. Yamato: "Baryons from instantons in holographic QCD". *Prog.Theor.Phys.* **117** (2007), 1157. arXiv: hep-th/0701280.

[269] D. K. Hong, M. Rho, H.-U. Yee, and P. Yi: "Nucleon form-factors and hidden symmetry in holographic QCD". *Phys. Rev. D* **77** (2008), 014030. arXiv: 0710.4615 [hep-ph].

[270] M. Elliot-Ripley, P. Sutcliffe, and M. Zamaklar: "Phases of kinky holographic nuclear matter". *JHEP* **10** (2016), 088. arXiv: 1607.04832 [hep-th].

[271] V. Kaplunovsky, D. Melnikov, and J. Sonnenschein: "Baryonic Popcorn". *JHEP* **11** (2012), 047. arXiv: 1201.1331 [hep-th].

[272] V. Kaplunovsky, D. Melnikov, and J. Sonnenschein: "Holographic Baryons and Instanton Crystals". *Mod. Phys. Lett. B* **29**.16 (2015), 1540052. arXiv: 1501.04655 [hep-th].

[273] N. Kovensky and A. Schmitt: "Holographic quarkyonic matter" (June 2020). arXiv: 2006.13739 [hep-th].

[274] O. Bergman, G. Lifschytz, and M. Lippert: "Holographic Nuclear Physics". *JHEP* **11** (2007), 056. arXiv: 0708.0326 [hep-th].

[275] M. Rozali, H.-H. Shieh, M. Van Raamsdonk, and J. Wu: "Cold Nuclear Matter In Holographic QCD". *JHEP* **01** (2008), 053. arXiv: 0708.1322 [hep-th].

[276] S.-w. Li, A. Schmitt, and Q. Wang: "From holography towards real-world nuclear matter". *Phys. Rev. D* **92**.2 (2015), 026006. arXiv: 1505.04886 [hep-ph].

[277] D. Areán, I. Iatrakis, M. Järvinen, and E. Kiritsis: "The discontinuities of conformal transitions and mass spectra of V-QCD". *JHEP* **11** (2013), 068. arXiv: 1309.2286 [hep-ph].

[278] T. Alho, M. Järvinen, K. Kajantie, E. Kiritsis, and K. Tuominen: "Quantum and stringy corrections to the equation of state of holographic QCD matter and the nature of the chiral transition". *Phys. Rev. D* **91**.5 (2015), 055017. arXiv: 1501.06379 [hep-ph].

[279] S. S. Gubser: "Curvature singularities: The Good, the bad, and the naked". *Adv. Theor. Math. Phys.* **4** (2000), 679–745. arXiv: hep-th/0002160.

[280] M. Panero: "Thermodynamics of the QCD plasma and the large-N limit". *Phys. Rev. Lett.* **103** (2009), 232001. arXiv: 0907.3719 [hep-lat].

[281] S. Borsanyi, Z. Fodor, C. Hoelbling, S. D. Katz, S. Krieg, and K. K. Szabo: "Full result for the QCD equation of state with 2+1 flavors". *Phys. Lett. B* **730** (2014), 99–104. arXiv: 1309.5258 [hep-lat].

[282] T. Alho, M. Järvinen, K. Kajantie, E. Kiritsis, C. Rosen, and K. Tuominen: "A holographic model for QCD in the Veneziano limit at finite temperature and density". *JHEP* **04** (2014). [Erratum: JHEP02,033(2015)], 124. arXiv: 1312.5199 [hep-ph].

[283] T. Alho, M. Järvinen, K. Kajantie, E. Kiritsis, and K. Tuominen: "On finite-temperature holographic QCD in the Veneziano limit". *JHEP* **01** (2013), 093. arXiv: 1210.4516 [hep-ph].

[284] N. Evans, A. Gebauer, K.-Y. Kim, and M. Magou: "Holographic Description of the Phase Diagram of a Chiral Symmetry Breaking Gauge Theory". *JHEP* **03** (2010), 132. arXiv: 1002.1885 [hep-th].

[285] O. Aharony, J. Sonnenschein, and S. Yankielowicz: "A Holographic model of deconfinement and chiral symmetry restoration". *Annals Phys.* **322** (2007), 1420–1443. arXiv: hep-th/0604161.

[286] N. Horigome and Y. Tanii: "Holographic chiral phase transition with chemical potential". *JHEP* **01** (2007), 072. arXiv: hep-th/0608198.

[287] U. Gürsoy: "Continuous Hawking-Page transitions in Einstein-scalar gravity". *JHEP* **01** (2011), 086. arXiv: 1007.0500 [hep-th].

[288] T. Drwenski, U. Gürsoy, and I. Iatrakis: "Thermodynamics and CP-odd transport in Holographic QCD with Finite Magnetic Field". *JHEP* **12** (2016), 049. arXiv: 1506.01350 [hep-th].

[289] U. Gürsoy, I. Iatrakis, M. Järvinen, and G. Nijs: "Inverse Magnetic Catalysis from improved Holographic QCD in the Veneziano limit". *JHEP* **03** (2017), 053. arXiv: 1611.06339 [hep-th].

[290] U. Gürsoy, M. Järvinen, and G. Nijs: "Holographic QCD in the Veneziano limit at finite Magnetic Field and Chemical Potential" (2017). arXiv: 1707.00872 [hep-th].

[291] F. Bruckmann, G. Endrődi, and T. G. Kovacs: "Inverse magnetic catalysis and the Polyakov loop". *JHEP* **04** (2013), 112. arXiv: 1303.3972 [hep-lat].

[292] K. Eskola, K. Kajantie, P. Ruuskanen, and K. Tuominen: "Scaling of transverse energies and multiplicities with atomic number and energy in ultrarelativistic nuclear collisions". *Nucl. Phys. B* **570** (2000), 379–389. arXiv: hep-ph/9909456.

[293] P. Kolb, U. W. Heinz, P. Huovinen, K. Eskola, and K. Tuominen: "Centrality dependence of multiplicity, transverse energy, and elliptic flow from hydrodynamics". *Nucl. Phys. A* **696** (2001), 197–215. arXiv: hep-ph/0103234.

[294] K. J. Eskola, H. Paukkunen, and C. A. Salgado: "An Improved global analysis of nuclear parton distribution functions including RHIC data". *JHEP* **07** (2008), 102. arXiv: 0802.0139 [hep-ph].

[295] H. Niemi, K. Eskola, and R. Paatelainen: "Event-by-event fluctuations in a perturbative QCD + saturation + hydrodynamics model: Determining QCD matter shear viscosity in ultrarelativistic heavy-ion collisions". *Phys. Rev. C* **93**.2 (2016), 024907. arXiv: 1505.02677 [hep-ph].

[296] M. Attems, J. Casalderrey-Solana, D. Mateos, I. Papadimitriou, D. Santos-Oliván, C. F. Sopuerta, M. Triana, and M. Zilhão: "Thermodynamics, transport and relaxation in non-conformal theories". *JHEP* **10** (2016), 155. arXiv: 1603.01254 [hep-th].

[297] S. s. Grozdanov and W. van der Schee: "Coupling Constant Corrections in a Holographic Model of Heavy Ion Collisions". *Phys. Rev. Lett.* **119**.1 (2017), 011601. arXiv: 1610.08976 [hep-th].

[298] M. Attems, J. Casalderrey-Solana, D. Mateos, D. Santos-Oliván, C. F. Sopuerta, M. Triana, and M. Zilhão: "Paths to equilibrium in non-conformal collisions". *JHEP* **06** (2017), 154. arXiv: 1703.09681 [hep-th].

[299] D. Steineder, S. A. Stricker, and A. Vuorinen: "Holographic Thermalization at Intermediate Coupling". *Phys. Rev. Lett.* **110**.10 (2013), 101601. arXiv: 1209.0291 [hep-ph].

[300] S. Waeber, A. Schäfer, A. Vuorinen, and L. G. Yaffe: "Finite coupling corrections to holographic predictions for hot QCD". *JHEP* **11** (2015), 087. arXiv: 1509.02983 [hep-th].

[301] S. Waeber: "Quasinormal modes of magnetic black branes at finite 't Hooft coupling". *JHEP* **08** (2019), 006. arXiv: 1811.04040 [hep-th].

[302] Y. Akiba et al.: "The Hot QCD White Paper: Exploring the Phases of QCD at RHIC and the LHC" (Feb. 2015). arXiv: 1502.02730 [nucl-ex].

[303] J. L. Nagle and W. A. Zajc: "Small System Collectivity in Relativistic Hadronic and Nuclear Collisions". *Ann. Rev. Nucl. Part. Sci.* **68** (2018), 211–235. arXiv: 1801.03477 [nucl-ex].

[304] W. Busza, K. Rajagopal, and W. van der Schee: "Heavy Ion Collisions: The Big Picture, and the Big Questions". *Ann. Rev. Nucl. Part. Sci.* **68** (2018), 339–376. arXiv: 1802.04801 [hep-ph].

[305] C. Ratti: "Lattice QCD and heavy ion collisions: a review of recent progress". *Rept. Prog. Phys.* **81**.8 (2018), 084301. arXiv: 1804.07810 [hep-lat].

[306] G. Aad et al. ATLAS: "Measurement of Z boson Production in Pb+Pb Collisions at $\sqrt{s_{NN}} = 2.76$ TeV with the ATLAS Detector". *Phys. Rev. Lett.* **110**.2 (2013), 022301. arXiv: 1210.6486 [hep-ex].

[307] G. Aad et al. ATLAS: "Centrality, rapidity and transverse momentum dependence of isolated prompt photon production in lead-lead collisions at $\sqrt{s_{\mathrm{NN}}} = 2.76$ TeV measured with the ATLAS detector". *Phys. Rev. C* **93**.3 (2016), 034914. arXiv: 1506.08552 [hep-ex].

[308] S. Chatrchyan et al. CMS: "Study of Z production in PbPb and pp collisions at $\sqrt{s_{\mathrm{NN}}} =$ 2.76 TeV in the dimuon and dielectron decay channels". *JHEP* **03** (2015), 022. arXiv: 1410.4825 [nucl-ex].

[309] F. Becattini, M. Bleicher, T. Kollegger, T. Schuster, J. Steinheimer, and R. Stock: "Hadron Formation in Relativistic Nuclear Collisions and the QCD Phase Diagram". *Phys. Rev. Lett.* **111** (2013), 082302. arXiv: 1212.2431 [nucl-th].

[310] A. Andronic, P. Braun-Munzinger, K. Redlich, and J. Stachel: "Decoding the phase structure of QCD via particle production at high energy". *Nature* **561**.7723 (2018), 321–330. arXiv: 1710.09425 [nucl-th].

[311] P. Koch, B. Müller, and J. Rafelski: "From strangeness enhancement to quark–gluon plasma discovery". *Int. J. Mod. Phys. A* **32**.31 (2017), 1730024. arXiv: 1708.08115 [nucl-th].

[312] R. Paatelainen, K. Eskola, H. Niemi, and K. Tuominen: "Fluid dynamics with saturated minijet initial conditions in ultrarelativistic heavy-ion collisions". *Phys. Lett. B* **731** (2014), 126–130. arXiv: 1310.3105 [hep-ph].

[313] URL: http://web.mit.edu/mithig/movies/LHCanmation.mov.

[314] A. Kurkela and Y. Zhu: "Isotropization and hydrodynamization in weakly coupled heavy-ion collisions". *Phys. Rev. Lett.* **115**.18 (2015), 182301. arXiv: 1506.06647 [hep-ph].

[315] W. van der Schee, P. Romatschke, and S. Pratt: "Fully Dynamical Simulation of Central Nuclear Collisions". *Phys. Rev. Lett.* **111**.22 (2013), 222302. arXiv: 1307.2539 [nucl-th].

[316] P. Romatschke: "Do nuclear collisions create a locally equilibrated quark–gluon plasma?" *Eur. Phys. J. C* **77**.1 (2017), 21. arXiv: 1609.02820 [nucl-th].

[317] A. Kurkela and G. D. Moore: "Thermalization in Weakly Coupled Nonabelian Plasmas". *JHEP* **12** (2011), 044. arXiv: 1107.5050 [hep-ph].

[318] A. Andronic et al.: "Heavy-flavour and quarkonium production in the LHC era: from proton–proton to heavy-ion collisions". *Eur. Phys. J. C* **76**.3 (2016), 107. arXiv: 1506.03981 [nucl-ex].

[319] J. Casalderrey-Solana and C. A. Salgado: "Introductory lectures on jet quenching in heavy ion collisions". *Acta Phys. Polon. B* **38** (2007). Ed. by M. Praszalowicz, M. Kutschera, and E. Malec, 3731–3794. arXiv: 0712.3443 [hep-ph].

[320] S. Chatrchyan et al. CMS: "Observation of Sequential Upsilon Suppression in PbPb Collisions". *Phys. Rev. Lett.* **109** (2012). [Erratum: Phys.Rev.Lett. 120, 199903 (2018)], 222301. arXiv: 1208.2826 [nucl-ex].

[321] B. B. Abelev et al. ALICE: "Suppression of $\Upsilon(1S)$ at forward rapidity in Pb-Pb collisions at $\sqrt{s_{\mathrm{NN}}} = 2.76$ TeV". *Phys. Lett. B* **738** (2014), 361–372. arXiv: 1405.4493 [nucl-ex].

[322] P. Foka and M. g. A. Janik: "An overview of experimental results from ultra-relativistic heavy-ion collisions at the CERN LHC: Hard probes". *Rev. Phys.* **1** (2016), 172–194. arXiv: 1702.07231 [hep-ex].

[323] J. Adam et al. ALICE: "Differential studies of inclusive J/ψ and ψ(2S) production at forward rapidity in Pb-Pb collisions at $\sqrt{s_{\mathrm{NN}}} = 2.76$ TeV". *JHEP* **05** (2016), 179. arXiv: 1506.08804 [nucl-ex].

[324] S. Chatrchyan et al. CMS: "Suppression of non-prompt J/ψ, prompt J/ψ, and Y(1S) in PbPb collisions at $\sqrt{s_{NN}} = 2.76$ TeV". *JHEP* **05** (2012), 063. arXiv: 1201.5069 [nucl-ex].

[325] A. Capella, L. Bravina, E. Ferreiro, A. Kaidalov, K. Tywoniuk, and E. Zabrodin: "Charmonium dissociation and recombination at RHIC and LHC". *Eur. Phys. J. C* **58** (2008), 437–444. arXiv: 0712.4331 [hep-ph].

[326] K. Ackermann et al. STAR: "Elliptic flow in Au + Au collisions at (S(NN))**(1/2) = 130 GeV". *Phys. Rev. Lett.* **86** (2001), 402–407. arXiv: nucl-ex/0009011.

[327] K. Aamodt et al. ALICE: "Higher harmonic anisotropic flow measurements of charged particles in Pb-Pb collisions at $\sqrt{s_{NN}}$=2.76 TeV". *Phys. Rev. Lett.* **107** (2011), 032301. arXiv: 1105.3865 [nucl-ex].

[328] G. Aad et al. ATLAS: "Measurement of the distributions of event-by-event flow harmonics in lead-lead collisions at = 2.76 TeV with the ATLAS detector at the LHC". *JHEP* **11** (2013), 183. arXiv: 1305.2942 [hep-ex].

[329] P. K. Kovtun and A. O. Starinets: "Quasinormal modes and holography". *Phys. Rev.* **D72** (2005), 086009. arXiv: hep-th/0506184 [hep-th].

[330] P. Romatschke and U. Romatschke: "Viscosity Information from Relativistic Nuclear Collisions: How Perfect is the Fluid Observed at RHIC?" *Phys. Rev. Lett.* **99** (2007), 172301. arXiv: 0706.1522 [nucl-th].

[331] H. Song, S. A. Bass, U. Heinz, T. Hirano, and C. Shen: "200 A GeV Au+Au collisions serve a nearly perfect quark-gluon liquid". *Phys. Rev. Lett.* **106** (2011). [Erratum: Phys.Rev.Lett. 109, 139904 (2012)], 192301. arXiv: 1011.2783 [nucl-th].

[332] B. Schenke, S. Jeon, and C. Gale: "Elliptic and triangular flow in event-by-event (3+1)D viscous hydrodynamics". *Phys. Rev. Lett.* **106** (2011), 042301. arXiv: 1009.3244 [hep-ph].

[333] M. Luzum and J.-Y. Ollitrault: "Extracting the shear viscosity of the quark-gluon plasma from flow in ultra-central heavy-ion collisions". *Nucl. Phys. A* **904-905** (2013). Ed. by T. Ullrich, B. Wyslouch, and J. W. Harris, 377c–380c. arXiv: 1210.6010 [nucl-th].

[334] J. E. Bernhard, J. S. Moreland, S. A. Bass, J. Liu, and U. Heinz: "Applying Bayesian parameter estimation to relativistic heavy-ion collisions: simultaneous characterization of the initial state and quark-gluon plasma medium". *Phys. Rev. C* **94**.2 (2016), 024907. arXiv: 1605.03954 [nucl-th].

[335] J. L. Albacete, Y. V. Kovchegov, and A. Taliotis: "Modeling Heavy Ion Collisions in AdS/CFT". *JHEP* **07** (2008), 100. arXiv: 0805.2927 [hep-th].

[336] J. L. Albacete, Y. V. Kovchegov, and A. Taliotis: "Asymmetric Collision of Two Shock Waves in AdS(5)". *JHEP* **05** (2009), 060. arXiv: 0902.3046 [hep-th].

[337] M. P. Heller, D. Mateos, W. van der Schee, and D. Trancanelli: "Strong Coupling Isotropization of Non-Abelian Plasmas Simplified". *Phys. Rev. Lett.* **108** (2012), 191601. arXiv: 1202.0981 [hep-th].

[338] H. Bantilan and P. Romatschke: "Simulation of Black Hole Collisions in Asymptotically Anti–de Sitter Spacetimes". *Phys. Rev. Lett.* **114**.8 (2015), 081601. arXiv: 1410.4799 [hep-th].

[339] P. M. Chesler and L. G. Yaffe: "Holography and off-center collisions of localized shock waves". *JHEP* **10** (2015), 070. arXiv: 1501.04644 [hep-th].

[340] P. M. Chesler and L. G. Yaffe: "Horizon formation and far-from-equilibrium isotropization in supersymmetric Yang-Mills plasma". *Phys. Rev. Lett.* **102** (2009), 211601. arXiv: 0812.2053 [hep-th].

[341] V. Balasubramanian, A. Bernamonti, J. de Boer, N. Copland, B. Craps, E. Keski-Vakkuri, B. Müller, A. Schafer, M. Shigemori, and W. Staessens: "Holographic Thermalization". *Phys. Rev.* **D84** (2011), 026010. arXiv: 1103.2683 [hep-th].

[342] H. Bantilan, T. Ishii, and P. Romatschke: "Holographic Heavy-Ion Collisions: Analytic Solutions with Longitudinal Flow, Elliptic Flow and Vorticity". *Phys. Lett. B* **785** (2018), 201–206. arXiv: 1803.10774 [nucl-th].

[343] G. T. Horowitz and V. E. Hubeny: "Quasinormal modes of AdS black holes and the approach to thermal equilibrium". *Phys. Rev.* **D62** (2000), 024027. arXiv: hep-th/9909056 [hep-th].

[344] D. T. Son and A. O. Starinets: "Minkowski space correlators in AdS / CFT correspondence: Recipe and applications". *JHEP* **09** (2002), 042. arXiv: hep-th/0205051 [hep-th].

[345] P. Kovtun and A. Starinets: "Thermal spectral functions of strongly coupled N=4 supersymmetric Yang-Mills theory". *Phys. Rev. Lett.* **96** (2006), 131601. arXiv: hep-th/0602059.

[346] D. Teaney: "Finite temperature spectral densities of momentum and R-charge correlators in N=4 Yang Mills theory". *Phys. Rev. D* **74** (2006), 045025. arXiv: hep-ph/0602044.

[347] S. S. Gubser, S. S. Pufu, and F. D. Rocha: "Bulk viscosity of strongly coupled plasmas with holographic duals". *JHEP* **08** (2008), 085. arXiv: 0806.0407 [hep-th].

[348] V. Keränen and P. Kleinert: "Thermalization of Wightman functions in AdS/CFT and quasinormal modes". *Phys. Rev. D* **94**.2 (2016), 026010. arXiv: 1511.08187 [hep-th].

[349] U. Gürsoy, S. Lin, and E. Shuryak: "Instabilities near the QCD phase transition in the holographic models". *Phys. Rev. D* **88**.10 (2013), 105021. arXiv: 1309.0789 [hep-th].

[350] U. Gürsoy, M. Järvinen, and G. Policastro: "Late time behavior of non-conformal plasmas". *JHEP* **01** (2016), 134. arXiv: 1507.08628 [hep-th].

[351] T. Ishii, E. Kiritsis, and C. Rosen: "Thermalization in a Holographic Confining Gauge Theory". *JHEP* **08** (2015), 008. arXiv: 1503.07766 [hep-th].

[352] R. A. Janik, G. Plewa, H. Soltanpanahi, and M. Spalinski: "Linearized nonequilibrium dynamics in nonconformal plasma". *Phys. Rev.* **D91**.12 (2015), 126013. arXiv: 1503.07149 [hep-th].

[353] R. A. Janik, J. Jankowski, and H. Soltanpanahi: "Nonequilibrium Dynamics and Phase Transitions in Holographic Models". *Phys. Rev. Lett.* **117**.9 (2016), 091603. arXiv: 1512.06871 [hep-th].

[354] T. Demircik and U. Gürsoy: "Holographic equilibration in confining gauge theories under external magnetic fields". *Nucl. Phys. B* **919** (2017), 384–403. arXiv: 1605.08118 [hep-th].

[355] R. A. Janik, J. Jankowski, and H. Soltanpanahi: "Real time dynamics and phase separation in a holographic first order phase transition" (2017). arXiv: 1704.05387 [hep-th].

[356] T. Springer: "Sound Mode Hydrodynamics from Bulk Scalar Fields". *Phys. Rev. D* **79** (2009), 046003. arXiv: 0810.4354 [hep-th].

[357] T. Springer, C. Gale, and S. Jeon: "Bulk spectral functions in single and multi-scalar gravity duals". *Phys. Rev. D* **82** (2010), 126011. arXiv: 1010.2760 [hep-th].

[358] S. Chandrasekhar and E. Milne: "The Highly Collapsed Configurations of a Stellar Mass". *Mon. Not. Roy. Astron. Soc.* **91**.5 (1931), 456–466.

[359] S. Chandrasekhar: "The highly collapsed configurations of a stellar mass (Second paper)". *Mon. Not. Roy. Astron. Soc.* **95** (1935), 207–225.

[360] P. A. Mazzali, F. K. Ropke, S. Benetti, and W. Hillebrandt: "A Common Explosion Mechanism for Type Ia Supernovae". *Science* **315** (2007), 825. arXiv: astro-ph/0702351.

[361] D. Viganò, N. Rea, J. A. Pons, R. Perna, D. N. Aguilera, and J. A. Miralles: "Unifying the observational diversity of isolated neutron stars via magneto-thermal evolution models". *Mon. Not. Roy. Astron. Soc.* **434** (2013), 123. arXiv: 1306.2156 [astro-ph.SR].

[362] D. Buckley, P. Meintjes, S. Potter, T. Marsh, and B. T Gänsicke: "Polarimetric evidence of a white dwarf pulsar in the binary system AR Scorpii". *Nature Astron.* **1** (2017), 0029. arXiv: 1612.03185 [astro-ph.HE].

[363] A. Hewish, S. Bell, J. Pilkington, P. Scott, and R. Collins: "Observation of a rapidly pulsating radio source". *Nature* **217** (1968), 709–713.

[364] J. M. Lattimer: "The nuclear equation of state and neutron star masses". *Ann. Rev. Nucl. Part. Sci.* **62** (2012), 485–515. arXiv: 1305.3510 [nucl-th].

[365] I. I. Shapiro: "Fourth Test of General Relativity". *Phys. Rev. Lett.* **13** (1964), 789–791.

[366] P. Demorest, T. Pennucci, S. Ransom, M. Roberts, and J. Hessels: "Shapiro Delay Measurement of A Two Solar Mass Neutron Star". *Nature* **467** (2010), 1081–1083. arXiv: 1010.5788 [astro-ph.HE].

[367] J. Antoniadis et al.: "A Massive Pulsar in a Compact Relativistic Binary". *Science* **340** (2013), 6131. arXiv: 1304.6875 [astro-ph.HE].

[368] H. T. Cromartie et al.: "Relativistic Shapiro delay measurements of an extremely massive millisecond pulsar". *Nature Astron.* **4**.1 (2019), 72–76. arXiv: 1904.06759 [astro-ph.HE].

[369] D. Barret, J.-F. Olive, and M. Miller: "An Abrupt drop in the coherence of the lower kilohertz QPO in 4U 1636-536". *Mon. Not. Roy. Astron. Soc.* **361** (2005), 855–860. arXiv: astro-ph/0505402.

[370] P. C. C. Freire, A. Wolszczan, M. v. d. Berg, and J. W. Hessels: "A Massive Neutron Star in the Globular Cluster M5". *Astrophys. J.* **679** (2008), 1433. arXiv: 0712.3826 [astro-ph].

[371] B. Margalit and B. D. Metzger: "Constraining the Maximum Mass of Neutron Stars From Multi-Messenger Observations of GW170817". *Astrophys. J. Lett.* **850**.2 (2017), L19. arXiv: 1710.05938 [astro-ph.HE].

[372] M. Shibata, S. Fujibayashi, K. Hotokezaka, K. Kiuchi, K. Kyutoku, Y. Sekiguchi, and M. Tanaka: "Modeling GW170817 based on numerical relativity and its implications". *Phys. Rev. D* **96**.12 (2017), 123012. arXiv: 1710.07579 [astro-ph.HE].

[373] M. Ruiz, S. L. Shapiro, and A. Tsokaros: "GW170817, General Relativistic Magnetohydrodynamic Simulations, and the Neutron Star Maximum Mass". *Phys. Rev. D* **97**.2 (2018), 021501. arXiv: 1711.00473 [astro-ph.HE].

[374] M. Miller et al.: "PSR J0030+0451 Mass and Radius from $NICER$ Data and Implications for the Properties of Neutron Star Matter". *Astrophys. J. Lett.* **887**.1 (2019), L24. arXiv: 1912.05705 [astro-ph.HE].

[375] T. E. Riley et al.: "A $NICER$ View of PSR J0030+0451: Millisecond Pulsar Parameter Estimation". *Astrophys. J. Lett.* **887**.1 (2019), L21. arXiv: 1912.05702 [astro-ph.HE].

[376] J. Nättilä, M. Miller, A. Steiner, J. Kajava, V. Suleimanov, and J. Poutanen: "Neutron star mass and radius measurements from atmospheric model fits to X-ray burst cooling tail spectra". *Astron. Astrophys.* **608** (2017), A31. arXiv: 1709.09120 [astro-ph.HE].

[377] J. Nättilä, A. W. Steiner, J. J. E. Kajava, V. F. Suleimanov, and J. Poutanen: "Equation of state constraints for the cold dense matter inside neutron stars using the cooling tail method". *Astron. Astrophys.* **591** (2016), A25. arXiv: 1509.06561 [astro-ph.HE].

[378] E. E. Flanagan and T. Hinderer: "Constraining neutron star tidal Love numbers with gravitational wave detectors". *Phys. Rev. D* **77** (2008), 021502. arXiv: 0709.1915 [astro-ph].

[379] T. Hinderer: "Tidal Love numbers of neutron stars". *Astrophys. J.* **677** (2008), 1216–1220. arXiv: 0711.2420 [astro-ph].

[380] D. Radice, S. Bernuzzi, and A. Perego: "The Dynamics of Binary Neutron Star Mergers and of GW170817" (Feb. 2020). arXiv: 2002.03863 [astro-ph.HE].

[381] K. Takami, L. Rezzolla, and L. Baiotti: "Constraining the Equation of State of Neutron Stars from Binary Mergers". *Phys. Rev. Lett.* **113**.9 (2014), 091104. arXiv: 1403.5672 [gr-qc].

[382] K. Takami, L. Rezzolla, and L. Baiotti: "Spectral properties of the post-merger gravitational-wave signal from binary neutron stars". *Phys. Rev. D* **91**.6 (2015), 064001. arXiv: 1412.3240 [gr-qc].

[383] M. Breschi, S. Bernuzzi, F. Zappa, M. Agathos, A. Perego, D. Radice, and A. Nagar: "kiloHertz gravitational waves from binary neutron star remnants: time-domain model and constraints on extreme matter". *Phys. Rev. D* **100**.10 (2019), 104029. arXiv: 1908.11418 [gr-qc].

[384] L. Rezzolla and K. Takami: "Gravitational-wave signal from binary neutron stars: a systematic analysis of the spectral properties". *Phys. Rev. D* **93**.12 (2016), 124051. arXiv: 1604.00246 [gr-qc].

[385] K. W. Tsang, T. Dietrich, and C. Van Den Broeck: "Modeling the postmerger gravitational wave signal and extracting binary properties from future binary neutron star detections". *Phys. Rev. D* **100**.4 (2019), 044047. arXiv: 1907.02424 [gr-qc].

[386] L. D. Landau: "On the Theory of Stars". *Phys.Z.Sowjetunion* **1** (1932), 285.

[387] D. G. Yakovlev, P. Haensel, G. Baym, and C. J. Pethick: "Lev Landau and the concept of neutron stars". *Phys. Usp.* **56** (2013), 289–295. arXiv: 1210.0682 [physics.hist-ph].

[388] W. Baade and F. Zwicky: "Remarks on Super-Novae and Cosmic Rays". *Phys. Rev.* **46** (1 1934), 76–77.

[389] R. C. Tolman: "Static solutions of Einstein's field equations for spheres of fluid". *Phys. Rev.* **55** (1939), 364–373.

[390] J. Oppenheimer and G. Volkoff: "On Massive neutron cores". *Phys. Rev.* **55** (1939), 374–381.

[391] J. B. Hartle: "Slowly rotating relativistic stars. 1. Equations of structure". *Astrophys. J.* **150** (1967), 1005–1029.

[392] J. B. Hartle and K. S. Thorne: "Slowly Rotating Relativistic Stars. II. Models for Neutron Stars and Supermassive Stars". *Astrophys. J.* **153** (1968), 807.

[393] H. Komatsu, Y. Eriguchi, and I. Hachisu: "Rapidly rotating general relativistic stars. I - Numerical method and its application to uniformly rotating polytropes". *Mon. Not. Roy. Astron. Soc.* **237** (1989), 355–379.

[394] G. B. Cook, S. L. Shapiro, and S. A. Teukolsky: "Rapidly rotating neutron stars in general relativity: Realistic equations of state". *Astrophys. J.* **424** (1994), 823.

[395] M. Fortin, C. Providencia, A. Raduta, F. Gulminelli, J. L Zdunik, P. Haensel, and M. Bejger: "Neutron star radii and crusts: uncertainties and unified equations of state". *Phys. Rev. C* **94**.3 (2016), 035804. arXiv: 1604.01944 [astro-ph.SR].

[396] M. Drews and W. Weise: "Functional renormalization group studies of nuclear and neutron matter". *Prog. Part. Nucl. Phys.* **93** (2017), 69–107. arXiv: 1610.07568 [nucl-th].

[397] K. Otto, M. Oertel, and B.-J. Schaefer: "Hybrid and quark star matter based on a nonperturbative equation of state". *Phys. Rev. D* **101**.10 (2020), 103021. arXiv: 1910.11929 [hep-ph].

[398] M. Leonhardt, M. Pospiech, B. Schallmo, J. Braun, C. Drischler, K. Hebeler, and A. Schwenk: "Symmetric nuclear matter from the strong interaction" (July 2019). arXiv: 1907.05814 [nucl-th].

[399] A. Kurkela and A. Vuorinen: "Cool quark matter". *Phys. Rev. Lett.* **117**.4 (2016), 042501. arXiv: 1603.00750 [hep-ph].

[400] T. Gorda, A. Kurkela, P. Romatschke, M. Säppi, and A. Vuorinen: "Next-to-Next-to-Next-to-Leading Order Pressure of Cold Quark Matter: Leading Logarithm". *Phys. Rev. Lett.* **121**.20 (2018), 202701. arXiv: 1807.04120 [hep-ph].

[401] E. Annala, T. Gorda, A. Kurkela, J. Nättilä, and A. Vuorinen: "Evidence for quark-matter cores in massive neutron stars". *Nature Phys.* (2020). arXiv: 1903.09121 [astro-ph.HE].

[402] V. E. Zavlin and G. Pavlov: "Modeling neutron star atmospheres". *270th WE-Heraeus Seminar on Neutron Stars, Pulsars and Supernova Remnants*. June 2002, 262–272. arXiv: astro-ph/0206025.

[403] N. Chamel and P. Haensel: "Physics of Neutron Star Crusts". *Living Rev. Rel.* **11** (2008), 10. arXiv: 0812.3955 [astro-ph].

[404] A. Kurkela, E. S. Fraga, J. Schaffner-Bielich, and A. Vuorinen: "Constraining neutron star matter with Quantum Chromodynamics". *Astrophys. J.* **789** (2014), 127. arXiv: 1402.6618 [astro-ph.HE].

[405] E. Annala, T. Gorda, A. Kurkela, and A. Vuorinen: "Gravitational-wave constraints on the neutron-star-matter Equation of State". *Phys. Rev. Lett.* **120**.17 (2018), 172703. arXiv: 1711.02644 [astro-ph.HE].

[406] E. Annala, T. Gorda, A. Kurkela, J. Nättilä, and A. Vuorinen: "Constraining the properties of neutron-star matter with observations". *12th INTEGRAL conference and 1st AHEAD Gamma-ray workshop (INTEGRAL 2019): INTEGRAL looks AHEAD to Multi-Messenger Astrophysics Geneva, Switzerland, February 11-15, 2019*. 2019. arXiv: 1904.01354 [astro-ph.HE].

[407] C. Hoyos, D. Rodríguez Fernández, N. Jokela, and A. Vuorinen: "Holographic quark matter and neutron stars". *Phys. Rev. Lett.* **117**.3 (2016), 032501. arXiv: 1603.02943 [hep-ph].

[408] C. Hoyos, N. Jokela, D. Rodríguez Fernández, and A. Vuorinen: "Breaking the sound barrier in AdS/CFT". *Phys. Rev.* **D94**.10 (2016), 106008. arXiv: 1609.03480 [hep-th].

[409] E. Annala, C. Ecker, C. Hoyos, N. Jokela, D. Rodríguez Fernández, and A. Vuorinen: "Holographic compact stars meet gravitational wave constraints". *JHEP* **12** (2018), 078. arXiv: 1711.06244 [astro-ph.HE].

[410] C. Ecker, C. Hoyos, N. Jokela, D. Rodríguez Fernández, and A. Vuorinen: "Stiff phases in strongly coupled gauge theories with holographic duals" (2017). [JHEP11,031(2017)]. arXiv: 1707.00521 [hep-th].

[411] K. Bitaghsir Fadafan, J. Cruz Rojas, and N. Evans: "Deconfined, Massive Quark Phase at High Density and Compact Stars: A Holographic Study". *Phys. Rev. D* **101**.12 (2020), 126005. arXiv: 1911.12705 [hep-ph].

[412] C. Ecker, M. Järvinen, G. Nijs, and W. van der Schee: "Gravitational Waves from Holographic Neutron Star Mergers" (2019). arXiv: 1908.03213 [astro-ph.HE].

[413] A. Akmal, V. Pandharipande, and D. Ravenhall: "The Equation of state of nucleon matter and neutron star structure". *Phys. Rev. C* **58** (1998), 1804–1828. arXiv: nucl-th/9804027.

[414] P. Haensel and B. Pichon: "Experimental nuclear masses and the ground state of cold dense matter". *Astron. Astrophys.* **283** (1994), 313. arXiv: nucl-th/9310003.

[415] F. Douchin and P. Haensel: "A unified equation of state of dense matter and neutron star structure". *Astron. Astrophys.* **380** (2001), 151. arXiv: astro-ph/0111092.

[416] M. Hempel and J. Schaffner-Bielich: "Statistical Model for a Complete Supernova Equation of State". *Nucl. Phys. A* **837** (2010), 210–254. arXiv: 0911.4073 [nucl-th].

[417] F. Fattoyev, C. Horowitz, J. Piekarewicz, and G. Shen: "Relativistic effective interaction for nuclei, giant resonances, and neutron stars". *Phys. Rev. C* **82** (2010), 055803. arXiv: 1008.3030 [nucl-th].

[418] S. Typel, G. Ropke, T. Klahn, D. Blaschke, and H. Wolter: "Composition and thermodynamics of nuclear matter with light clusters". *Phys. Rev. C* **81** (2010), 015803. arXiv: 0908.2344 [nucl-th].

[419] P. M. Chesler, N. Jokela, A. Loeb, and A. Vuorinen: "Finite-temperature Equations of State for Neutron Star Mergers". *Phys. Rev. D* **100**.6 (2019), 066027. arXiv: 1906.08440 [astro-ph.HE].

[420] G. D. Moore: "Stress-stress correlator in ϕ^4 theory: poles or a cut?" *JHEP* **05** (2018), 084. arXiv: 1803.00736 [hep-ph].

[421] S. Grozdanov and A. O. Starinets: "Adding new branches to the "Christmas tree" of the quasinormal spectrum of black branes". *JHEP* **04** (2019), 080. arXiv: 1812.09288 [hep-th].